

Miniaturized Bioanalytics to Probe the Function of Membrane Proteins

THÈSE N° 4209 (2008)

PRÉSENTÉE LE 31 OCTOBRE 2008

À LA FACULTÉ DES SCIENCES DE BASE

Laboratoire de chimie physique des polymères et membranes

SECTION DE CHIMIE ET GÉNIE CHIMIQUE

ÉCOLE POLYTECHNIQUE FÉDÉRALE DE LAUSANNE

POUR L'OBTENTION DU GRADE DE DOCTEUR ÈS SCIENCES

PAR

Pedro PASCOAL

Biochimiste diplômé de l'Université de Genève
et de nationalité portugaise

acceptée sur proposition du jury:

Prof. G. Bodenhausen, président du jury

Prof. H. Vogel, directeur de thèse

Dr G. Turcatti, rapporteur

Dr R. Wagner, rapporteur

Prof. M. Winterhalter, rapporteur



ÉCOLE POLYTECHNIQUE
FÉDÉRALE DE LAUSANNE

Suisse

2008

Este trabalho é dedicado aos meus pais Ilda e Alípio,
e à minha mana Catarina
e ao grupo d'amigos cujo nome ficará no meu coração

Abstract

G-protein coupled receptors (GPCRs) are the most abundant class of proteins in the cell body. Such receptors are of major interest as potential therapeutic targets. Downscaling and parallelization of bioanalytics opens novel routes to rapidly screen and identify potential drugs with a decrease in regard to the costs, and elucidate novel functions of signaling networks under physiological conditions. Native vesicles are small autonomous biological containers, which are efficiently produced from all cell lines. They are composed of their mother cell plasma membrane and enclose part of their cytoplasm. Membrane receptors are then exposed at their surface and already demonstrate to induce cellular signaling when exposed to receptor ligands.

Native vesicles were investigated in this present work, as novel possibilities to downscale receptor investigation in live cells, using neurokinin 1 receptor (NK₁R) as a representative model. Here native vesicle production and purification was optimized. The influence of the cell cycle on the production efficiency was demonstrated. Biological proteins were downregulated in order to produce blebbing cells. Native vesicle characterization was achieved. The receptors also demonstrate to be efficiently labeled by agonist and antagonist, allowing to access information about the binding kinetics as well as K_D values. The results are in agreement with those obtained in live cells. Native vesicles also demonstrate to internalize agonist after application, demonstrating receptor desensitization and signaling performance similar as live cells.

Confocal microscopy shows that cells expressing the NK₁R-CFP have two binding affinities for their main agonist, substance P. Similar results could be observed with flow cytometry. The high affinity binding is related to cholesterol content in the cell membrane and was abolished by cholesterol depletion with methyl- β -cyclodextrin.

Micro-contact printing (μ CP) was used to (bio)functionalize surfaces with proteins, polymers or functionalized nanoparticles. Precise sample positioning by micro-contact printing shows improves nuclear magnetic resonance excitation and detection, when performed with a planar microcoil probe. μ CP was used to produce native vesicle arrays by two procedures, and fluorescent binding assay shows the binding of fluorescent ligands to the receptor.

Laser tweezers allow manipulating cell membranes without requiring the use of polystyrene beads. From pulled membranes, native vesicles were produced. In addition from pulled membranes, large tethers were produced and artificial connections were established with neighboring cells. Intercellular communication was investigated by whole-cell patch clamp in dissociated primary dorsal root ganglion neurons after optical induced connection, as well as in HEK cells expressing Cx36.

The lab-on-chip assay development demonstrates: the high production of native vesicles in microchannels; the efficient purification obtained by negative dielectrophoresis depletion in MEMS chips; perfect trapping and thus immobilization of native vesicles in a new optical multi-tweezer array. Fluorescence labeling was performed with native vesicles trapped in a multi-tweezer array inside microfluidic channel in the presence of two laminar flows.

Optical multi-tweezer array setup shows to be the fastest and more efficient technique in order to perform immobilization and labeling of native vesicles in the microfluidic channel. It is presently the only technique to perform fluorescence measurements when maintaining objects trapped.

KEYWORDS: Native Vesicles; G-protein coupled receptor (GPCR); NK₁R; SP; Dorsal Root Ganglions (DRGs); Primary cells; Cx36; Ligand affinity; Cholesterol; Planar Microcoil Confocal Microscopy; Flow Cytometry; Nanoparticle; Patch Clamp; Laser Tweezer; NMR; Optical Multi-Tweezer Array; Dielectrophoresis, MEMS; Micro-Contact Printing (μ CP); Microfluidics.

Version Abrégée

Les récepteurs couplés aux protéines G (RCPGs) forment la classe la plus abondante de protéines. Ces récepteurs sont d'un intérêt majeur comme cibles thérapeutiques. La parallélisation et la miniaturisation des bioanalyses ouvrent la voie à la découverte de médicaments avec une réduction effective des coûts. Les vésicules natives sont de petits conteneurs capables d'être produits à partir de nombreux types cellulaires. Elles se forment à partir de la membrane plasmique de la cellule mère et renferment une partie de son cytosol. Elles contiennent les récepteurs membranaires et sont capables d'effectuer de la signalisation cellulaire.

Les vésicules natives ont été étudiées comme une alternative pour effectuer la recherche à une échelle plus petite que la cellule. Le récepteur neurokinin 1 (NK₁R) a été utilisé comme modèle. La production et la purification de vésicules natives ont été optimisées. L'implication du cycle cellulaire lors de la production a été démontrée. Le taux d'expression de certaines protéines a été abaissé induisant une vésiculation de la cellule. La caractérisation des vésicules a démontré que l'on pouvait suivre la liaison de l'agoniste, ainsi que de l'antagoniste, permettant dans les deux cas d'obtenir des valeurs de K_D en accord avec celles obtenues en cellule. Les vésicules natives ont aussi permis l'internalisation du ligand, démontrant la désensibilisation ainsi que l'activité de signalisation.

La microscopie confocale a montré que les cellules exprimant le NK₁R-CFP possèdent deux affinités différentes pour le même agoniste, la substance P. Ces résultats ont été confirmés avec la cytométrie en flux. Cet effet a été abrogé lors de l'utilisation de méthyle-β-cyclodextrine, un chélateur du cholestérol.

Le "micro-contact printing" (μCP) a été utilisé pour (bio)fonctionnaliser les surfaces avec des protéines, polymères ou des nanoparticules. Le positionnement précis de l'échantillon par μCP améliore notablement la qualité d'excitation et de détection lors de mesures de résonance magnétique nucléaire faites avec des bobines planaires. Le μCP a en outre permis de réaliser, par deux méthodes différentes, des réseaux de vésicules natives pour réaliser des tests de liaison entre un ligand fluorescent et son récepteur.

Des pinces optiques ont permis la manipulation de la membrane cellulaire sans l'aide de billes de polystyrène. Des vésicules natives ont pu ainsi être produites. Dans d'autres expériences, des connections artificielles ont été réalisées entre deux cellules en tirant des filaments membranaires. Dans ces derniers cas, ces expériences ont permis d'étudier la communication cellulaire dans des cellules neuronales des ganglions dorsaux préalablement dissociés, et dans des HEK exprimant la protéine : Cx36. Lors de ces expériences, les mesures ont été réalisées par "whole-cell patch clamp".

Le développement d'un laboratoire sur puce a démontré: une grande production de vésicules natives dans des microcanaux; l'efficacité d'une purification réalisée par négative diélectrophorèse déviation dans des puces MEMS; un piégeage optique de vésicules natives dans un flux laminaire. Un test de liaison de ligand a été ensuite réalisé en microcanaux en maintenant les vésicules piégées dans le flux.

Cet instrument de pinces optiques multiples a démontré une très grande efficacité à maintenir les vésicules piégées dans le flux laminaire. Elle permet en outre un échange rapide d'échantillon, mais surtout de pouvoir suivre en temps réel le marquage fluorescent.

MOTS CLEFS: Vésicules Natives; Récepteurs Couplés aux Protéines G (RCPGs); R-NK₁; SP; Ganglions Dorsaux (DRGs); Cellules Primaires; Cx36; Affinité du Ligand; Cholestérol; Microbobine Planaire; Microscopie Confocale; Cytométrie en Flux; Nanoparticules; Patch Clamp; Pince Optique; RMN; Réseau de Pinces Optiques; Diélectrophorèse, MEMS; Impression par Microcontact (μCP); Microfluidique.

Table of Contents

ABSTRACT	5
VERSION ABRÉGÉE	6
TABLE OF CONTENTS	7
ABBREVIATIONS AND SYMBOLS	10
CHAPTER 1	14
1.INTRODUCTION	14
1.1 AIM OF THE THESIS	17
CHAPTER 2	19
2. NATIVE VESICLES	19
2.1 CELL CYTOSKELETON	20
2.1.1 Actin Regulation	25
2.2 CELL CYTOSKELETON AND ITS ROLE FOR NATIVE VESICLES PRODUCTION	27
2.2.1 Liposomes	28
2.2.2 Cell Motility	29
2.2.3 Membrane Protein Expression and Downregulation	33
2.2.4 Synaptogenesis	39
2.2.5 Other Mechanisms of Vesicle Formation	40
2.3 RESULTS AND DISCUSSION	42
2.4 CYTOCHALASIN EFFECT ON CELL CYTOSKELETON	43
2.5 OPTIMIZATION PARAMETERS FOR NATIVE VESICLE PRODUCTION	45
2.5.1 Influence of Growth Medium on native vesicle production	46
2.5.2 Influence of Cell Cycle on Native Vesicle Production	47
2.5.3 Production by Small Hairpin RNA (shRNA)	49
2.6 PURIFICATION	51
2.6.1 Centrifugation and Filtration	52
2.6.2 Ultracentrifugation on Continuous Percoll® Density Gradient	52
2.7 NATIVE VESICLES CHARACTERIZATION	54
2.7.1 Native Vesicle Size Distribution	54
2.7.2 Intracellular Components Present in Native Vesicles	58
2.7.3 Production of Native Vesicles from Attached vs. in Suspension Cells	60
2.8 CONCLUSIONS AND OUTLOOK	61
2.9 MATERIAL AND METHODS	63

CHAPTER 3	67
3. INVESTIGATING MEMBRANE PROTEINS ON CELLS AND NATIVE VESICLES	67
3.1 GPCR CHARACTERIZATION	68
3.1.1 The Neurokinin 1 Receptor as a Model Cell Surface Receptor	69
3.2 RESULTS AND DISCUSSION	71
3.3 THE NEUROKININ ₁ RECEPTOR	74
3.3.1 Agonist Binding	74
3.3.1.1 Cells	74
3.3.1.2 Influence of Cholesterol on NK ₁ R	79
3.3.1.3 Native Vesicles	81
3.3.1.4 Internalization in Native Vesicles	83
3.3.2 Antagonist Labeling	84
3.3.2.1 Cells	84
3.3.2.2 Native Vesicles	85
3.4 CONCLUSION AND OUTLOOK	86
3.5 MATERIAL AND METHODS	88
CHAPTER 4	90
4. SURFACE FUNCTIONALIZATION BY MICRO-CONTACT PRINTING	90
4.1 IMMOBILIZATION OF LIPOSOMES FOR NMR MEASUREMENTS	93
4.2 NANOPARTICLES FOR SURFACE FUNCTIONALIZATION	97
4.3 IMMOBILIZATION OF NATIVE VESICLES IN MICRO-ARRAYS	101
4.3.1 Immobilization Via Biotin-Streptavidin Interaction	101
4.3.2 Suppression of Unspecific Attachment	107
4.3.3 COMB Polymer for Suppressing Unspecific Vesicles Adsorption	110
4.3.4 Hyaluronic Acid for Suppressing Unspecific Vesicles Adsorption	113
4.4 CONCLUSIONS AND OUTLOOK	115
4.5 MATERIAL AND METHODS	117
CHAPTER 5	122
5. ARTIFICIAL CELLULAR CONNECTIONS WITH OPTICAL TWEEZERS	122
5.1 INTERCELLULAR COMMUNICATION	125
5.1.1 Primary Cells	127
5.2 ELECTROPHYSIOLOGY	128
5.3 RESULTS AND DISCUSSION	130
5.3.1 Single Vesicle Investigation	130
5.3.2 Artificially Induced Intercellular Contact	131
5.3.3 Neuronal Communication in Primary Cells	133
5.3.4 Artificial Electrical Synapses between HEK Cells	138
5.4 CONCLUSIONS AND OUTLOOK	140
5.5 MATERIAL AND METHODS	142

CHAPTER 6	146
6. LAB-ON-CHIP FOR INVESTIGATING NATIVE VESICLES	146
6.1 MICROFLUIDICS FOR PRODUCTION OF NATIVE VESICLES	148
6.1.1 Adherent Cells	150
6.1.2 Single cells in suspension	152
6.2 PURIFICATION	157
6.2.1 Electrophoresis	157
6.2.2 Dielectrophoretic Depletion (DEPD)	158
6.3 IMMOBILIZATION OF VESICLES BY NEGATIVE DIELECTROPHORESIS	161
6.4 PARALLEL ANALYSIS WITH LASER MULTI TWEEZERS	162
6.5 NEW LAB-ON-CHIP DESIGNS	165
6.6 CONCLUSIONS AND OUTLOOK	169
6.7 MATERIALS AND METHODS	171
BIBLIOGRAPHY	175
ACKNOWLEDGMENTS	184
CURRICULUM VITAE	186

Abbreviations and Symbols

5HT ₃	5-hydroxytryptamine
7TM	seven transmembrane
ABP	actin-binding protein
ACP	acyl carrier protein
ADP / ATP	adenosine diphosphate / triphosphate
APs	adaptator proteins
AR	adrenergic receptor
BE	beam expander
BLAST	Basic Local Alignment Search Tool
bPEG	biotinylated-poly(ethylene glycol)
BSA	bovine serum albumin
cAMP	cyclic adenosine-5-monophosphate
CCD :	charge-coupled device
CFP:	cyan fluorescent protein
CHO	Chinese Hamster Ovary
CMC	critical micelle concentration
CNGs	cyclic nucleotide gated channel
CNS	central nervous system
CTC	cubic ternary complex
DAG	diacylglycerol
DAPI	4',6-diamidino-2-phenylindole
DEPD	dielectrophoretic depletion
DHPE	1,2-dihexadecanoyl-sn-glycero-3-phosphoethanolamine
DHPE-biotin	1,2-dihexadecanoyl-sn-glycero-3-phosphoethanolamine-biotin
DM	dichroic mirror
DMEM	Dulbecco's Modified Eagle's Medium
DNA	deoxyribonucleic acid
DOPG	1,2-dioleoyl-sn-glycero-3-[phospho-rac-(1-glycerol)]
DPPC	1,2-dipalmitoyl-sn-glycero-3-phosphocholine
DRG	dorsal root ganglions
DSPE	1,2-distearoyl-sn-glycero-3-phosphoethanolamine
ECFP	enhanced cyan fluorescent protein
EDTA	ethylenediaminetetraacetic acid
EGFP	enhanced green fluorescent protein
ER	endoplasmic reticulum
ERM	ezzrin/radixin/moesin
ESCRT	endosomal sorting complex required for transport
ETC	extended ternary complex
FACS	fluorescence activated cell sorter
FCS	fetal calf serum
FID	free induction decay

FITC	fluorescein isothiocyanate
FL	field lense
FRET	Fluorescence Resonance Energy Transfer
GAPs	GTPase-activating proteins
GASP	G protein-coupled receptor-associated sorting protein
GDI _s	guanine dissociation inhibitors
GEFs	guanine exchange factors
GIT1	G protein-coupled receptor kinase-interacting protein
GPCRs	G protein-coupled receptors
GPI	glycosylphosphatidylinisitol
GRK	G protein-coupled receptor kinase
HA	hyaluronic acid
HEK	human embryonic kidney
HeLa	Henrietta Lacks cells
HEPES	(4-(2-hydroxyethyl)-1-piperazineethanesulfonic acid)
HPOEM	hydroxy- poly(oxyethylene) methacrylate
IP ₃	inositol-1,4,5-triphosphate
IR	infra red
LBPA	lyso-bisphosphatidic acid
LPA	lysophosphatidic acid
LSM	laser scanning microscope
M-β-CD	methyl-β-cyclodextrin
M	mirror
M2	melanomas cell lines
MAC	membrane attack complex
MAPK	mitogen-activated protein kinase
MEMS	microelectromechanical systems
MLA	microlenses array
MO	microscope objective
MTOCs	microtubule organizing centers
MVB	multivesicular bodies
nDEP	negative dielectrophoresis
NHE1	Na-H exchanger isoform 1
NHS-biotin	N-hydroxysuccinimide-biotin
NIR	near infrared
NK ₁ R	neurokinin 1 receptor
NMR	nuclear magnetic resonance
NO	nitric oxide
OG	oregon green
OGP	n-octyl-β-D-glucopyranoside
PBF	passband filter
PBS	phosphate buffer saline
PC	phosphocholine
PCR	polymerase chain reaction

pDEP	positive dielectrophoresis
PDMS	polydimethylsiloxane
PEG	poly(ethylene glycol)
PI(4,5)P2	phosphatidylinositol-4,5-bisphosphate
PI	phosphatidylinositol
PIs	phosphoinositide lipids
PKC	protein kinase C
PLC	phospholipase C
PLL	poly-L-lysine
PLL-g-PEG	poly-L-lysine-grafted-poly(ethylene glycol)
PMMA	poly(methyl methacrylate)
POEM	poly(oxyethylene) methacrylate
PPTase	phosphopantetheine transferase
QDs	quantum dots
RNA	ribonucleic acid
RNAi	interference RNA
ROIs	regions of interest
RT	room temperature
shRNA	small hairpin RNA
siRNA	small interference RNA
SM	scanning mirror
SP	substance P
SR	sarcoplasmic reticulum
TRITC	N-(6-tetramethylrhodaminethiocarbonyl)
UV	ultra violet
WASP	Wiskott-Aldrich syndrome protein
WGA	wheat germ agglutinin
μ CP	micro-contact printing
μ -TAS	miniaturized total chemical analysis systems

Chapter 1

1. Introduction

Life relies on cells' capabilities to sense external signals and translate them into intracellular chemical responses. Evolution lead to sophisticated membrane proteins, which play pivotal role in cellular signaling. In complex organisms, a major class of membrane proteins, called G protein-coupled receptors (GPCRs), mediate such elaborated reactions. They function as specialized molecular transducers capable efficiently to discriminate subtle differences in chemical signals.

GPCRs (Gether 2000), also referred as 7TMs due to their common structural feature of having seven transmembrane spanning α -helices, are the largest superfamily of proteins accounting for about 1% of the human genome. They are subdivided into three major classes: class A receptors, comprising the β_2 -adrenergic, rhodopsin, neurokinin 1 (figure 1.1) and olfactory receptors, have the shortest N-terminal domain; class B receptors, with the glucagon receptor, have several disulfide bridges connecting their extracellular domain; and class C receptors, comprising the glutamate and γ -aminobutyric acid (GABA) receptors, are characterized by large extracellular domains.

As a prototypical GPCRs is the neurokinin 1 receptor (NK₁R). This receptor has been investigated in this thesis. Its structural model is illustrated in

figure 1.1. The NK₁R couples to the G_{αq/11} protein signaling pathway in HEK293 cells, which leads to a transient increase of the intracellular calcium ion concentration (for more details refer to section 3.1.1).

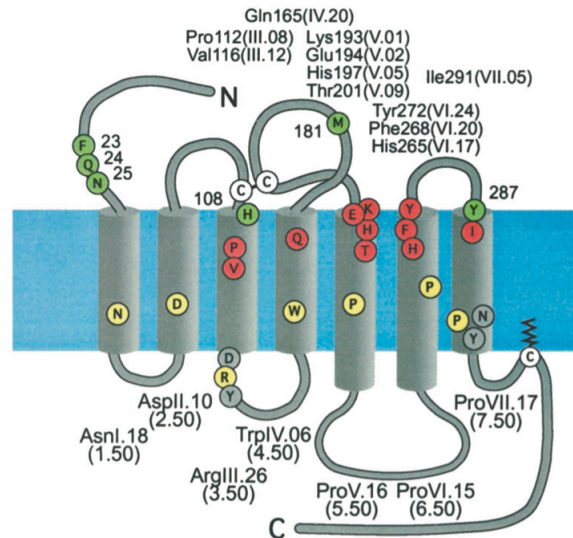


Figure 1.1: Scheme of the NK₁R. In yellow are depicted the most conserved residues, in green those that are supposed to interact with its agonist (Substance P), and in red those that are supposed to interact with the antagonist (CP 96,435). Image taken from Gether et al. 2000 (Gether 2000).

At an early stage of pharmacology, a receptor was considered as a protein interacting simply with its specific ligands (Kenakin 2004). In the 1930s, Clark is considered to be at the origin of receptor theory. Early in the 1980s, De Lean introduced the ternary complex model, which was the first model to take into account allosteric interactions of the receptor and the G protein. Latter in this decade, the simple ternary complex model could not explain observations made by Costa and Hertz about constitutive activity of GPCRs. In 1993, Samana proposed a new extended ternary complex (ETC) model, which can take in consideration infinite receptor states when the receptor is bound to a ligand. In 1996, thermodynamic considerations lead to its extension to the cubic ternary

complex (CTC) model that includes the interaction between the inactive receptor and the G protein (Weiss, Morgan et al. 1996). Despite such a complex model, an increasing number of GPCR-interacting partners are being discovered and should be also considered to draw a complete dynamic picture of GPCR-mediated signaling reactions. Indeed, cholesterol and specific lipids are today considered as important modulators of receptor activity, leading to a higher level of complexity. Taking all these partners in consideration can only be achieved by a different approach. A good candidate is the probabilistic model proposed by Onoran and Costa in 1997. This model considers that the receptor unoccupied by a ligand can adopt many different conformational states. Ligand binding or interaction with other proteins might trap the receptor in one particular conformational state.

The elucidation of physiology regulation of biochemical pathways is an important field in biomedical research and is essential for the development of new medicines by the pharmaceutical industry. The complexity of the cellular functions will be only solved by a multidisciplinary approach of research.

1.1 Aim of the Thesis

During my Ph.D Thesis, the major goal was to downscale membrane receptor bioanalysis below the single cell level, using 100 nm - μm sized native vesicles. Such native vesicles are biological containers produced by treating with cytochalasin live mammalian cells. Native vesicles are composed of cellular membranes and enclose parts of the cytoplasm of the mother cell.

The second chapter focuses on different aspects concerning the production and characterization of native vesicles in order to obtain reproducible and well-controlled quantities of material to perform bioanalysis of membrane receptors. Native vesicles production and purification was investigated as a function of several parameters, such as the cellular cycle and the type of growth medium.

The third chapter describes the functionality of membrane receptors in native vesicles with a focus to the neurokinin 1 receptor (NK_1R). Binding assays of fluorescent ligand agonists and antagonists have been performed revealing interesting features of the NK_1R on cells and native vesicles.

The fourth chapter is dedicated to the use of micro-contact printing, a method developed to biofunctionalize surfaces, in order to immobilize native vesicles as arrays on solid supports. The characterization of native vesicles provides a bioanalytical platform for screening receptor functions. Moreover, micro-contact printing offers substantial advantages for precise sample positioning for new microcoil nuclear magnetic resonance analysis. Finally, streptavidin-functionalized nanoparticles have proven to offer novel tools for labeling.

The fifth chapter is dedicated to biological applications of optical tweezers. First experiments are provided to form intercellular connections using optical tweezers. This approach enables to study intercellular communication in primary cells and in cultured cells.

Finally, the sixth chapter describes the development of a bioanalytical platform in order to perform lab-on-chip assays with native vesicles. Several microtechnologies are used, such as microfluidics, microelectromechanical systems and a multiple optical tweezers setup.

Chapter 2

The present chapter focuses on the biological mechanism of formation of native vesicles, as well as on the preparation, purification and characterization of native vesicles with a protocol recently established. The investigation of new parameters influencing native vesicle production is discussed. Small hairpin RNA technology allows down-regulating protein expression and stably producing blebbing cells.

2. Native Vesicles

Understanding receptor-mediated signaling pathways and their underlying protein-protein interactions are of major interest to discover effective treatments for many diseases like cancer, diabetes or autoimmunity, which are often caused by a dysfunction of the flow of information in living cells. The molecular analysis of these processes is difficult to perform in live cells due to the high complexity of the structural components involved and their dynamical regulation by numerous partners. The dissection of whole cells into smaller units by the controlled preparation of native vesicles, as discussed below, opens novel possibilities for downscaling the analysis of cell signaling and will provide novel insights into the molecular mechanisms of these complex processes. In comparison to classical *in vitro* techniques comprising several manipulation steps such as protein purification and reconstitution into liposomes, native vesicles are produced from living cells in one step by chemically induced membrane extrusion, and represent

the smallest autonomous units capable of performing cellular signaling reactions (Pick, Schmid et al. 2005). These sub-micrometer sized containers provide a valuable platform in many aspects similar to living cells, with important functional characteristics such as the native membrane lipid composition, the presence of integral membrane receptors correctly exposing their extracellular ligand binding sites on the outer vesicle surface and intracellular component essential to perform cellular signaling. However, they are lacking central cellular compartments especially the cell nucleus accounting for the fact that native vesicles cannot replicate themselves. The general downscaling of cellular functions provided by the native vesicles, offers the major advantage of requiring low reactant volumes necessary to perform assays, with regard to chemical costs and some biological rare materials. This approach allows multiplexing of cell-based bioanalytics.

2.1 Cell Cytoskeleton

The cell cytoskeleton (Lodish, Berk et al.; Stryer, Berg et al.) is composed of three helical protein filaments: microtubules, actin and intermediate filaments (figure 2.1). These filaments are inter-connected by proteins forming a three-dimensional network, also known as cell architecture (Geiger 1983). This network is able to interact with many diverse scaffolding proteins (Grashoff, Thievensen et al. 2004), membrane associated proteins (Small, Stradal et al. 2002) or protein domains with specific lipids head-groups (Raucher, Stauffer et al. 2000). These complexes connected to the cellular membrane achieve to maintain membrane integrity providing each cell type its particular shape. Cell cytoskeleton regulation is a highly dynamic process that permanently leads the cytoskeleton to disassemble and assemble and allowing it to perform many different functions such as for

instance, cell locomotion, or intracellular transport of organelles, mitosis/meiosis, to mention a few.

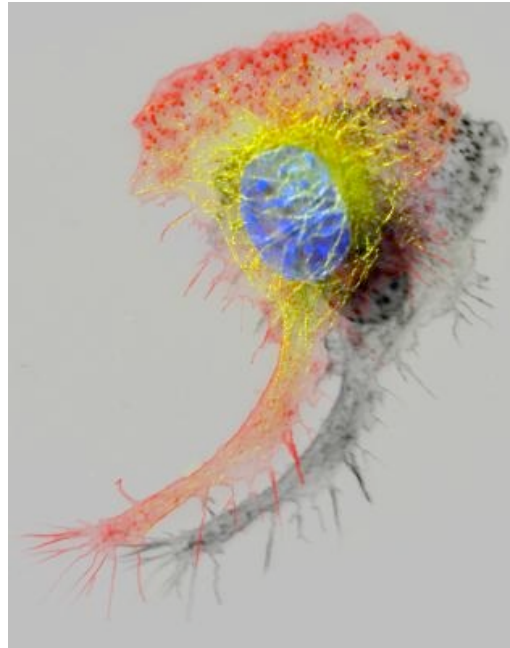


Figure 2.1: Fluorescence confocal microscopic image of a macrophage cell cytoskeleton labeled with fluorescent antibodies against tubulin (yellow) and actin (red); the nucleus is stained with DAPI (blue). The image was recorded by Dr. James Evans (Whitehead Institute, MIT Boston MA, USA; <http://www.svi.nl/support/wiki/EvansMacrophage>)

Microtubules are present in all mammalian cells. They are the biggest filaments (25 nm in diameter) and are composed of dimers of α - and β - tubulin. Microtubule dimers possess an ATP binding region and an intrinsic hydrolase activity. When bound to ATP they assemble into protofilaments and after hydrolysis of ATP into ADP, the building blocks have tendency to dissociate from them. Microtubules are composed of 13 protofilaments. Their organization radiates from two common starting points usually located close to the cell nucleus, the MTOCs (microtubule organizing centers). Microtubules have the functional property of being polarized with a minus (-) end, associated with the

MTOCs, and a plus (+) end where tubulin heterodimers are added. The two principal functions of microtubules are to position and interconnect the intracellular membrane compartments, such as the endoplasmic reticulum and Golgi apparatus, and to provide tracks for the transport of vesicles within the cell, which are essential for cellular trafficking. They are the tracks for the two motor proteins: kinesin, which generally moves towards the (+)-end, and dynein to the other direction. Microtubules have a second major function in chromosome segregation during mitosis and meiosis. Drugs such as taxanes, nocodazole or colchicine, have demonstrated their perturbing efficiency and specificity and were used since decades to study microtubule dynamics, cell cycle dependent events and for cancer treatment in medicine.

Intermediate filaments (Chou, Skalli et al. 1997) are cytoskeletal elements formed by a family of proteins, classified in 6 types according to their primary structure, with diameters lying between that of microtubules and microfilaments, typically 9-11 nm. Their expression patterns are more related to tissue specificity and are principally involved in cell-cell or cell-substrate interactions. They distribute proteins or organelles to defined subcellular localizations. In contrast to the other cytoskeletal filaments they are not polarized.

Finally actin filaments, also called microfilaments, are the thinnest components of cell cytoskeleton, approximately 5-9 nm in diameter and are present in all cell types. They can be distributed across the entire cell body, such as in muscular or motile cell lineages, or in other cell types they could be localized preferentially in close proximity to the plasma membrane, thus termed cortical actin network. Similar as microtubules, actin building blocks have the ability to bind GTP and hydrolyze it, giving rise to actin polymerization. G-actin (or globular actin), which is the only building block, polymerizes to form filaments,

which are named F-actin (or filamentous actin). Like microtubules, microfilaments are polarized and possess a minus and a plus end, also termed pointed and barbed ends, respectively, with distinct physical characteristics (Reisler and Egelman 2007). Even if the two ends possess the capability to elongate or shrink by addition or removal of subunits, the main difference between both is that they possess different association constants and association/dissociation kinetics. Under physiological conditions, the general assumption is that the minus end dissociates and the plus end polymerizes and only the association/dissociation ratio of both ends reveals finally if filaments are elongating or shrinking, which is commonly named actin treadmilling (figure 2.2). Actin filaments can inter-associate too, thus forming actin bundles, also known as stress fibers. These larger structures interact with a specific family of motor proteins: the myosins, which have a more tissue specific expression and their interaction gives rise to the contractile property of cells, like for instance in muscle cells. They are mainly involved in cell contractility and motility (Small, Stradal et al. 2002), but also in membrane partitioning (Gaus, Le Lay et al. 2006), and in trafficking of particular components or organelles, such as mitochondria.

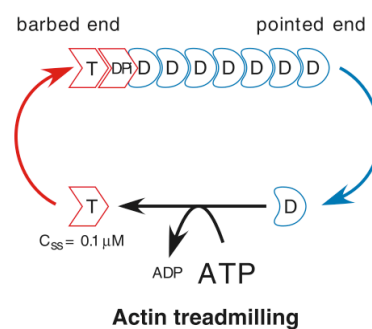


Figure 2.2: Scheme of actin treadmilling. Image taken from Pantaloni et al. 2001 (Pantaloni, Le Clainche et al. 2001).

Natural compounds, known to interact and to modify the actin cytoskeleton are mostly derived from fungi, among which the two classes of poisons, cytochalasins and phallotoxins, allow the specific inhibition of the actin filament elongation at one of the two ends. On one hand phalloidin, a compound of the phalloxin family, attaches to the minus end inhibiting the dissociation of actin filaments in its basic building blocks G-actin. On the other hand cytochalasins can interact at the plus-end inhibiting further polymerization of actin filaments. Another interesting class of compounds derived from marine biology, are the latrunculins, which have demonstrated their efficiency in interacting with actin filaments.

Cytochalasins (Greek cytos, cell; chalasis, relaxation) represent a family of fungal cell permeable metabolites discovered in 1964 by the Pharmaceuticals Division of Imperial Chemicals Industries, Ltd (Carter 1967). Since then, an increasing number of publications compare and quantify their different biological effects. Diverse effects of cytochalasins on the inhibition of cell division and cell movement, induction of nuclear extrusion or inhibition of glucose transport, have been described and some of these effects seem to be cell type specific. Since then, their molecular interaction with the actin cytoskeleton was analyzed, demonstrating their capping activity of the plus end in actin filaments resulting in the inhibition of actin polymerization, and their severing activity creating new sites for actin nucleation. All initially observed effects could probably be correlated to interactions with actin filaments and their remodeling.

The next section will describe the functional role of the cell cytoskeleton and will explain molecular pathways and proteins, which are involved in the regulation and structure of the cellular architecture.

2.1.1 Actin Regulation

Actin treadmilling has a profound influence on cell membrane shape (Hagmann, Burger et al. 1999), on formation of membrane domains (Lillemeier, Pfeiffer et al. 2006), and is responsible for almost all membrane deformations (Hall 1998; Ridley 2006). Many different terms are used to specify membrane deformations in relation to their underlying regulatory mechanisms, which however can be simplified by using a classification according to the relative orientation to the cytoplasm (McMahon and Gallop 2005). Deformations are considered as positive, when the plasma membrane and cytoplasm moves outwards, and negative, when the movement is directed inwards.

Actin filaments are the major component of cell cytoskeleton, which are regulated by more than fifty cytosolic proteins and mainly remodeled by external signals transmitted by membrane receptors. Among these fifty cytosolic proteins, which are able to influence the actin cytoskeleton, it is possible to distinguish two main classes: actin-interacting and actin-regulating proteins.

On one hand, actin-interacting proteins (Small, Stradal et al. 2002) which can be classified according to their diverse functions like, actin crosslinking (also termed gelating), bundling, capping, sequestering, severing or even side-binding proteins all are under the control of cellular signaling cascades. They are responsible for the maintenance of the actin filament network.

On the other hand, actin-regulating proteins belong to a superfamily named Ras that is divided into 5 major branches: Ras, Rho, Rab, Ran and Arf. All these guanine nucleotide binding proteins are small GTPases, acting as binary molecular switches, because they exhibit high-affinity binding for GDP and GTP,

and possess at the same time low intrinsic GTP hydrolysis and GDP/GTP exchange activity. Small GTPases are inactive when bound to GDP and become active when exchanging GDP to GTP, a mechanism apparently driven by GDP/GTP local intracellular concentration changes. Like for the other members of the Ras superfamily, the GDP/GTP-bound states are regulated by two other main classes of proteins: guanine exchange factors (GEFs) and GTPase-activating proteins (GAPs). A supplementary class of regulating proteins, the guanine dissociation inhibitors (GDIs), is only involved in the regulation of the Rho family (figure 2.3). The most investigated family is the Rho family, comprising Rho, Rac and Cdc42 which are involved in actin cytoskeleton treadmilling (Hall 1998). Rho activation promotes the assembly of contractile stress fibers, Rac activation induces formation of lamellipodia and membrane ruffles, Cdc42 induces extension of filopodia. The interplay of all these proteins make actin polymerization one of the most complex and precise cell regulation system which remains extremely difficult to understand in its entire complexity.

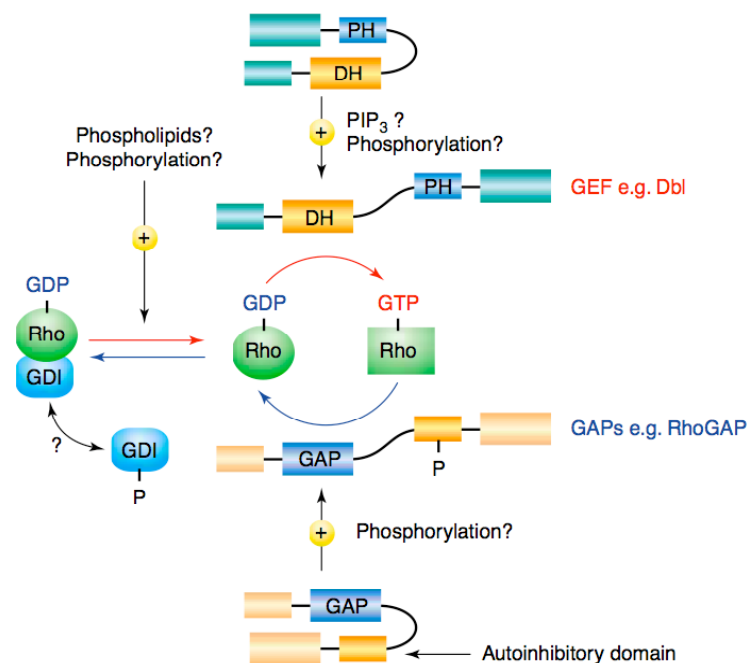


Figure 2.3: Proteins regulating Rho family GTPases. Guanine nucleotide dissociation inhibitors (GDIs), which are not always present, form a complex with Rho GTPases maintaining them in an inactive form. After binding to

phosphatidylinositol (3,4,5)-trisphosphate (PIP3), GDP-GTP exchange factors (GEFs) increase the rate of nucleotide exchange, resulting in Rho protein activation. When activated, GTPase-activating proteins (GAPs) downregulate Rho proteins by activating their intrinsic GTPase activity. Figure taken from Ridley et al. 2001 (Ridley 2001).

2.2 Cell Cytoskeleton and its Role for Native Vesicles Production

Principally, native vesicles can be produced from any eukaryotic cell type. Although not fully elucidated, two forces, the intracellular osmotic pressure and the rearrangement of the actin cytoskeleton apparently drive their formation (Cunningham 1995; Pedersen, Hoffmann et al. 2001). The actin cytoskeleton underneath the cell membrane forms a network that is connected to membrane proteins by scaffolding proteins (Berrier and Yamada 2007). A variety of natural compounds can affect directly the actin cytoskeleton and are able to induce changes to this cytoskeleton-membrane connection and/or are responsible for changes in the molecular pathways regulating the cytoskeletal architecture. For a general understanding of the parameters influencing native vesicle formation, particular interest is given to literature describing the molecular pathways regulating the cytoskeleton architecture, which for instance is important for cell motility (Pantaloni, Le Clainche et al. 2001) contractility, and neurogenesis (Luo 2002), or mechanisms affecting directly positive (outwards) membrane curvature, also known as budding, such as viral particle release (Pornillos, Garrus et al. 2002) or multivesicular body formation (Katzmann, Odorizzi et al. 2002). Chemicals capable of inducing plasma membrane vesicle formation will be also discussed.

Outward movements of the membrane, giving rise to positive membrane curvature, can be observed in different cell types according to their functional implications and are reported (Revenu, Athman et al. 2004) for cell cytokinesis, motility, immunity, axonal and synapse grow, microvilli formation, multivesicular bodies formation, viral budding or apoptosis. As the regulation of such cellular membrane extrusions is not totally elucidated, attention was given to cellular mechanisms capable of inducing membrane remodeling in a similar way to that one observed with cytochalasins, allowing a better understanding of cytochalasin influence on vesicle formation.

2.2.1 Liposomes

Membrane positive curvature was observed in model membranes. For example, physical phase separation between two different lipids is sufficient to induce lipid bilayer curvature (Parthasarathy, Yu et al. 2006) (Lipowsky and Dimova 2003). The modification of lipids by phospholypase A2 can also induce budding and even fission of vesicles (Staneva, Angelova et al. 2004). Most interestingly is the demonstration that cholesterol (Bacia, Schwille et al. 2005), known to promote phase separation and resulting in bilayer domain formation, can also give rise to positive membrane curvature (Binder, Barragan et al. 2003). The main deficiency of such physical approaches to membrane curvature is that the properties of artificial lipid vesicles are quite distant from biological membranes due to their simple lipid composition and especially due to the absence of membrane proteins, and the absence of the cytoskeleton that has been proven to play a major role in cell membrane stabilization. For these reasons, more attention was given to biological regulated mechanisms that allow obtaining initial positive curvature of the membrane.

2.2.2 Cell Motility

One of the best-studied membrane positive curvature occurs during cell motility, which has been investigated in mammalian cells, such as fibroblasts (Kole, Tseng et al. 2005). Cell motility requires that the cell locally extends its membrane surface to create new anchorage points with the extracellular matrix, contracts to move cell body and finally releases its adhesion at the rear of the cytoplasm. External signals sense by membrane proteins (Halloran and Wolman 2006) spatial control of actin polymerization, which is the driving force allowing cell motility. This polymerization gives rise to the formation of an actin filament network that pushes the membrane outwards the cytoplasm, thus creating plasma membrane ruffles, known as lamellipodia or leading edges from where new protrusions expand, known as filopodia (figure 2.1). The family of integrins (van der Flier and Sonnenberg 2001), which are cell-matrix adhesion proteins, present at the tip of filpodia search then for new contacts with the extracellular matrix (Berrier and Yamada 2007), where subsequent clustering give rise to new focal points and membrane partitioning (Gaus, Le Lay et al. 2006).

Main interest was concentrated on the mechanism of lamellipodium formation where actin polymerization (Disanza, Steffen et al. 2005) (Zicha, Dobbie et al. 2003) occurs in a site-directed and signaling-controlled fashion. In response to the activation of plasma membrane receptors, such as GPCRs, growth factor receptors, receptor tyrosine kinases or integrins, the recruitment and activation of phosphoinositide-kinases gives rise to the modification of phosphoinositide lipids (PIs) head-groups (Welch, Coadwell et al. 2003) (Bettache, Baisamy et al. 2003) (Honda, Nogami et al. 1999). This particular family of lipids constitutes only 1% of total membrane lipids but their implications and also cellular signaling are essential for membrane integrity. The

phosphatidylinositol-4,5-bisphosphate (PI(4,5)P₂) is one of the most important lipids, known to play an essential role as a second messenger (Raucher, Stauffer et al. 2000) and is the major component of the plasma membrane responsible for making connections with the cytoskeleton (Sechi and Wehland 2000) (McLaughlin, Wang et al. 2002). The partitioning of such lipids at cell membrane is one of the first consequences and requirements for actin microfilaments segregation and assembly in a controlled fashion (Kwik, Boyle et al. 2003). Different membrane-associated proteins, generally known as GTP exchange factors (GEFs), part of which is the Rho GTAses family (like Rac, Rho or Cdc42), are then recruited to form a signaling complex. Other cytosolic proteins, such as SH3 domain-containing proteins (like Grb2) or profilin, can also be directly recruited by cooperative binding to the receptors or to lipids making part of such signaling complexes. The formation of these complexes targets others scaffolding proteins, like the Wiskott-Aldrich syndrome protein (WASP), which will finally recruit actin filaments (figure 2.4).

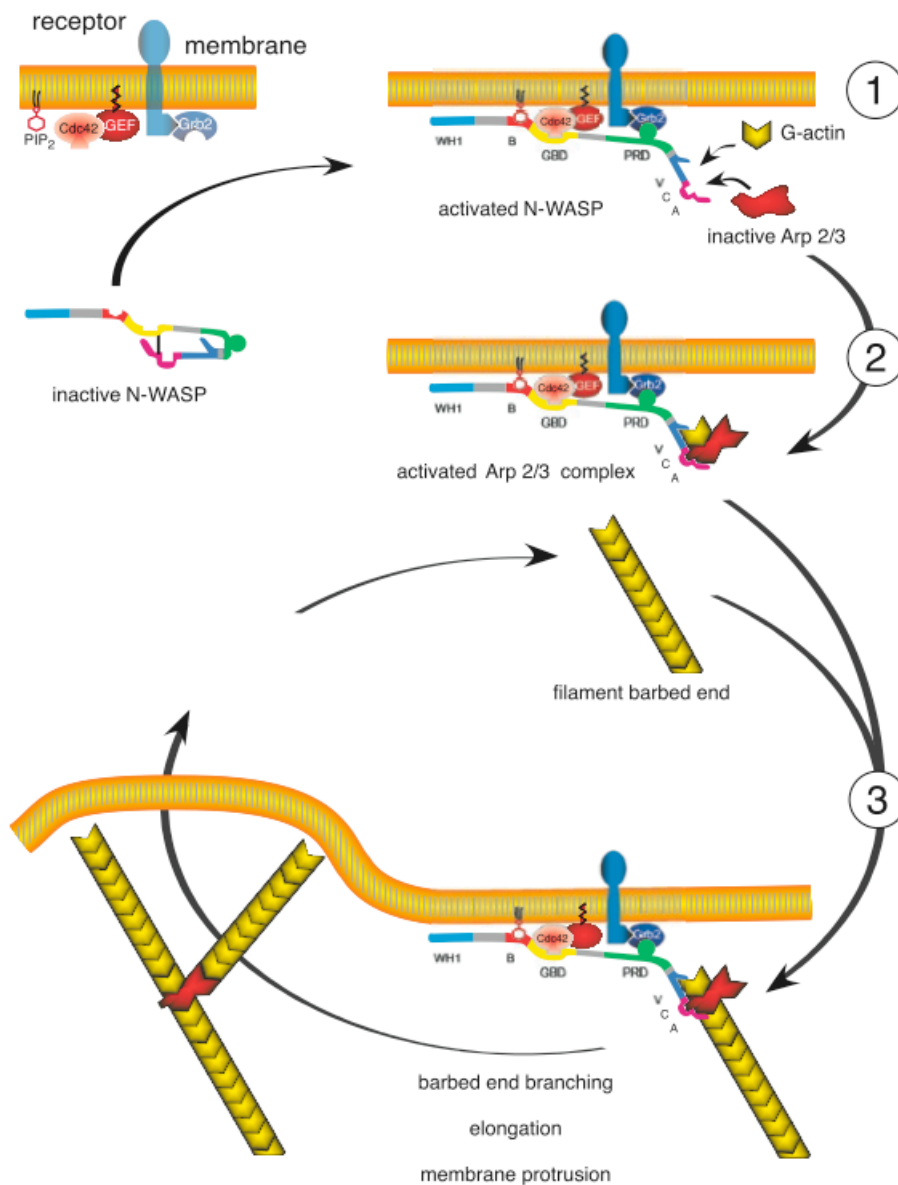


Figure 2.4: Mechanism of WASP protein regulation at the lamellipodium. Activation of WASP leads to its recruitment to the plasma membrane and association with PIP₂ and Grb2 proteins (1). WASP promotes actin filament and Arp2/3 complex formation. Taken from Pantaloni 2001 (Pantaloni, Le Clainche et al. 2001).

WASP is implicated in the recruitment of another main actuator in actin polymerization, the Arp2/3 complex (Higgs and Pollard 2001), which is the cellular factor that generates side branching, also known as Y-branching, of the

actin filaments resulting in an increased number of barbed ends and the subsequent addition of G-actin, driving actin polymerization in a site-directed fashion.

Another similar mechanism, where the actin cytoskeleton plays an essential role and is regulated in a very similar fashion is phagocytosis in immunity (Ridley 2001), where assembly, necessary for enclosing of the phagocytosed particle, and disassembly, occurring after maturation of the phagosome. PI(4,5)P₂ seems to be extremely important in such regulation too.

As already discussed above, the formation of actin bundles and their continuous growth by addition of G-actin subunits induces also the formation of filopodia which in turn 'search' for new cell-matrix contacts with the surface substrate finally resulting in the activation of new integrins and the formation of focal contacts. A parallel regulation mechanism discovered in fibroblasts was the antiporter Na-H exchanger isoform 1 (NHE1). Additionally to its main function, NHE1 was reported to have a supplementary plasma membrane anchorage function (Bernstein and Bamberg 2004) (Denker, Huang et al. 2000) (Pedersen, Hoffmann et al. 2001), by his interaction with the ezrin/radixin/moesin (ERM) actin-binding proteins, and then to be a main actuator for focal adhesion assembly and downstream regulation of the lamellipodium (figure 2.5). Its downregulation was reported to impair integrin and Rho signaling resulting in a loss of directed migration by the formation of multiple pseudopodia in all directions. Other ion transporters (Denker and Barber 2002) were reported to play similar roles as important regulators of actin filament recruitment and are also implicated in cell volume regulation.

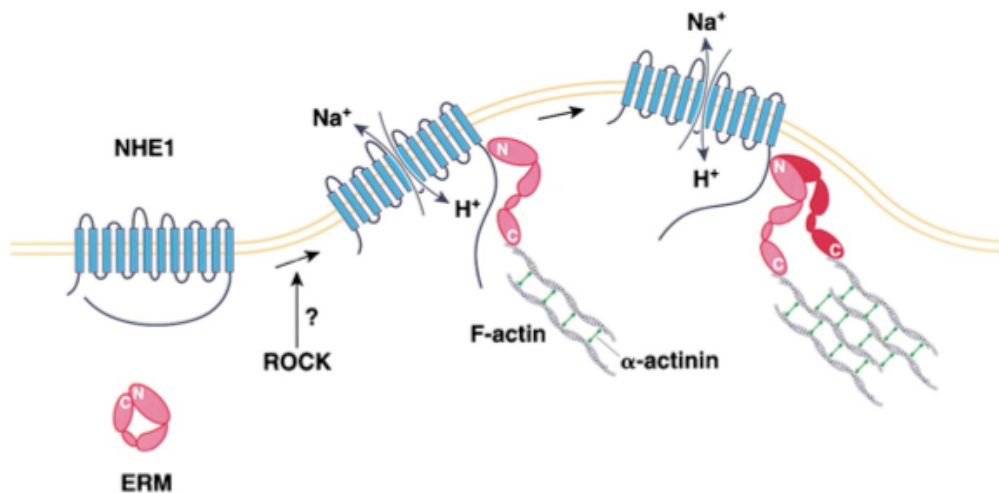


Figure 2.5: Proposed mechanism of regulation for the ion exchanger NHE1 and its interaction to the actin cytoskeleton. Taken from Denker et al. 2000 (Denker, Huang et al. 2000).

2.2.3 Membrane Protein Expression and Downregulation

Another well-studied cellular budding is the formation of intracellular vesicles, which are implicated in the two main cellular trafficking pathways: protein biosynthesis and protein endocytosis. The formation of endocytotic vesicles starts by a negative curvature of the membrane, which is the opposite process as compared to native vesicles formation induced by cytochalasin. It is important to mention the complexity and the regulation of endocytotic vesicle formation, which results from the assembly of membrane interacting proteins that initiate the formation of well defined macrostructures responsible for the pulling of the membrane (figure 2.6). In a final step, multivesicular body (MVB) formation leads to a positive membrane curvature. MVBs are involved in protein degradation and share part of the endocytic machinery with the conventional receptor-recycling pathway, where β -arrestins are implicated.

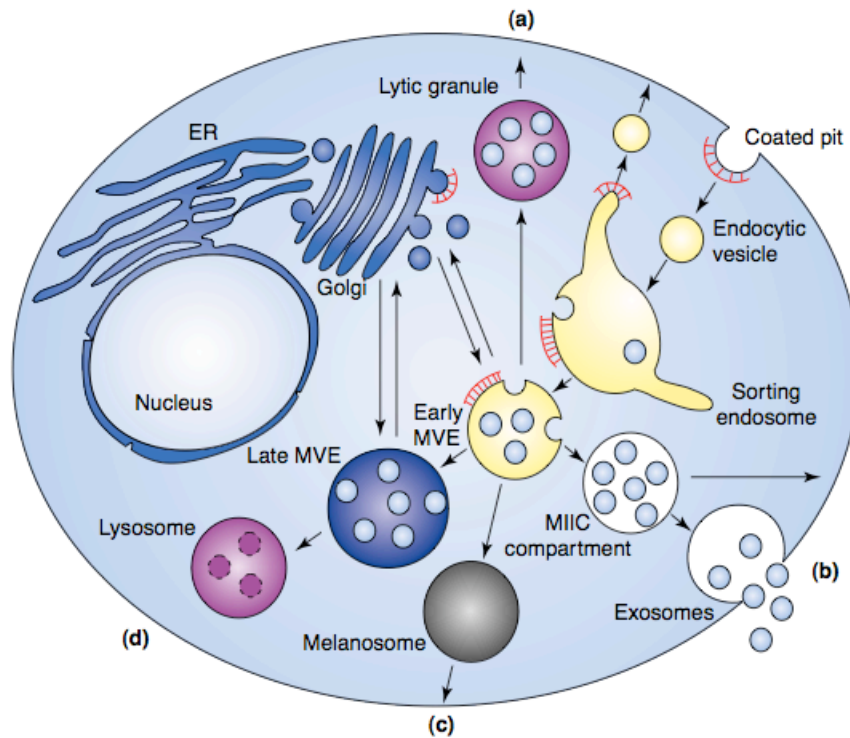


Figure 2.6: Compilation of major routes leading to the formation of intracellular vesicles in different cell lines: (a) lytic granules in T lymphocytes, (b) exosomes from antigen-presenting cells, (c) melanosomes in melanocytes, (d) clathrin-coated vesicles and MVEs present in all cells. Taken from Raiborg et al 2003 (Raiborg, Rusten et al. 2003).

Briefly, membrane protein and secretory protein biosynthesis requires trafficking of vesicles between the endoplasmic reticulum and the Golgi apparatus, which is essential for post-translational modifications. The main actuators in such vesicle formation are the family of COP proteins, but more recently the importance of lipid partitioning was also pointed out, bringing increasing interest to the particular class of inositol lipids (Caroni 2001; Bennett, Onnebo et al. 2006). From the Golgi apparatus, proteins are addressed to their final destination also via COP-coated vesicles with the only exception of lysosomal proteins, which are addressed through clathrin-coated vesicles. The driving force for the formation of all these vesicles is energy dependent.

In general endocytosis is induced by external signals and is processed by clathrin-coated vesicles, playing a major role in receptor desensitization and recycling. After receptor activation by its ligand, G protein-coupled receptor kinases (GRKs) are recruited to phosphorylate the receptor, which then interacts with β -arrestins (Lefkowitz 1998). β -arrestins are scaffolding proteins driving the assembly of a macrostructure complex implying adaptator proteins (APs), which in turn recruit clathrin triskelions. Their subsequent assembly drives the pulling of plasma membrane and leads the formation of clathrin-coated vesicles. These endocytic vesicles are addressed and fuse with early endosomes, which play an important role in the sorting of proteins, addressing them back to the plasma membrane or to degradation. From these early endosomes, most receptors recycle back to the plasma membrane, apparently if they are non-ubiquitinated (Hicke 2001).

Ubiquitin was reported to be the main signaling molecule addressing proteins to MVBs (Hicke 2001) and can occur at different steps along the endocytic pathway. Membrane receptors, which have been ubiquitinated at the plasma membrane by cellular ubiquitin ligases, such as Nedd4 or Cbl, are directly addressed to the degradation pathway. Non-ubiquitinated proteins, by association with cargo proteins, such as Epsin or Eps15, themselves ubiquitinated, can also enter the degradation pathway at the plasma membrane or in early endosomes. Another MVBs sorting protein able to target non-ubiquitinated δ -opioid receptors to MVBs was recently discovered, and is so called GASP protein (G-protein-coupled receptor-associated sorting protein) (Heydorn, Sondergaard et al. 2004). These findings seem to demonstrate that cargo proteins play also an essential role for addressing proteins to specific intracellular pathways.

When proteins are addressed for degradation, by these molecular signals, a cellular mechanism gives rise to a positive membrane curvature and multivesicular body formation, also known as late endosomes. Although these mechanisms are not completely understood on a molecular level, important findings were obtained in yeast (*S.cerevisiae*), where MVBs sorting was elucidated; from similarities in coding sequence alignments, potential candidates were also found in the human genome (Katzmann, Odorizzi et al. 2002) (Babst, Katzmann et al. 2002) (Piper and Luzio 2001). In early endosomes, microdomains are formed through the activation of a class III PI3-kinase that phosphorylates PI head-group to PI-(3)P (Raiborg, Rusten et al. 2003). Hrs protein recognizes PI-(3)P by its FYVE-domain and by a particular motif sequence of residues, P(S/T)AP, recruits Tsg101 (tumor susceptibility gene 101). Tsg101 is part of a multi-protein complex called ESCRT I, that finally engages others multi-protein complexes also known as ESCRT II and III directly implicated in the assembly of MVBs (figure 2.7).

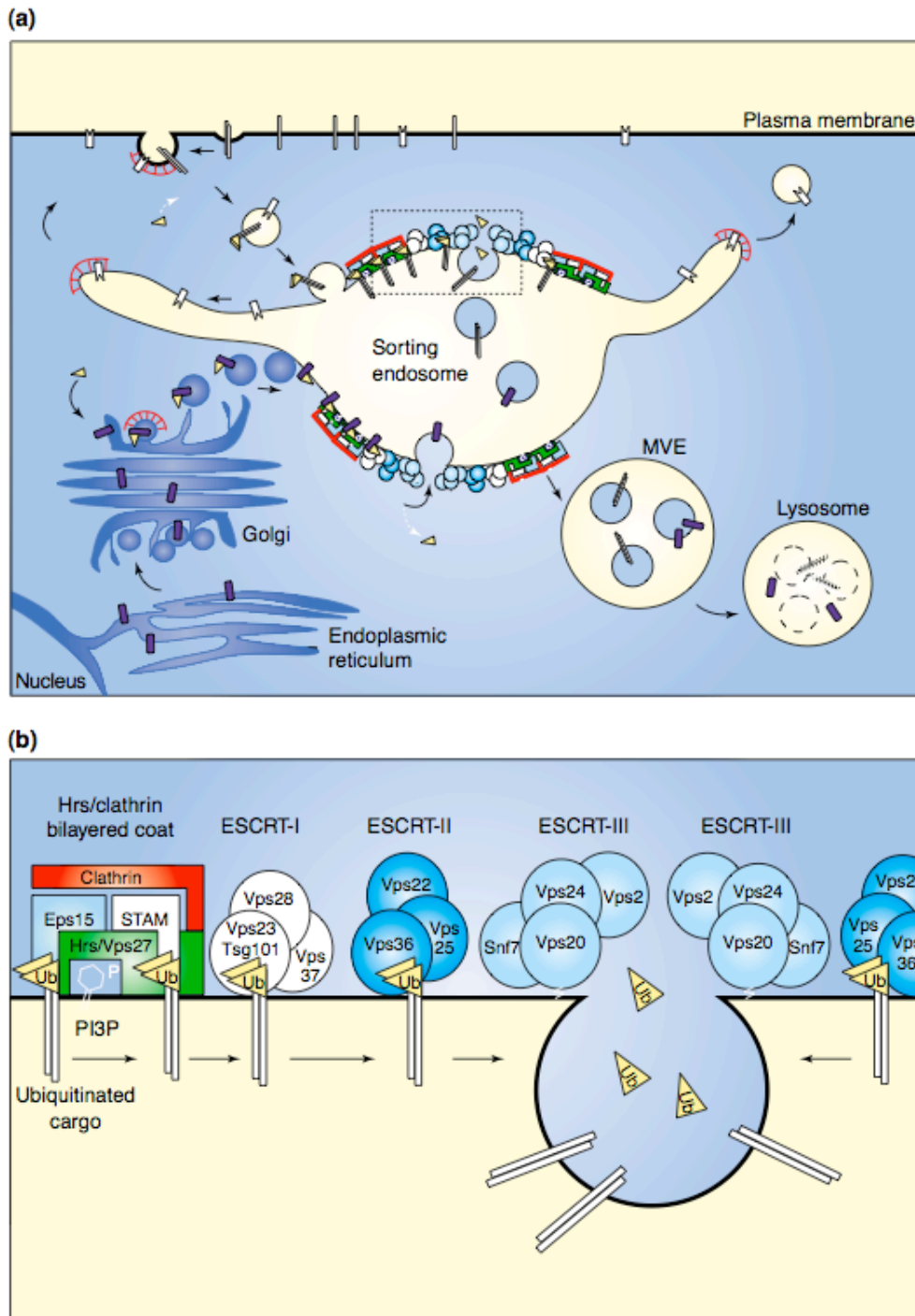


Figure 2.7: Internalization pathways implicated in receptor recycling. (a) Internalization of membrane proteins via clathrin-coated pits and early endosomes. (b) Sorting of ubiquitinated proteins to late endosomes, the formation of which leads to positive membrane curvature. Taken from Raiborg et al 2003 (Raiborg, Rusten et al. 2003).

The presence of another unconventional lipid, the lyso-bisphosphatidic acid (LBPA), is only detectable in cytoplasmic vesicles. Due to its unusual structure, giving it a cone shape, it is only inefficiently degraded by lipases, which makes it a suitable candidate for mediating inward membrane curvature, giving then rise to a positive curvature (figure 2.8). Other results demonstrate the enrichment of tetraspanins and GPI-anchored proteins in intracellular vesicles, which are usually, associated with cholesterol and sphingolipids domains. All these observations seem to demonstrate a particular partitioning of lipids to specific microdomains in such vesicles, which might also influence protein segregation.

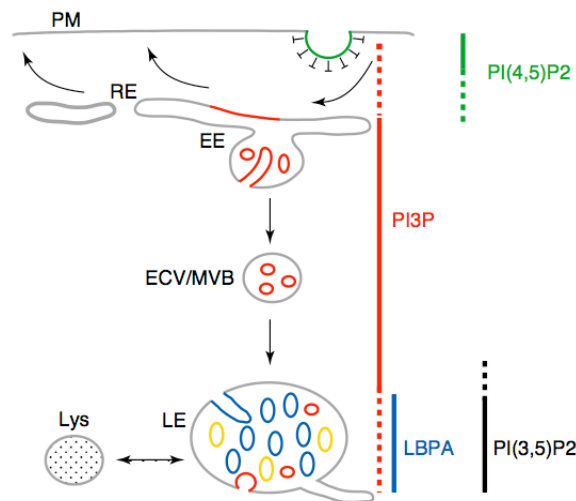


Figure 2.8: Lipid partitioning in intracellular compartments. Taken from Gruenberg et al 2003 (Gruenberg and LBPA 2003).

Also quite interesting is the mimicry strategy used by certain classes of viruses that reproduce the sequence motif, P(S/T)AP, in a protein encoded by their genome (Garrus, von Schwedler et al. 2001) (Amara and Littman 2003). This protein, named Gag, hijacks the MVBs machinery (Pornillos, Garrus et al. 2002), targets it to the cellular membrane and uses it to produce new viral particles by outward budding of the plasma membrane (figure 2.9). It is important

to mention that in macrophages viral particles are also accumulating in MVBs (Pornillos, Higginson et al. 2003).

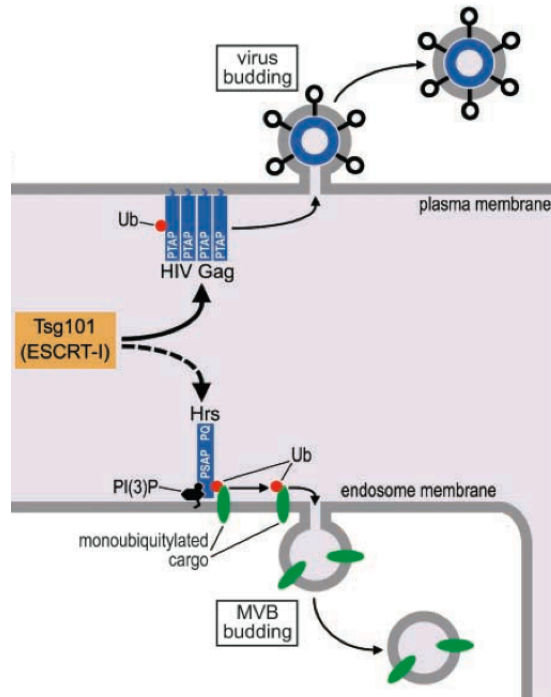


Figure 2.9: Molecular mechanism of viral budding. Taken from Pornillos et al 2003 (Pornillos, Higginson et al. 2003).

2.2.4 Synaptogenesis

Another cellular mechanism giving rise to positive membrane curvature can be found in synaptogenesis (Luo 2002). As previously described for the WASP protein, activation of Rho GTPases is essential for inducing synapse formation. In this case a G protein-coupled receptor kinase-interacting protein (GIT1) (Zhang, Webb et al. 2003) was reported to be essential as a scaffolding protein leading to the assembly of multiprotein signaling complexes, comprising actin regulators such as PIX, a Rac GEF, and PAK, a Rac effector, finally implicated in cytoskeleton remodeling (figure 2.10). GIT1 protein was also reported to be implicated in the regulation of fibroblast motility and their protrusive activity.

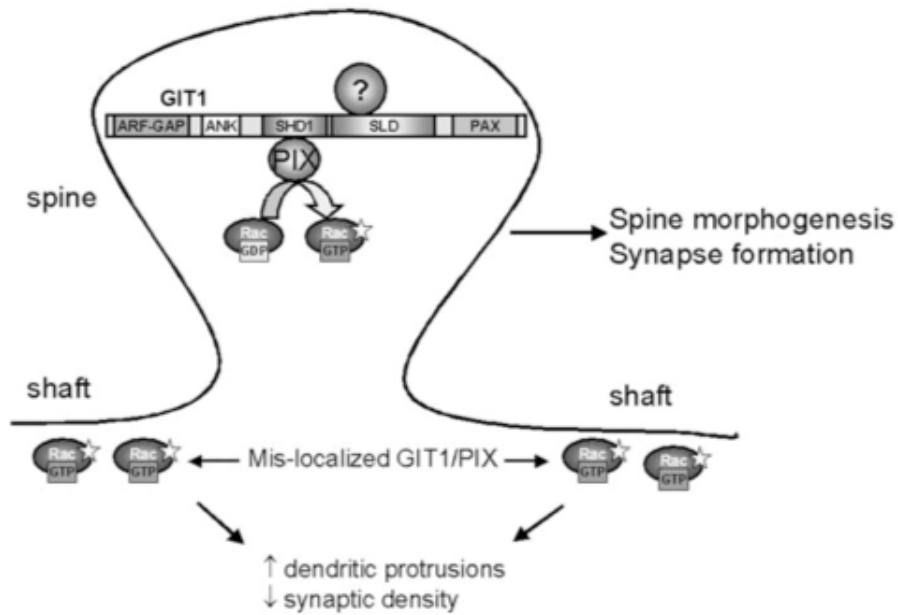


Figure 2.10: Mechanism of GIT1 regulation and its role in synapse formation. Taken from Zhang et al 2003 (Zhang, Webb et al. 2003).

2.2.5 Other Mechanisms of Vesicle Formation

Another biological mechanism was reported to result in positive membrane curvature, the exocytosis of lytic granules (ectosomes) in T lymphocytes (Pilzer, Gasser et al. 2005). Similarly exosomes are produced like MVBs, which results in the vesiculation of a membrane organelle into its proper lumen (figure 2.11). The final fusion event of the cellular vesicle with the plasma membrane leads to the release of exosomes.

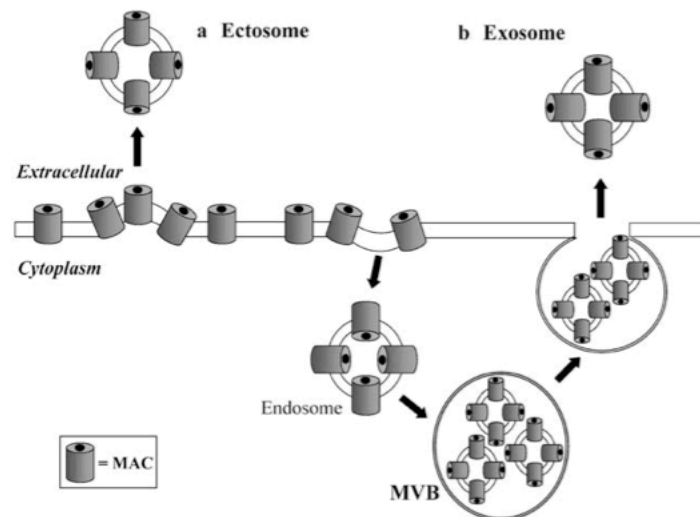


Figure 2.11: Formation of ectosomes and exosomes by membrane attack complex (MAC). Taken from Pilzer et al. 2005 (Pilzer, Gasser et al. 2005).

Hagmann et al. reported that neuroblastoma cells undergo a transient blebbing when exposed to lysophosphatidic acid (LPA) (Hagmann, Burger et al. 1999). Cells bleb due to a general cell body contraction and can be inhibited by different chemicals such as staurosporine, KT 5926 (an inhibitor of myosin light chain kinase), and cytochalasin B. They suggested that this effect is myosin light chain dependent. They also showed the potent effect of calyculin, an inhibitor of protein phosphatase 2A, sustaining prolonged cell blebbing.

Baba et al. reported a spherical membrane extrusion in okadaic acid-treated K562 cells induced by crosslinking of membrane microdomains (Baba, Udaka et al. 2003). Cell treatment with okadaic acid, another protein phosphatase inhibitor, induces clustering of surface bound F-actin. The authors were able to increase this effect by a subsequent external cell membrane crosslinking using a biotinylated-polyethylene glycol derivative of cholesterol (bPEG-Chol) and subsequent streptavidin binding. The accumulation of clusters finally results in the formation of a spherical cell extrusion. The same kind of extrusion could also

be induced by direct crosslinking of a raft marker, CD59, which was inhibited when the gene encoding for a raft-associated non-receptor tyrosine kinase, Fyn, was knocked out in murine T-cells. These findings demonstrate the importance of the actin cytoskeleton in the production of cell surface extrusions and offer novel strategies to enrich such extrusions in cholesterol microdomains by manipulating cholesterol-associated proteins.

Other interesting acting-related effects on cell extrusions were described by Cunningham (Cunningham 1995), who demonstrated that M2 melanoma cell lines lacking the actin-binding protein ABP-280 undergo a persistent blebbing during the initial stages of spreading after plating.

Finally apoptosis in which a programmed sequence of events leads to the breakdown of the cytoskeleton resulting in cell death has to be mentioned as a process producing cell extrusions. Apoptotic stimuli activate caspases which leads to ROCK-1 activation resulting in phosphorylation of myosin light chains, increased contractility and finally cell blebbing.

2.3 Results and Discussion

In our lab, Pick et al. (Pick, Schmid et al. 2005) focused to a special effect induced by cytochalasins. Certain compounds, mainly cytochalasin B, a metabolite extracted from *Helminthosporium dematioideum*, or cytochalasin D, a metabolite extracted from *Metarrhizium anisopliae*, applied on cultured mammalian cells at defined concentration ranges, induce cytoskeletal remodelling giving rise to a transient outwards membrane expansion, known as membrane blebbing, blistering or even budding. When the cell membrane pinches off,

leading to the enclosure of the bleb, the formed vesicle can be separated from the cell body and is thus called native vesicle.

2.4 Cytochalasin Effect on Cell Cytoskeleton

When HEK cells are subjected to a cytochalasin B at 25 a concentration of 25 $\mu\text{g}/\text{ml}$, transient blebbing was observed (figure 2.12) leading to the formation of large membrane extravasations, or blebs. Those blebs enclose parts of the cytoplasm and bud off as native vesicles, which can be regarded as independent entities derived from a living cell. In the presented experiment HEK cells express the EGFP-Neurokinin 1 receptor (EGFP-NK₁R) and a cytosolic protein, DsRed2.

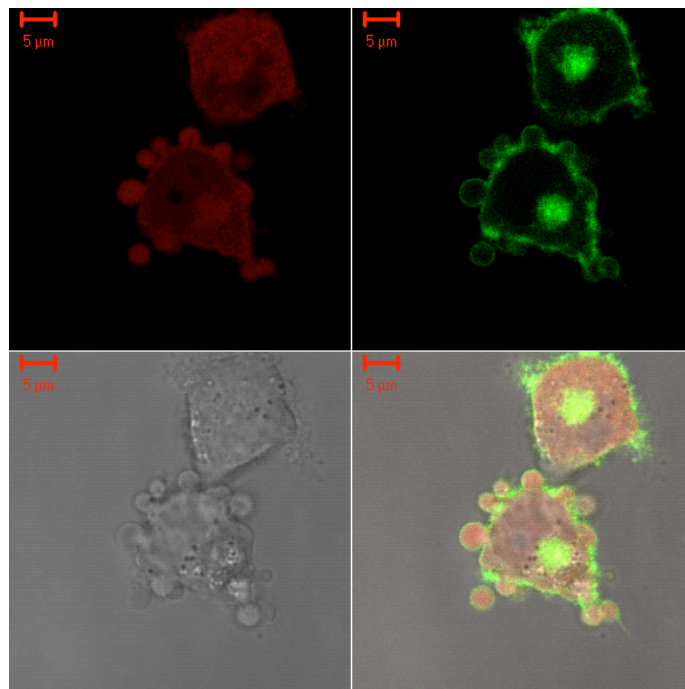


Figure 2.12: HEK cell expressing membrane EGFP-NK₁R (green) and the cytosolic protein DsRed2 (red) after cytochalasin B treatment (25 $\mu\text{g}/\text{ml}$ in PBS). After formation of blebs, some enclose and form native vesicles.

When cells were exposed to cytochalasin B, two main effects could be observed: (i) cell body contraction and (ii) plasma membrane blebbing. The severing (Urbanik and Ware 1989) and capping (Flanagan and Lin 1980) effects of cytochalasin on the actin filaments can explain both. When cytochalasin traverses the cell membrane, it encounters the actin cortical network. The first actin structures encountered are probably the actin filaments located at the focal contact points, which are involved in maintaining the cell contact to the substrate surface. If this interaction is perturbed the disassembly of the focal contact points leads to the release of the tension maintained on cell membrane, resulting in cell detachment and cell body contraction (figure 2.13). Cell body contraction does not necessarily involve cell blebbing. Experiments demonstrated that cells can contract without blebbing, or vice versa they can bleb without apparent contraction. Several mechanisms seem to interplay to induce cell membrane blebbing. Probably cell blebbing requires attenuation of the interaction between the plasma membrane and the actin cytoskeleton. Other reports indicate that release of parts of the cell membrane from the cytoskeleton also affects internal cell pressure (Pedersen, Hoffmann et al. 2001) (Mills, Falsig Pedersen et al. 2000) and the activation of myosin light chains (Hagmann, Burger et al. 1999).

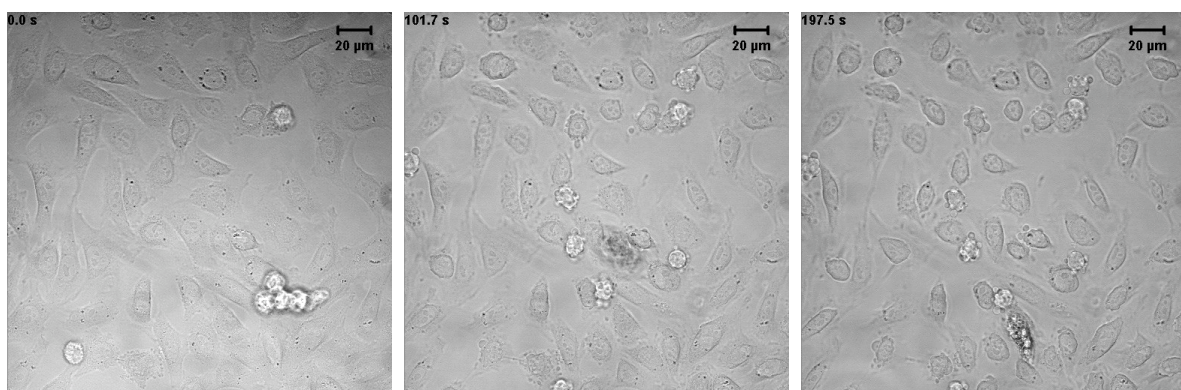


Figure 2.13: Micrographs of cell body contraction in CHO cells induced by cytochalasin B treatment at 25 µg/ml can also be observed.

2.5 Optimization Parameters for Native Vesicle Production

The optimization of parameters influencing native vesicle production has been already investigated during my master thesis. The influence of cytochalasin B concentration, the appropriate medium for production, the influence of temperature or the agitation strength have been investigated. The best results were obtained using physiological PBS buffer without calcium, and a cytochalasin B concentration of 25 $\mu\text{g}/\text{ml}$ (52 μM), with prewarmed solutions at 37°C, under vigorous agitation (800 rpm/min). Such conditions allow the production of many vesicles from a single cell (figure 2.14). However, the quantity of vesicles produced was extremely variable from day to day, suggesting that some others parameters were not totally under control.

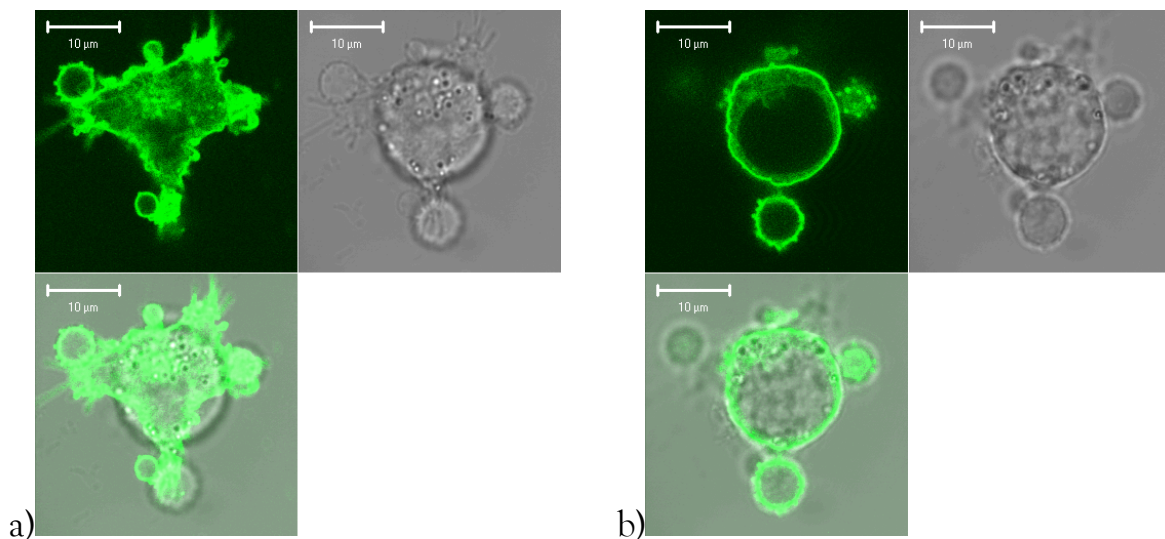
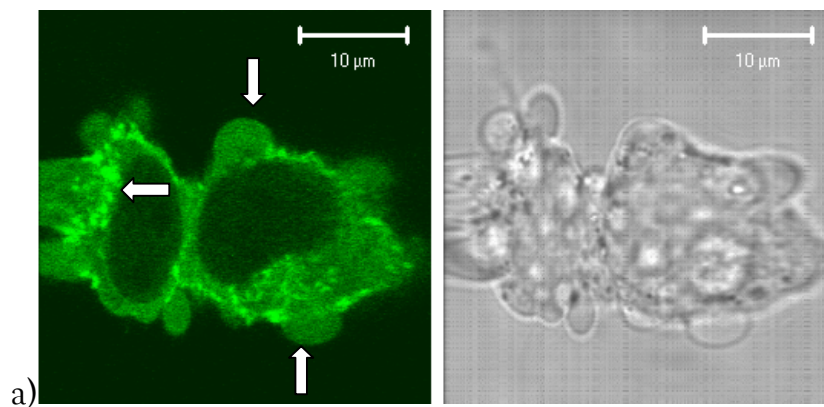


Figure 2.14: Fluorescence confocal micrographs of a HEK293 cell expressing EGFP-NK₁R after cytochalasin B treatment (25 $\mu\text{g}/\text{ml}$). After the formation of blebs, some of them bud off and form native vesicles. On the membrane surface of bigger vesicles some smaller one's can also be observed, whose size is lower than 1 μm in diameter. Two different planes of the same cell are shown: (a) is at proximity of glass surface and (b) in the middle of cell body.

2.5.1 Influence of Growth Medium on native vesicle production

The influence of the growth medium in which cells were maintained represents an interesting parameter to be addressed. The percentage of serum supplemented to the standard Dulbecco's Modified Eagle's Medium (DMEM) commonly used for HEK293 cell cultivation, influences directly the speed of cell growth. As native vesicle production is directly related to cytoskeletal changes, it was interesting to test the influence of the serum content in the cell medium.

Experimental evidence tends to demonstrate that cells don't bleb in the same way when kept in culture condition with high or low serum concentrations. At 10% FCS (fetal calf serum), cells show a slightly reduced blebbing efficiency and the shape of the vesicles produced seems smaller and spherical. When cells were maintained in the absence of FCS prior to experiments, cells bleb easier. The size of blebs are bigger and their shape is more variable and it would be more appropriate to call them blisters. The neck of blisters is more extended, the actin cytoskeleton seems also to be more fragmented (figure 2.15), which probably could lead to a lower probability to bud off and separate from the mother cell, impairing the efficiency of native vesicle production.



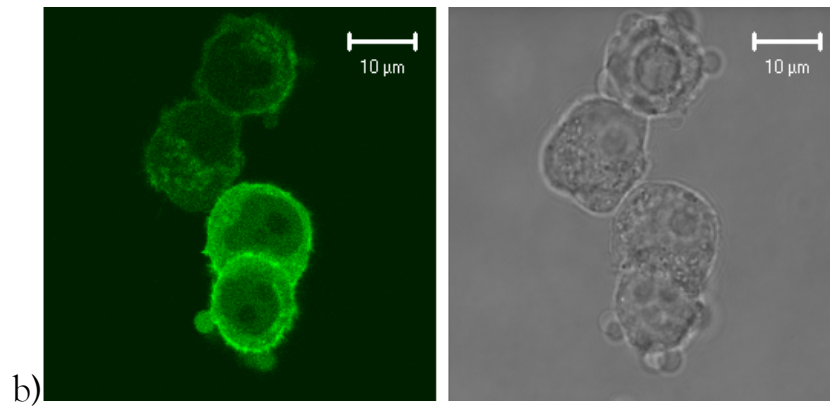


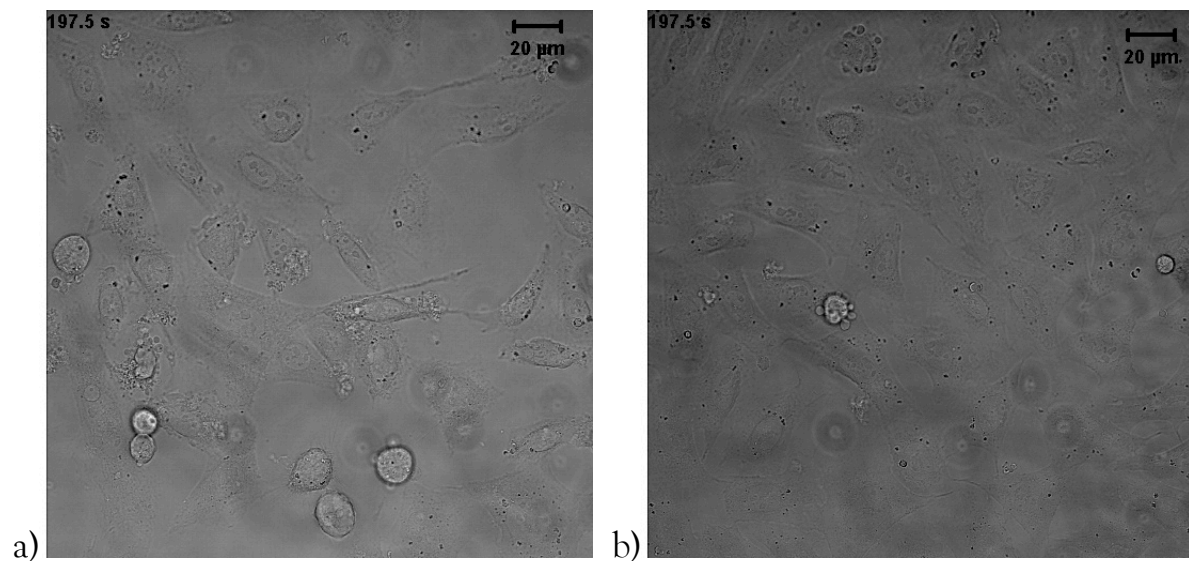
Figure 2.15: Confocal fluorescence micrographs of HEK293 cells labeled with actin-EGFP after cytochalasin B treatment (25µg/ml). Upper panel (a) shows cell blebbing when cells were maintained in 0% FCS and lower panel (b) when they are in 10% FCS. Magnification is slightly different between both panels. Arrows indicate blisters, which probably are not able to close and form vesicles due to a larger neck, and will probably return back.

2.5.2 Influence of Cell Cycle on Native Vesicle Production

One of the most intriguing observations is that not all cells of the same batch bleb simultaneously when exposed to cytochalasin B treatment. The fact that the percentage of cells blebbing upon cytochalasin treatment can drastically vary from a few to 100%, indicates that the cell should be in an appropriated state of cell cycle to produce such membrane extrusion.

Cell synchronization was therefore investigated following the eukaryotic “baby machine” approach (Cooper 2002), which consists in collecting freshly ‘newborn’ cells from a population of mitotic adherent mother cells. This technique was slightly modified avoiding the use of any filtration and can be accomplished in a common growing flask, when working with strong adherent cells or by the use of surface treatment impairing mother cell detachment. When

an adherent cell population is dividing, the newborn cells have a tendency to detach from the solid support and remain in suspension for a short period of time (30 minutes to 1 hour) before attaching again to the support. Under these conditions, it is possible to collect the newborn cells without displacing the population of mother cells by careful replacement of the medium. This approach works perfectly with strong adherent cells, like CHO, which avoids the collection of mother cells and permits to obtain an almost synchronized population for cell cycle investigation. Following such an approach, cell blebbing efficiency appears to dependent on cell cycle (figure 2.16). This was investigated with three types of cells: HEK, CHO and HeLa, and similar results were obtained with nocodazole treatment, which is often used to synchronize cell populations (Didichenko, Fragoso et al. 2003) .



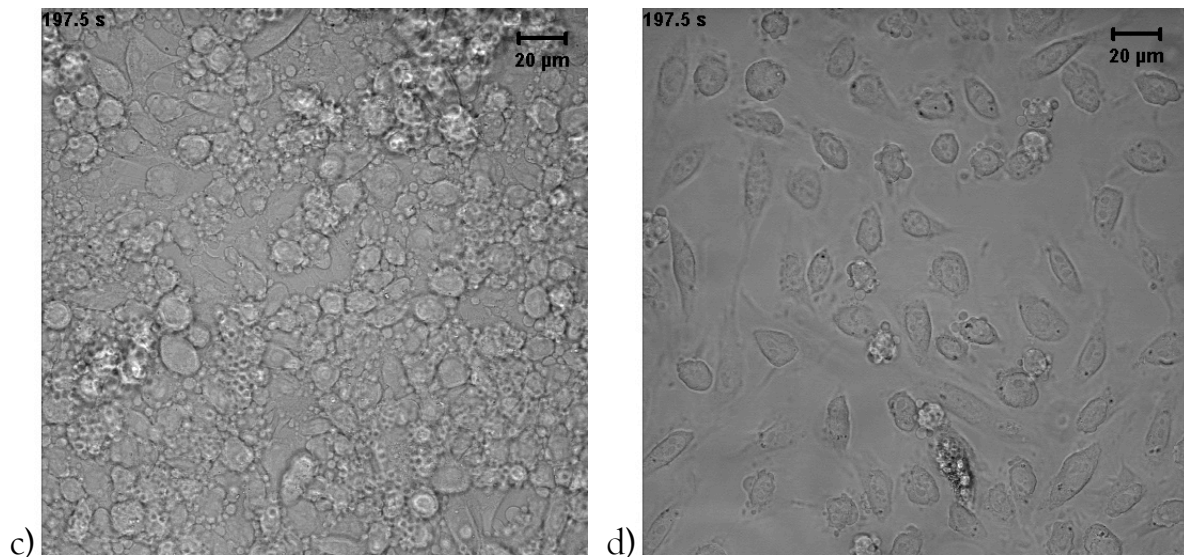


Figure 2.16: Confocal micrographs showing the cell cycle dependency of blebbing on CHO cells. Cells are collected at intervals of 1h and plated on fibronectin-coated cover slides for improved and faster cell attachment and are grown under blebbing culture conditions (DMEM + 2.2% FCS). Cytochalasin B is then applied and blebbing efficiency is followed over time by microscopy. Only few cells have a tendency to bleb after plating at 4h (a) and 15h (b). Around 16h after plating (c) drastic increase of blebbing is observed. At 21h after plating (d) cell blebbing is only observable in a few cells again.

2.5.3 Production by Small Hairpin RNA (shRNA)

As already mentioned above, cells without filamin (also known as ABP280) have a tendency to bleb for prolonged periods after plating (Cunningham 1995). Another publication (Yamaji, Suzuki et al. 2004) demonstrates that the down-regulation of affixin (also known as β -parvin) in fibroblasts induces a persistent cell blebbing, apparently without perturbing cell survival. Affixin is an additional protein forming a complex with membrane integrins, which connects the actin cytoskeleton to cell plasma membranes. With the final goal to produce native

vesicles without using any chemical treatment, an RNA interference technology based on small hairpin RNAs (shRNA) was chosen for gene silencing.

In order to obtain reproducible results and apply them for native vesicles production, shRNA against affixin were designed according to already discovered sequences or by BLAST sequence alignments. Following the protocol of Knockout™ RNAi Systems from Clontech, four constructions matching different sequence regions were produced, two of them for each protein. Co-transfection with cytosolic GFP allows visualizing positively transfected cells, subsequent imaging and 3D reconstruction (figure 2.17).

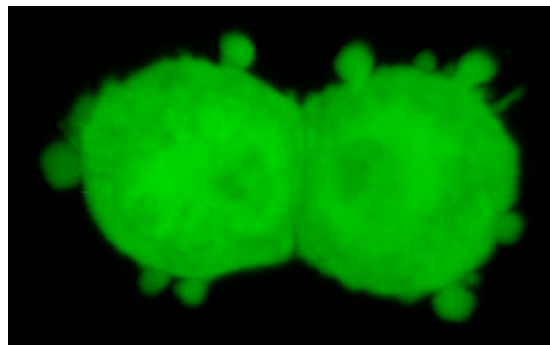


Figure 2.17: HEK293 cells transfected with shRNA against affixin. GFP cotransfection allows clear visualization of vesicle formation on the cell surface.

According to cell morphology, constructs against affixin gave the best blebbing efficiency. The blebbing is persistent over days and native vesicles can be produced from these cells. Affixin downregulation should have been demonstrated by Western Blot analysis, but unfortunately due to the commercially unavailability of the corresponding antibody and regarding the costs of generating a new one, this was not achieved. Northern Blot analysis could also provide a quantification of affixin mRNA, but was not achieved. After maintenance under selection culture conditions (puromycin against cell not

inserting de shRNA), resistant cell clones were obtained, demonstrating the stable transfection with this construct. Cells that contain also the GFP were then easily visualized. By comparison, cells transfected with only the GFP construct are efficiently selected and die after two days under these conditions. The percentage of blebbing cells does not reach 100% and despite maintenance under selection growth conditions, after two weeks in culture, cells show a significant decrease in blebbing efficiency, phenomenon that can be attributed to the silencing of the expression of siRNA. This fact is difficult to overcome and hinders to create stable cell lines.

On the other hand, isolation of single clones using flow fluorescence activated cell sorting (FACS) has not been done due to the probably inappropriate discrimination of fluorescence signals from scattering. Other approaches, presented in the next chapter, such as negative dielectrophoresis or sorting in optical multi-tweezers could be more appropriate to reach such achievement, due to the possibility of combining imaging with sorting.

2.6 Purification

The first approach used for purification involves two differential centrifugation steps, one for pelleting cells and the second to concentrate native vesicles. Unfortunately this approach was not efficient enough with regard to the fact that some cells remain in the vesicle pellet and 100% purity was thus not achieved. To avoid the presence of undesirable cell bodies after vesicle purification a more efficient method had to be achieved. Optimization of purification was then investigated with different techniques.

2.6.1 Centrifugation and Filtration

The obvious alternative was to use filtration using filters with different pore sizes. This approach clearly proves a better efficiency in comparison to simple centrifugation steps and filter pore sizes ranging from 0.8 μm to 10 μm were tested. With filter pore sizes ranging from 0.8 μm to 3 μm 100% pure native vesicle preparations were achieved enabling also the selection of adequate native vesicles size. When the filter pore size was low, the overall quantity of native vesicles decreased. With filters of higher pore sizes (above 5 μm), purity was not anymore fully achieved and cells bodies were again present in resuspended native vesicle pellets. A centrifugation round remains necessary at the end for pelleting native vesicles, get rid of cytochalasin and resuspension in appropriated medium for subsequent experiments. Different efficiencies were obtained according to filter composition due to unspecific absorption of vesicles and the use of polycarbonate filters proved to give the highest vesicle concentrations and no apparent vesicle damage has been observed.

Others filtration methods were also investigated such size exclusion chromatography with no convincing results probably due to very high absorption of native vesicles with the column. Dialysis cassettes were also tested and despite good efficiency remain inappropriate due to the very high dilution of the sample.

2.6.2 Ultracentrifugation on Continuous Percoll[®] Density Gradient

Promising results were obtained by ultracentrifugation in Percoll gradient. In comparison to sucrose density gradient centrifugation with discrete layers of

different sucrose concentrations, the use of Percoll is an interesting approach due to its ability to create a continuous gradient. In this continuous gradient, native vesicles could set to their real density and are not constrained to remain between to phases as observed using sucrose gradient centrifugation. This allows a better discrimination of native vesicles density and a much more precise separation. Surprisingly this approach shows the instauration of several discrete populations appearing around the density of 1.02 (figure 2.18). These populations can probably be related to native vesicle size, more than vesicle composition or protein content. Unfortunately this approach, which seems the most appropriated for large-scale purification shows some disadvantages such as the difficulty of collecting independent fractions or final removal of Percoll, which requires a final step of very high centrifugation speed to pellet the Percoll that can be damageable for native vesicles. This experiments point on the possibility to use such approach as preparative method to identify and isolate a special population of native vesicles sizes more appropriated for further analysis or in the collection of special native vesicle content as it can be coupled to a direct fluorescence detection.

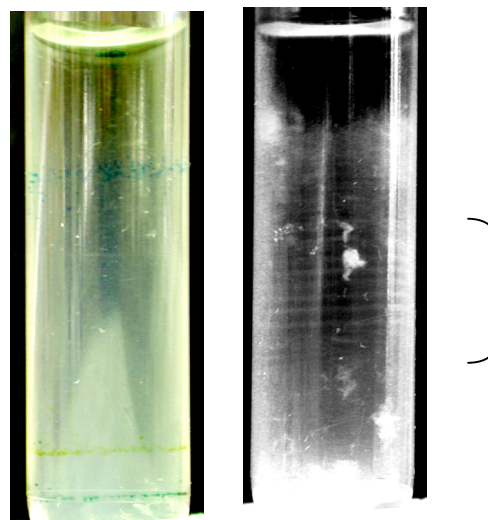


Figure 2.18: Ultracentrifugation in 20% Percoll gradient of calibration beads (left panel) and the appearance of discrete native vesicles populations (right panel).

Beads density: blue (1.018), yellow (1.033), green (1.049). Some membrane aggregates can also be observed.

2.7 Native Vesicles Characterization

Native vesicles are composed of the plasma membrane and enclose part of the cytoplasm of their mother cell, without the nucleus. By their mode of production it is possible to transfer recombinantly expressed membrane receptors and cytoplasmic proteins into native vesicles, which are much smaller than whole cells. The presence of specific cytoplasmic organelles in native vesicles, such as the endoplasmic reticulum, opens the possibility of recording Ca^{2+} signaling responses mediated by membrane receptor activation. This aspect was here investigated in more detail. Others (Cunningham 1995) (Hagmann, Burger et al. 1999) (Keller, Rentsch et al. 2002) (Charras, Hu et al. 2006) (Charras, Coughlin et al. 2008) also investigate blebbing and the partitioning of some proteins at their membrane. The characterization of the membrane receptors characterization in native vesicles will be discussed in the following chapter.

2.7.1 Native Vesicle Size Distribution

Native vesicles can adapt variable shapes and exhibit a broad range of sizes. Native vesicles are not always perfectly spherical (figure 2.19), probably due to cytoskeletal rearrangements of newly formed filaments or by lipid partitioning. Sometimes the formation of additional vesicles on the surface of an already formed one occurs in cluster that cannot always be separated.

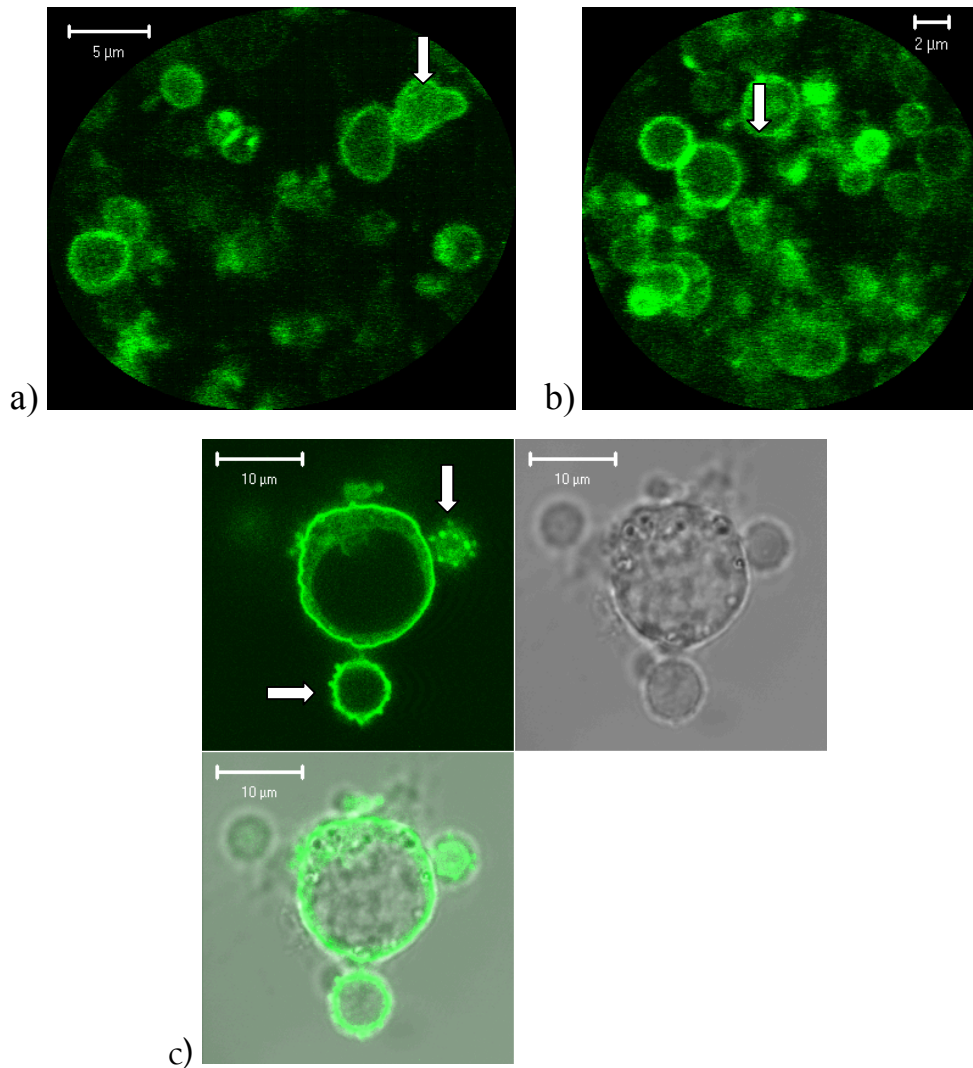


Figure 2.19: Confocal micrographs of native vesicles (a - b) produced from HEK cells (c) expressing EGFP-NK₁R. (a) Vesicles of non-spherical shapes, (b) native vesicle with smaller vesicles on top, (c) native vesicles before release from cells with a multitude of smaller vesicles on their surface, which can be observed separately after purification and immobilization on surface.

As explained before, native vesicles produced from living cells exhibit a quite heterogenous size distribution (figure 2.20), which ranges from hundreds of nanometers to a few micrometers in diameter (figure 2.21). Vesicles of size slightly bigger than the cutoff of the filter are found probably because they are able to deform under the constraints during filtration by the imposed pressure. Vesicles smaller than 500 nm can exist but are removed by filtration.

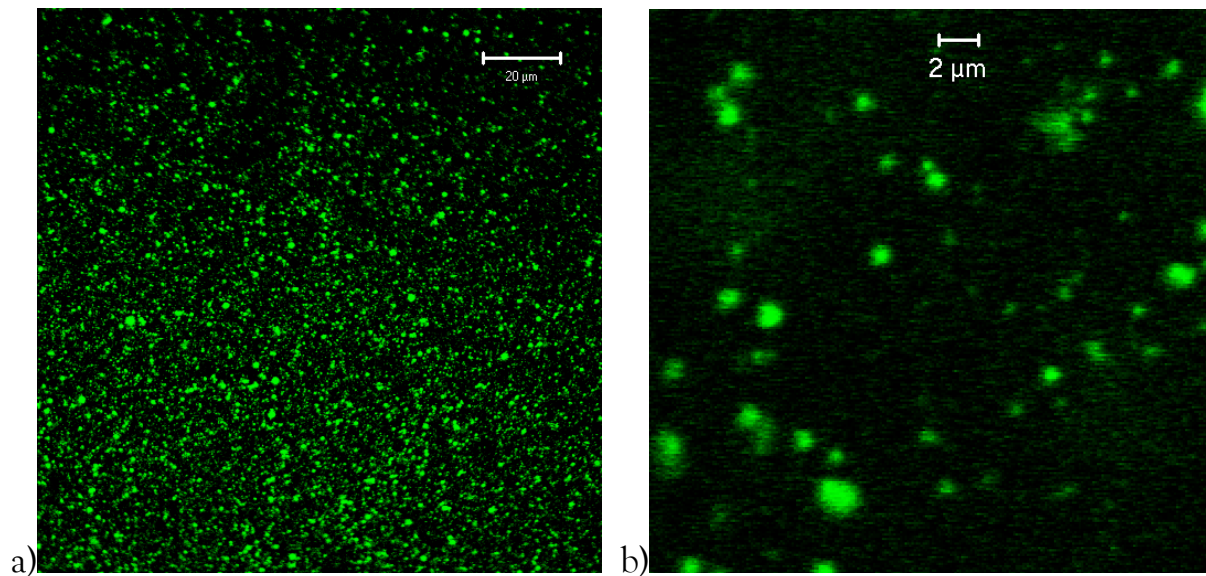


Figure 2.20: Confocal micrographs of native vesicles produced from a stable HEK cell line expressing EGFP-5HT3-R, separated by filtration through a 3 μm pore size filter. (a) shows a native vesicle population after immobilization on a poly-lysine coated glass surface. (b) is a magnification where vesicles smaller than 1 μm can be observed.

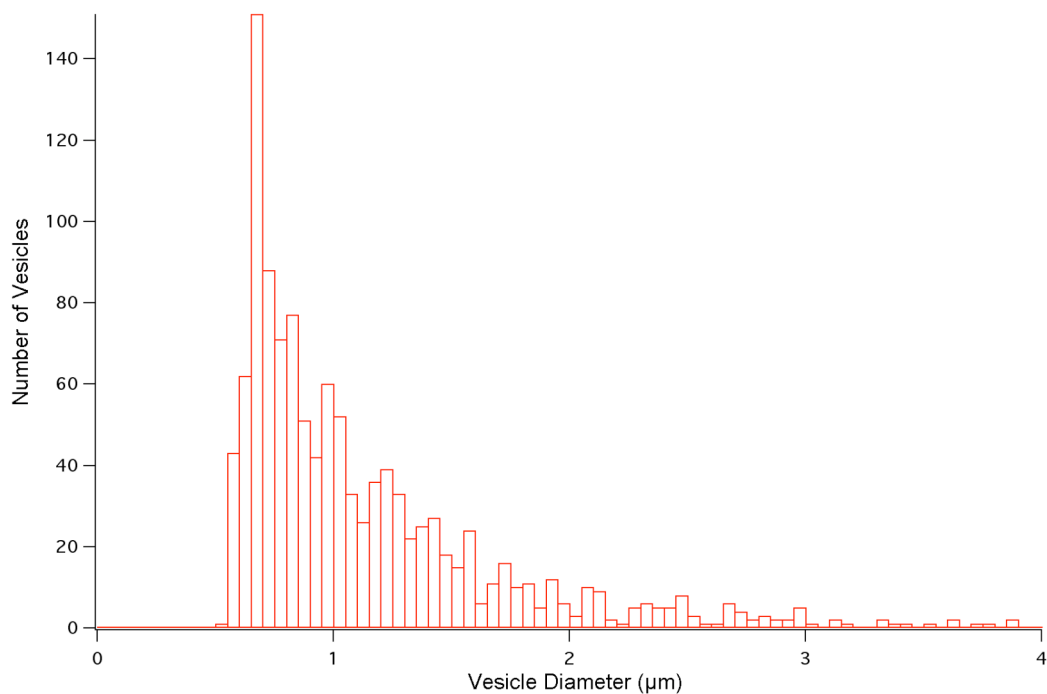


Figure 2.21: Histogram of native vesicle size distribution. Figure 2.20a is analyzed by IgorPro software and by a particle analysis procedure sizes are extracted. The threshold is fixed for vesicles smaller than 500 nm.

When the number of bins of the histogram is properly adjusted, as in the previous figure, some distinct size subpopulations can be probably be distinguished. Does this reflect the observations done in Percoll gradient where distinct populations appeared? This remains unclear and only analytical ultracentrifugation would provide such information. Such analytic methods allows in fact recording fluorescence at the same time than performing ultracentrifugation, and allows detecting thus fractions of interesting native vesicles populations.

To quantify native vesicles production, no precise technique is available allowing measuring vesicles of such small sizes. Despite flow cytometry analysis seems the most appropriated technique, the experimental obtained results tend to demonstrate that the sensitivity of the instrument is insufficient to detect the smallest vesicles inducing thus a drastic error on the number of vesicles. Fluorescence spectrometer was tested to detect the overall average signal of fluorescently labelled membrane proteins and of lipids previously inserted, but do not permit to assess directly the sizes of vesicles. Then confocal fluorescence microscopy was used. After sample production and purification, different dilutions of native vesicles were attached on a poly-lysine surface and diluted until distinct/individual vesicles could be observed. The quantification of any vesicle detected on the surface observed, multiplied by the dilution factor and normalized by the number of cells, provides a rough estimation of around 20 vesicles produced per cell.

2.7.2 Intracellular Components Present in Native Vesicles

Native vesicles could contain several cytoplasmic components from their mother cell. With the aim to characterize the most important components present after production several cytoplasmic proteins and organelles have been labeled in mother cells and their detection and quantification was then followed after production. The presence of cytoskeleton fibers, such as actin fibers or microtubules, and the main subcellular compartments have been analyzed, such as the endoplasmic reticulum, golgi apparatus, nucleus and mitochondria.

As previously introduced, the actin cytoskeleton is responsible for membrane partitioning and protein localization. An actin-EGFP stable cell line was produced to observe if actin polymerization is playing a role during native vesicles production by pushing outwards the plasma membrane and if actin remains present and polymerizes in native vesicle.

After their production native vesicles contain actin-EGFP and some of them show structures comparable to newly formed filaments (figure 2.22). These structures are probably assembled after native vesicle release from mother cells, or if occurring during that time, do not influence enclosure and are then restricted to a part of the vesicle. These newly formed filaments seem capable of interacting with lipids or proteins at the membrane and can be responsible for subsequent partitioning. These observations are in agreement with more recent literature, which demonstrate rapid meshwork reassembly beneath the membrane of the new bleb (Charras, Hu et al. 2006).

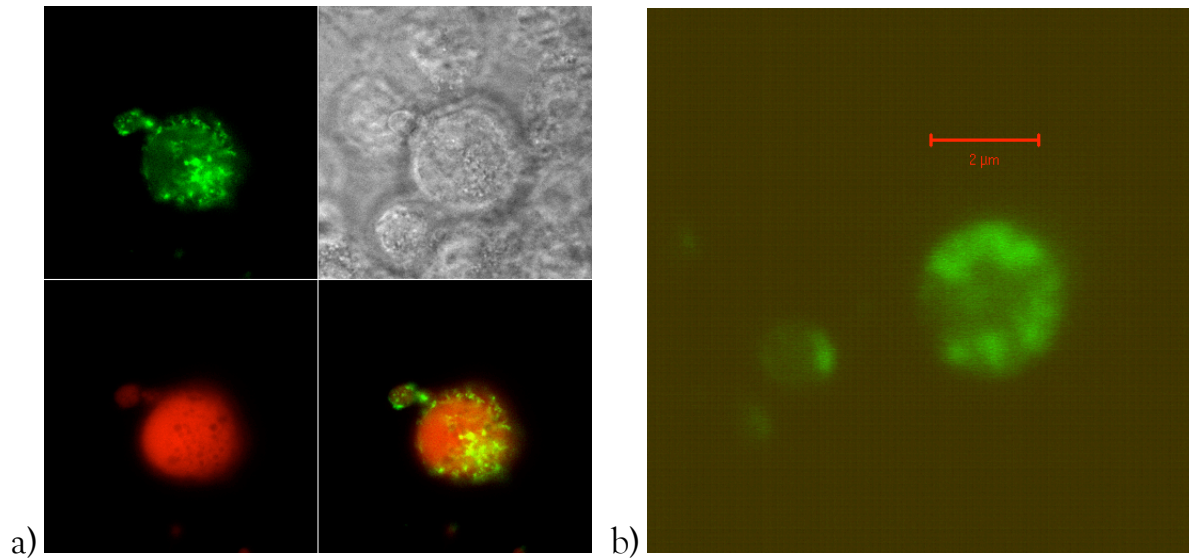


Figure 2.22: Confocal fluorescence micrographs of a HEK293 cell transfected with actin-EGFP and the cytosolic protein DsRed, during blebbing induced by cytochalasin treatment. (a) shows the presence and the formation of actin filaments. (b) shows the presence of newly formed actin structures in native vesicles, which can maybe contribute to membrane or receptor partitioning.

Interesting cellular organelles, such as mitochondria or parts of the endoplasmic reticulum, can be entrapped in native vesicles during formation and observed by microscopy (figure 2.23). Only vesicles $> 1 \mu\text{m}$ micrometer contain organelles.

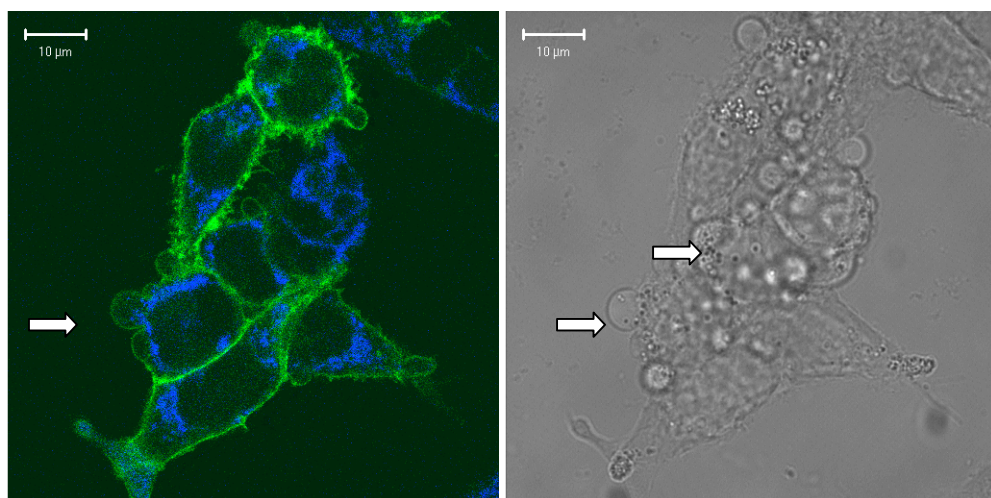


Figure 2.23: Confocal fluorescence micrographs of HEK293 cells expressing EGFP-NK₁R (green) and labeled with MitoTracker 633 for mitochondria (blue). Left panel shows fluorescence microscopy after cytochalasin treatment and right panel shows fluorescence microscopy before cytochalasin treatment.

the corresponding fluorescence image. Arrows indicate vesicles containing organelles.

Finally, the presence of other cellular components in native vesicles, such as tubulin and the Golgi apparatus was investigated by fluorescence labeling techniques. None of these components have been found probably due to their direct association with the cell nucleus. Calcium ion influx could be performed by coupling receptor signaling to a calcium membrane channel, such as the cyclic nucleotide gated channel (CNGs) (Berridge, Bootman et al. 2003). Other possibilities are to monitor receptor activation via signaling proteins, such as GRK or β -arrestin recruitment, which are involved in the first steps of signaling after ligand binding.

2.7.3 Production of Native Vesicles from Attached vs. in Suspension Cells

Here we investigate whether cells are able to produce vesicles in the same way when attached to supports or suspended in the medium. Our experiments show that the number of native vesicles is similar in both cases but small differences are detected when analyzed by flow cytometry. Two parameters were investigated: forward scattering, which scales with particle size, and sideward scattering, which depends on cell granularity, showed the presence of a distinct native vesicles population with increased granularity and a smaller size. This might have two reasons: first, native vesicles could contain more intracellular components when produced from cells in suspension; second, the apparition of a smaller native vesicles population with an increased granularity (figure 2.24). This observation was not correlated to the observations made by microscopy, because

such last technique doesn't allow accessing the power of static data obtained with the flow cytometry technique.

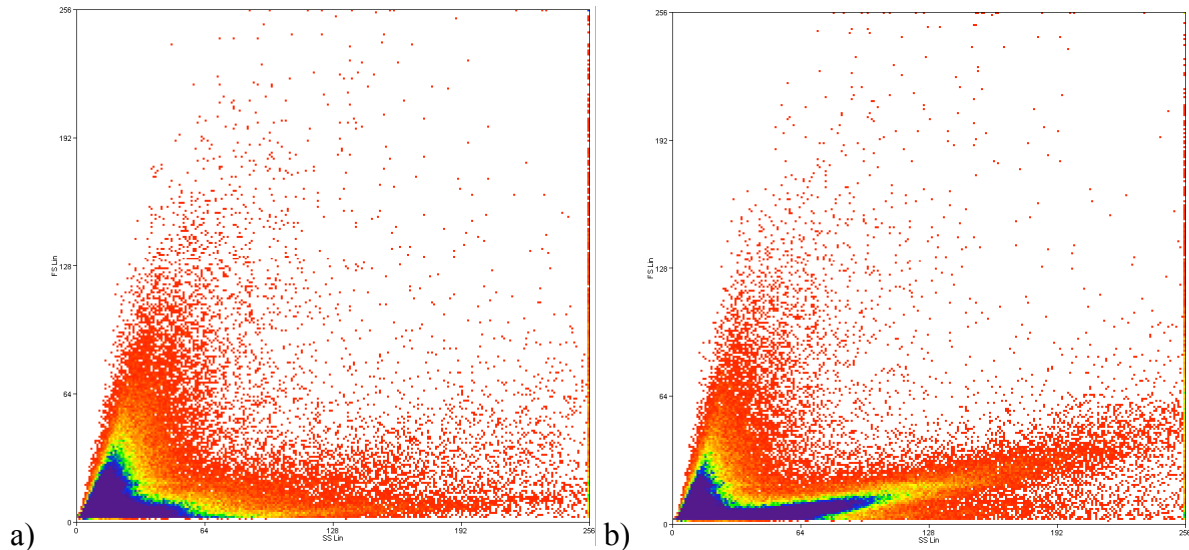


Figure 2.24: Native vesicles produced with the same protocol from attached cells (a) and from cells in suspension (b). On the right panel a new population of native vesicles appears with higher side scattering (blue area extending on the right).

2.8 Conclusions and Outlook

In this chapter we investigated the influence of the actin cytoskeleton to native vesicle production. Both, the growth medium and the cell cycle could be shown to influence the properties of the native vesicles produced. For cell blebbing, probably a combination of different cellular biochemical pathways is influenced by cytochalasin B treatment. The finding that shRNA downregulates affixin expression demonstrates the possibility to influence membrane-cytoskeleton interaction and by this to induce membrane blebbing without chemical treatment. Different purification techniques were applied to obtain the most pure native vesicle preparation. Almost all native vesicles contain cytosolic proteins, while intracellular components are only present in larger vesicles. Actin

structures could be detected in native vesicles after their production, in agreement with investigation done by others; (Charras, Hu et al. 2006), demonstrated that native vesicles have a similar cell membrane organization like whole intact cells. Their formation gives rise to different shapes with a broad range of sizes between hundreds of nanometers to a few micrometers, which opens interesting opportunities for the development and downscaling of new bioanalytical techniques.

2.9 Material and Methods

Cell Culture

Adherent HEK293 cells were grown in culture in DMEM F-12 medium (Gibco, Invitrogen) supplemented with 2.2% or 10% foetal calf serum (FCS) at 37°C in an humidified atmosphere with 5% CO₂. Cells were splitted every 2 to 3 days with 0.1% trypsin / EDTA solution.

Transfecting Cells and Producing Stable Cell Lines

Dr. Bruno Meyer produced in our laboratory DNA constructs for the following receptors: EGFP-5HT₃R, EGFP-NK₁R.

DNA constructs for the proteins EGFP-tubulin, EGFP-Actin, DsRed2 were purchased from DB Biosciences (Clontech).

Cells were transfected with DNA constructs using the calcium phosphate method. The previous to transfection, cells were splitted at a concentration of $1.5 \cdot 10^5$ cells/ml and grown at 37°C for 16-20 h. Per ml of medium, 2.5 µg of DNA were mixed with 50 µl of 250 mM CaCl₂ at pH 7.05 and then with 50 µl of HEPES / 50mM PO₄. After 1 min the reaction was stopped by adding DMEM + 10% FCS to the cells. 4 h later the medium was exchanged by fresh one.

Stable cell lines were established by selection with the appropriate antibiotic for 2-3 weeks and isolated by FACS.

Native vesicle production

Cells were splitted 16 hours prior to native vesicles production and maintained in DMEM F-12 + 2.2% FCS. Cells were collected in PBS⁻ buffer containing 5mM EDTA and resuspended in 1 ml PBS⁻. They were added in a solution of 4 ml PBS⁻ containing 10 µl cytochalasin B (10 mg/ml in DMSO) (final concentration of cytochalasin B was 25 µg/ml). Native vesicles were separated from cells during 10 minutes of agitation at 700 rpm (IKA MS1 Minishaker). Native vesicles were then purified from cells by filtration (2 µm TPPC filter, Millipore). Native vesicles were then collected by centrifugation at 7000 rpm (6300 g) for 10 min and finally resuspended in PBS⁻ buffer for investigation.

Native vesicles were also produced from adherent cells by replacement of grown medium by a solution of 25 µg / ml of cytochalasin in PBS⁻, previously warmed at 37°C. Agitation, filtration and collection followed the same protocol.

Affixin siRNA

According to the siRNA sequence against affixin (Yamaji, Suzuki et al. 2004), two complementary oligonucleotides strands were designed to be used as shRNA.

Sequence 1:

5' -GATCCGCTGAATGTGGCTGAGGTGTTCAAGAGACACCTCAGCCACATTCAGCTTTTTTGCTAGCG -3'
3' -GCGACTTACACCGACTCCACAAGTCTCTGTGGAGTCGGTGTAAAGTCGAAAAAACGATCGCTTAA-5'

Sequence 3:

5' -GATCCGCTGAATTTGGAGGTGACGTTCAAGAGACGTCACCTCCAAATTCAGCTTTTTTGCTAGCG -3'
3' -GCGACTTAAACCTCCACTGCAAGTCTCTGCAGTGGAGGTTTAAAGTCGAAAAAACGATCGCTTAA-5'

Oligonucleotides (Microsynth) were inserted into RNAi-Ready pSiren-RetroQ Vector (BD Biosciences Clontech) following manufacturer protocol. For

annealing, oligonucleotide strands were resuspended in TE buffer at a concentration of 100 μ M and mixed in 1:1 ratio to reach a final concentration of 50 μ M of double stranded oligonucleotide. This mixture was then sequentially heated at 95°C for 30 seconds, 72°C for 2 minutes, 37°C for 2 minutes, 25°C for 2 minutes and stored on ice. Annealing solution was diluted in TE buffer to a concentration of 0.5 μ M. Ligation was realized for 3 hours at RT with a solution of: 2 μ l of pSIREN vector (25 ng/ml), 1 μ l of annealed oligonucleotide (0.5 μ M), 1.5 μ l 10 X T4 DNA ligase buffer, 0.5 μ l BSA (10 mg/ml), 9.5 μ l nuclease-free H₂O, 0.5 μ l T4 DNA ligase (New England Biolabs). Transfection of adherent HEK cells was done according to an Effecten protocol (Qiagen). Per ml of medium 0.1 μ g of DNA is diluted in 50 μ l of EC buffer. 0.8 μ l of enhancer solution is added, vortexed for 1s and incubated at maximum for 5 minutes. 1 μ l of Effecten solution was added, vortexed for 10s, incubated for 10 minutes and added to the cell culture.

Cell Synchronization

HEK, CHO and HeLa cells were grown under similar conditions as previously described.

The “baby machine” protocol (Cooper 2002) to collect freshly newborn cells was modified to avoid any filtration. Adherent cells were grown in a culture flask, whose surface was previously treated with fibronectin (Sigma–Aldrich) to improve cell adhesion. Newborn cells were collected in suspension by careful replacement of culture medium. This operation was continually repeated between 30 minutes to 1 hour. Cells were then centrifuged and resuspended in DMEM + 2.2% FCS and kept in culture at 37°C.

Synchronization was also achieved by 400 ng/ml nocodazole (Sigma-Aldrich) treatment in culture medium for 16 hours. Nocodazole was then withdrawn by 3 times medium exchange. Cells were put again in culture at 37°C. In both cases, cytochalasin B was applied at 25 µg/ml in PBS⁻.

Percoll Gradient

Percoll (Amercham Pharmacia Biotech) was mixed with PBS⁻ (20% Percoll / 80% PBS) and filled in two 3 ml centrifugation tubes. Density marker beads (Amercham Pharmacia Biotech) were added to one tube. Native vesicle preparations were added to the second tube. The two tubes were placed in a TLA 100.4 rotor and run at 23000 rpm for 30 minutes in a Beckman Optima TLX Ultracentrifuge. Gradients were automatically established during ultracentrifugation.

Flow Cytometry

Flow Cytometry measurements were done at the Flow Cytometry Core Facility at EPFL with an CyAn ADP analyser from Beckman Coulter.

FACS was performed at Ludwig Institute of Lausanne with a Calibur Instrument from Becton Dickinson Biosciences.

Chapter 3

The goal of this chapter is to demonstrate that the receptors present at the surface of the vesicles are not affected by the production of the vesicles, thus remaining functional. In order to test such functionality receptors are labeled on cells and on native vesicles with their agonist as well as their antagonist.

3. Investigating Membrane Proteins on Cells and Native Vesicles

Membrane proteins are the main actuators for the transduction of external signals (i.e. neurotransmitters, peptides, odorants, hormones, taste) into intercellular responses of second messengers, such as calcium, cAMP (cyclic adenosine-5-monophosphate), or even NO (nitric oxide). Single GPCR can interact with various molecular species with different affinities, and induce a variety of second messenger responses through the activation of different effector proteins (Azzi, Charest et al. 2003).

Activation of GPCR leads also to the activation of others pathways. As previously introduced in section 2.1.2.3, β -arrestins are scaffolding proteins that can generate a multitude of downstream signals by multiple interactions and whose principal function is receptor desensitization and recycling. Recent reports demonstrate that they are able to couple and activate other pathways (Lefkowitz, Rajagopal et al. 2006). β -Arrestin 2 was recently reported to play a role in

chemotaxis regulation (Fong, Premont et al. 2002; Sun, Cheng et al. 2002), and to mediate coupling to a cellular proliferation pathway known as MAPK (mitogen-activated protein kinase) (Azzi, Charest et al. 2003). In this context, β -arrestin 1 in conjunction with $G_{\alpha q/11}$ protein was reported to coordinate the activation of RhoA (Barnes, Reiter et al. 2005), one of the main players in cytoskeletal remodeling. At such levels of regulation, conflicting results start appearing, probably due to the interplay of several regulation pathways or due to the use of different cell line models.

Downscaling receptor analysis below the single cell level can have important implications. For example, the cost of such investigations can be reduced. More importantly, for the first time the dissection of cellular biochemical pathways by analysis of partial molecular components would be possible.

3.1 GPCR Characterization

Our laboratory investigates GPCR such as olfactory receptors, α_{1B} -adrenregic (α_{1B} -AR) and the neurokinin 1 receptor (NK₁R). Due to the availability of different receptor constructs, of fluorescently labeled agonists and antagonists and also of specific antibodies, NK₁R was in particular the best candidate to test its expression and functionality in native vesicles in comparison to the cells. The NK₁R was used as a model to investigate formation immobilization and function of native vesicle. Amongst different fluorescent techniques confocal microscopy and flow cytometry were most appropriated for characterization of native vesicles.

3.1.1 The Neurokinin 1 Receptor as a Model Cell Surface Receptor

Tachykinins are a family of peptides, sharing a common C-terminal amino acid sequence (Phe-Xaa-Gly-Leu-MetNH₂), and since its discovery in the 1930ies, substance P (SP) became the most used compound. In the 1960ies the first discoveries point on the implication of tachykinins in the central nervous system (CNS). Since then other tachykinins were discovered in the 1980ies and the major interest of pharmacological research for such class of compounds lead finally to the identification and the isolation of the three tachykinins receptors in the 1990ies, known as neurokinin-1, -2 and -3 receptors (NK₁R, NK₂R and NK₃R respectively), belonging to the superfamily of GPCRs, also known as seven transmembrane (7TM) receptors. Tachykinin receptors are responsible for nociception, but are also reported to mediate neurogenic inflammation, vasodilatation, regulation of gastrointestinal secretion and motility by the regulation of smooth muscle contraction. As a potential therapeutic target, NK₁R is the most studied receptor of his family with discoveries of new specific agonists and antagonists. NK₁R expression occurs in a variety of tissues, where it leads principally to the depolarization of primary afferent neurons. NK₁R is principally activated by its natural agonist SP, but was also demonstrated to be activated by other tachykinins with the potency order SP > Neurokinin A > Neurokinin B, the latter two are respectively the main agonists for NK₂-R and NK₃-R (Fong, Huang et al. 1992; Maggi and Schwartz 1997). Numerous radioligand binding experiments have been reported for the NK₁R (Perrone, Diehl et al. 1983; Knaus, Knaus et al. 1991; Fong, Huang et al. 1992; Fong, Yu et al. 1992; Johnson and Johnson 1992; Heuillet, Menager et al. 1993; Huang, Huang et al. 1995; Maggi 1995; Maggi and Schwartz 1997; Turcatti, Zoffmann et al. 1997), delivering contradicting results about the precise affinity of the interaction of SP with NK₁R. Most recent reports indicate that the NK₁R is able to display two distinct binding

affinities for SP which could be due to two distinct conformational states (Alves, Delaroche et al. 2006). These investigations report the difficulty of evaluating the interaction of a receptor with its ligand and point to the existence of many interactions of surface receptors with intracellular proteins or extracellular matrix that can influence such affinities.

NK1R was reported to mainly activate $G_{\alpha q/11}$ protein (McConalogue, Corvera et al. 1998; McConalogue, Dery et al. 1999), but was also reported to activate at lower levels G proteins of the class $G_{\alpha s}$ or $G_{\alpha i}$. The main activation pathway, implying the $G_{\alpha q/11}$ protein leads to the final release of calcium (Ca^{2+}) from the internal cellular stores, at the endoplasmic reticulum (ER) and sarcoplasmic reticulum (SR). This traditional pathway implies the activation by $G_{\alpha q/11}$ protein of PLC (phospholipase C) inducing the degradation of the plasma membrane lipid PIP_2 (phosphatidyl-inositol-4,5-biphosphate) into DAG (diacylglycerol) and IP_3 (inositol-1,4,5-triphosphate) that after binding to IP_3 -R on internal stores leads to the release of Ca^{2+} . But NK_1R was also reported to induce the formation of cyclic AMP, probably due to the activation of $G_{\alpha s}$ protein, which in turn activates adenylate cyclase. These effects seem more be related to the used cell type.

NK_1R desensitization follows normal endocytic routes after agonist interaction, implying GRK activation and β -arrestin recruitment leading to his internalization by clathrin-coated pits. In early endosomes, sorting occurs and NK_1R recycles back to the membrane. Recycling occurs by two distinct routes according to NK_1R interaction with β -arrestin 1 or β -arrestin 2. NK_1R desensitization has further implications on the desensitization NK_3R (Schmidlin, Dery et al. 2002). When NK_1R is internalized, NK_3R can not be. This

mechanism supposed implying probably the sequestration of β -arrestin is supposed to allow cells responding permanently to tachykinins peptides.

3.2 Results and Discussion

The use of the NK₁R as a typical example of GPCR in native vesicles revealed soon to encounter with difficulties. Native vesicles are heterogeneous in terms of comprising functional receptors. In this study, fluorescence microscopy was used for characterizing the native vesicles on glass surfaces because it allows to record images with high sensitivity and high spatial and temporal resolution.

In order to easily visualize the presence of the NK₁R, we used a fluorescence receptor version, the EGFP-NK₁R, which expresses very well in HEK cells resulting in high concentrations in the cell membrane. Receptor binding of the fluorescent agonist SP-Cy5 was measured using a Plate Reader and confocal microscopy. Experiments with the Plate Reader were performed at different SP-Cy5 concentrations and fluorescence of EGFP and Cy5 was simultaneously acquired in two separate channels. The signal of Cy5 was normalized to the EGFP signal of the receptor (figure 3.1). A plot of these normalized fluorescence intensities as a function of the ligand concentration was then fitted by a Hill equation:

$$y = base + \frac{(\max - base)}{\left[1 + \left(\frac{x_{half}}{x}\right)^{rate}\right]}$$

where the obtained *xhalf* value corresponds to the K_D.

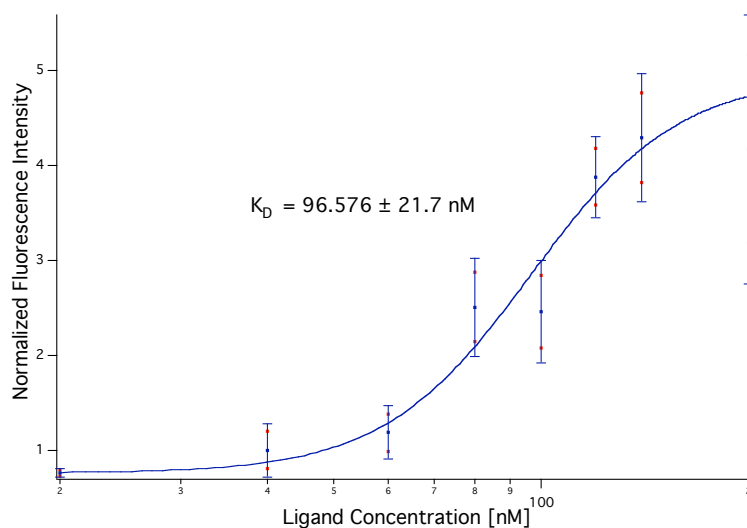


Figure 3.1: HEK cells expressing EGFP-NK₁R labeled with SP-Cy5. Fluorescence was recorded using a Plate Reader (Flexstation) and normalized to receptor expression via the EGFP fluorescence. Error bars represent average of two replicates.

The confocal microscopy data were evaluated by two procedures. The first consists to evaluate B_{\max} values for each SP-Cy5 concentration, when labeling reaches the equilibrium plateau. Normalization was performed as described previously and K_D values were calculated from the Hill plot.

Within this procedure the following difficulties appeared. At very low concentrations below K_D , the equilibrium was not always easily observed. Fortunately, this experimental uncertainty only gives rise to a minimal error on the calculated K_D value. At high and intermediate concentrations, above and around the K_D , the equilibrium is easily observed, but here a major biological difficulty is present. As soon as receptor is activated, receptor desensitization occurs resulting in receptor internalization and influences the fluorescence measurements. This problem might be overcome by performing the labeling experiments at 4°C, where major cellular pathways are inhibited. Here we used the

following procedure to overcome the difficulties: we analyzed only the very first data points of the time courses of the fluorescence intensity changes during labeling. Plotting such values as a function of SP-Cy5 concentration and evaluating the data by the Hill equation, finally delivered accurate K_D values (figure 3.2)

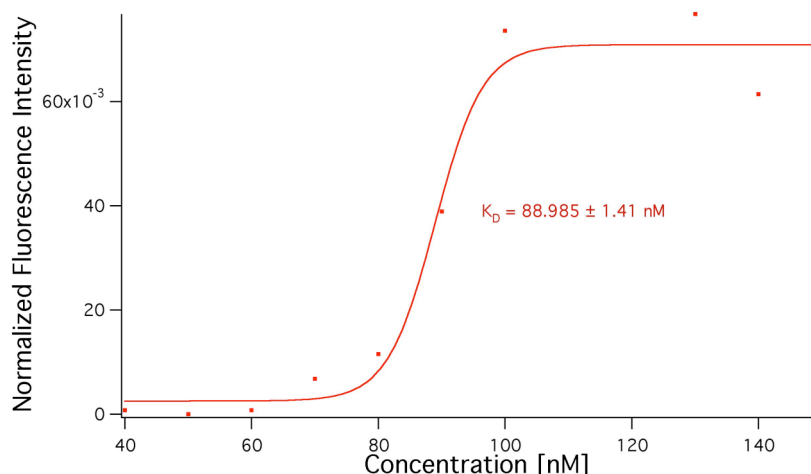


Figure 3.2: HEK Cells expressing the EGFP-NK₁R labeled with the agonist SP-Cy5. Kinetic data were extracted from the fluorescence intensity changes at the beginning of the experiment. Data were corrected for background and were normalized by dividing the ligand signal by the signal of the receptor (Cy5/GFP). The first points were extracted and plotted as a function of the ligand concentration. Hill plot of the data allows evaluating the K_D value.

This second approach was preferred for evaluating K_D values from labeling experiments performed on cells and on native vesicles.

For analyzing the fluorescence intensities distribution of the individual vesicles an IgorPro semi-automated program was developed. It is based on an IgorPro Particle Analysis Program and allows choosing automatically regions of interest. Several parameters could be adjusted such as: i) The minimal area to take

in account depending on the resolution of the image, and if desired the program allows to set a threshold excluding native vesicles below a particular size. ii) Filtering can be applied on the image to improve particle analysis, but we analyzed always the original images. iii) A threshold could be introduced to remove fluorescence background; once the evaluation parameters are fixed, automated analysis defines several regions of interest (ROIs). iv) It is possible to select a particular registration channel out of three color images for analysis and store the data in a worksheet. Such procedure was used for native vesicles analysis.

3.3 The Neurokinin₁ Receptor

Several constructs of the NK₁R were available in the laboratory, but we concentrated mostly on the NK₁R-CFP and the wtNK₁R. NK₁R-CFP expresses homogenously at cell plasma membrane without big differences between individual cells.

3.3.1 Agonist Binding

Substance P labeled with Cy5 (SP-Cy5) was mostly used for labeling NK₁R in cells and in native vesicles because it shows no unspecific adsorption on cells that do not express the NK₁R.

3.3.1.1 Cells

Confocal microscopy images shows that a certain proportion of cells displayed a more efficient ligand binding at intermediate concentrations of SP-

Cy5 despite a comparable membrane expression of the receptor in the different cells (figure 3.3) indicating the existence of two different cell populations with two different receptor binding affinities. We were able to separate two apparent binding affinities by single cell analysis for each particular concentration; this required manual selection of ROIs, because the automated analysis was unable to perform such separation. If images were analyzed according to their average fluorescence intensities a bimodal binding was sometimes observed. The bimodal effect reflects the averaging and was never observed in single cell analysis.

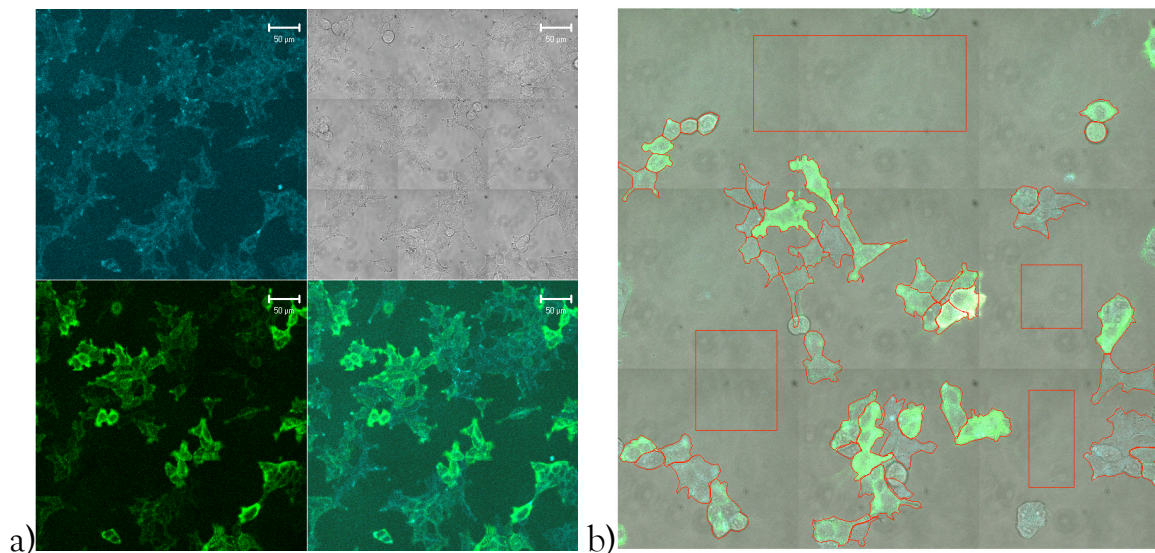


Figure 3.3: (a) HEK cells stably expressing NK_1R -CFP (blue) labeled with SP-Cy5 (green) at a concentration of 2 nM. Despite similar membrane expression cells clearly demonstrates different ligand affinities. (b) Similar experiment at 1 nM SP-Cy5 showing typical single cells analysis with hand made ROIs. The squares are taken in account for background subtraction.

This labeling experiment was performed with a broad range of ligand concentrations (from 10 pM to 100 nM). Two identical channels for recording ligand (SP-Cy5) concentrations were used, whose settings differ only in acquisition sensitivity (figure 3.4). This approach was used because the more

sensitive channel can saturate at very high concentrations. A third channel was used to measure receptor fluorescence (NK₁R-CFP). Nevertheless, the more sensitive fluorescence channel for Cy5 allows obtaining the two binding curves (red for the cell population with the highest affinity for the ligand and green for the population with lower affinity). The less sensitive channel for Cy5 allows obtaining the blue curve (only for the low affinity cell population). When comparing the green and blue curve for the low affinity population of cells, a decrease of the points at the highest concentrations is observed, which results from the exclusion of saturated image pixels.

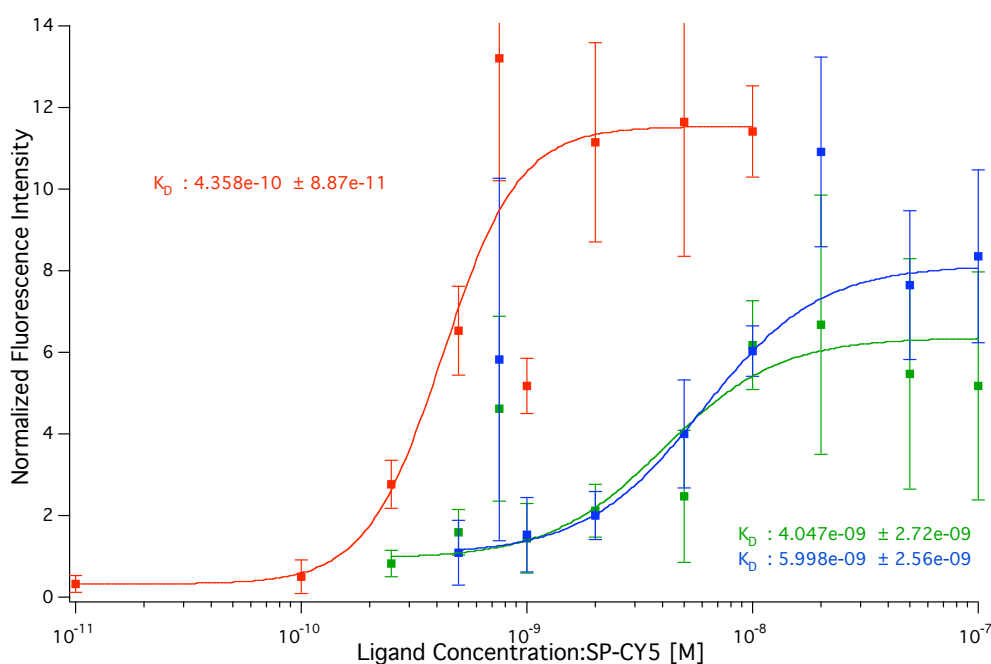


Figure 3.4: HEK cells expressing NK₁-CFP with two distinct cell populations demonstrating different affinities for their ligand despite similar receptor expression levels. Cells were labeled with the agonist SP-Cy5 and fluorescence was recorded by confocal microscopy in three different channels: one for CFP and two different settings for the ligand SP-Cy5 (red and green curves with a high sensitive settings and blue with lower sensitive settings). Fluorescence signal was corrected for background and normalized to cell expression. Cells were analyzed independently with single cell ROIs and data were plotted using IgorPro analysis software. Data were fitted using the Hill equation (1nM was removed for red curve

and 750pM was removed for green and blue curves). Error bars indicate the variation in cell population for a given concentration.

In order to confirm such results a flow cytometry analysis was performed yielding many more data for a reliable statistical analysis. Similar experiments performed over a large range of concentrations. Also, here two cell populations were observed, each showing a different ligand binding affinity at intermediate concentrations (figure 3.5 f-i). As seen at intermediate concentrations two peaks (depicted by the arrows) are overlapped, which do not allow obtaining a K_D value with accuracy to compare with those obtained by confocal microscopy. Nevertheless, it appears that such observations were in agreement.

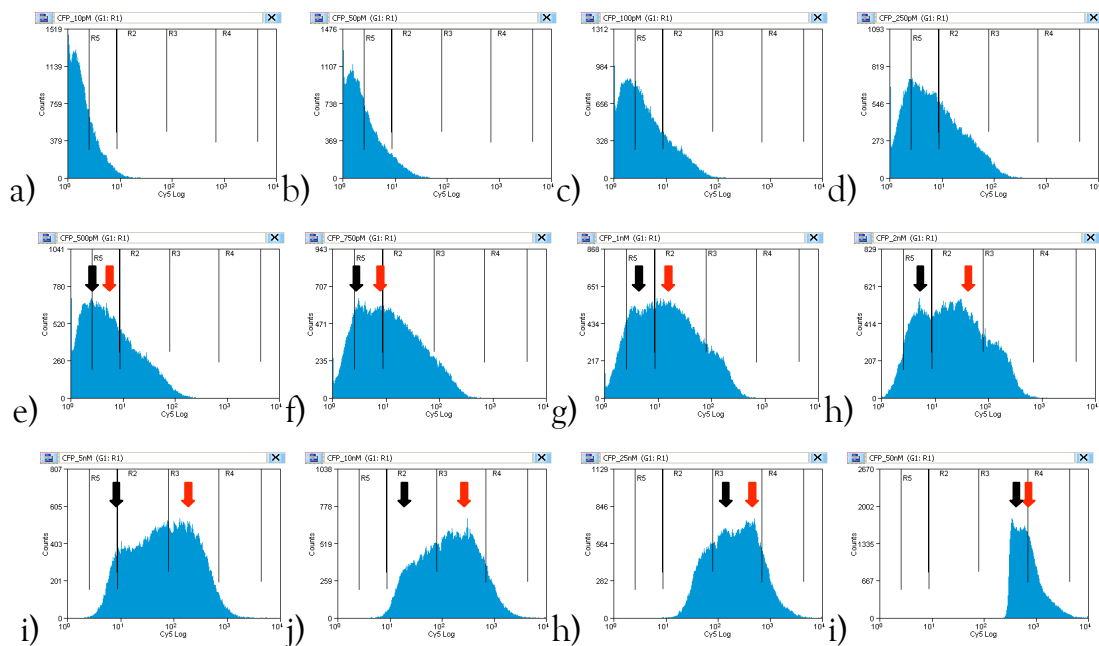


Figure 3.5: Flow cytometry analysis of NK₁R-CFP labeled with SP-Cy5. For each concentration a plot of the signal of SP-Cy5 in a logarithm (horizontal axis) is displayed in function of the number of counts, which corresponds to the number of cells acquired (vertical axis). At intermediate concentration, black arrows indicate the population with a low affinity, whereas the red arrow shows the high affinity population. At intermediate concentrations from f) to i), the two populations of

cells demonstrate different affinities for the ligand with an order of magnitude of difference. Concentration ranges from 10pM, 50pM, 100pM, 250pM, 500pM, 750pM, from a) to f), respectively and from 1nM, 2nM, 5nM, 10nM, 25nM and 50 nM from g) to i), respectively.

About the biological relevance of such observations we presently can speculate the following. (i) Do the two binding affinities reflect two distinct conformational states of the NK₁ as claimed by Alves et al. (Alves, Delaroche et al. 2006)? Alves et al. demonstrate that NK₁R shows two different affinities for his major ligand SP, but also for a neurokinin A (the ligand for NK₂R), which is known to bind to the NK₁R with a lower affinity. To resolve such two populations by flow cytometry analysis, a new experiment could be performed by double labeling the receptor with SP and neurokinin A. Substance P can saturate the first population of cells with high affinity and neurokinin A the lower affinity one. The difference of affinities for such two ligands can probably discriminate the two cellular populations. (ii) Do the results reflect receptor partitioning into microdomains at the cellular membrane? Monastarkaya et al. (Monastyrskaya, Hostettler et al. 2005) claimed that NK₁R signaling is dependent on membrane microdomains and that treatment with methyl- β -cyclodextrin (M- β -CD), a cholesterol chelator can abolish receptor signaling to PKC. (iii) Does this reflect different cellular states or receptors interactions with other proteins? NK₁R is known to interact with different effectors proteins and this two binding affinities could also be due to different receptor associated proteins, such as two different G proteins. In any case the fluorescent measurement of such two binding affinities can provide new opportunities to identify such kind of partners.

Similar behavior was also observed with the wtNK₁R. Unfortunately the full separation of such two populations was not successful, probably due to different levels of expression of the receptor in the two cell populations.

Other receptor constructs were also investigated by confocal fluorescence microscopy in order to test whether the two ligand binding affinities were present in the same cell or if this was related to a particular cellular state, maybe related to cell cycle. First experiments were performed to determine the K_D of SP binding to the ACP-NK₁R (figure 3.6). Because experiments were done without any labeling normalization for receptor expression was not possible. This receptor shows only one binding affinity for the ligand.

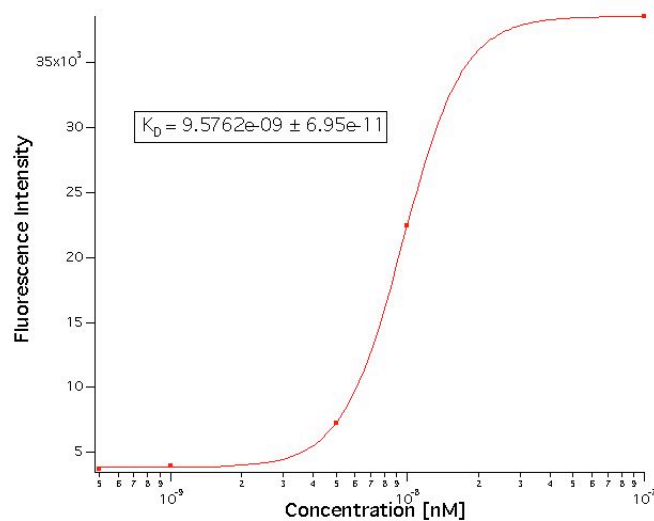


Figure 3.6: Binding of SP-Cy5 to ACP-NK₁R shows only one binding affinity.

3.3.1.2 Influence of Cholesterol on NK₁R

In order to test if cholesterol has a major effect on the binding affinity of SP to the NK₁R-CFP, cells were subjected to two concentrations of ligand (1nM and 25nM) within a short period of time to avoid major receptor internalization.

15 minutes after treating the cells with 4% M- β -CD to remove major part of the cell membrane cholesterol, ligands were added in two steps. This experiment showed that the high affinity ligand interaction with the NK₁R was abolished by cholesterol removal from cellular membrane. The high affinity population of NK₁R-CFP demonstrates to be labeled with the two concentrations of ligand (figure 3.7a). The low affinity population demonstrates poor ligand binding with the first concentration, but efficiently labeled with the higher concentration (figure 3.7b). When subjected to M- β -CD treatment, the two populations of NK₁R-CFP could not anymore be distinguished and all cells response only to the higher concentration of ligand (figure 3.7c). During such experiment, calcium signaling was followed with an intracellular calcium dye and all analyzed cells demonstrate efficient calcium responses.

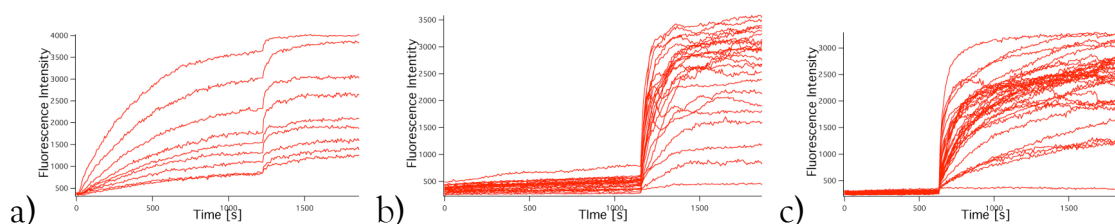


Figure 3.7: (a) High affinity population of NK₁R-CFP cells challenged with two concentrations of ligand: 1nM applied at t: 0s and 25 nM at t: 1224s. (b) Low affinity populations of NK₁R-CFP cells demonstrate poor affinity for the ligand: when 1 nM was applied at t: 0s and efficient labeling when labeled at 25 nM at t: 1153s. (c) After M- β -CD treatment to remove cell membrane cholesterol, no more cells could bind the ligand when applied at 1 nM and demonstrate efficient labeling when subjected to 25 nM concentration at t: 632s. These results tend to demonstrate that receptor affinity could be influenced by cellular membrane cholesterol content.

3.3.1.3 Native Vesicles

NK₁R was also investigated in native vesicles to test receptor functionality and if its affinity was influenced by the procedure of production or by the higher membrane curvature in the vesicles.

Obtaining ligand binding curves with native vesicles appears to be even more challenging than with cells. From experiments where native vesicles were labeled with SP-Cy5 prior to measurements, data analysis did not allow to obtain binding curves. The only explanation for that was that native vesicles could maybe perform internalization. However, results could be obtained by extracting the values of kinetic data as previously described. Native vesicles were labeled with increasing concentrations of SP-Cy5 and demonstrate efficient binding (figure 3.8). The results only show one population of vesicles because only high concentrations have been investigated.

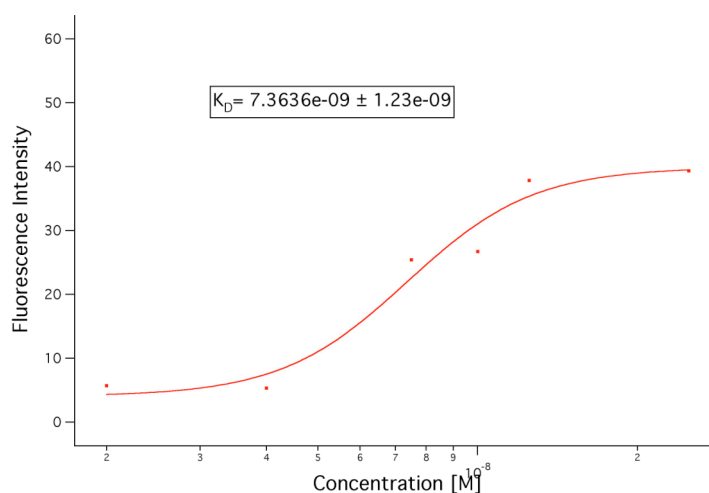


Figure 3.8: Data points are averages obtained from single native vesicles, all of them show similar behavior (2nM: n=22; 4nM: n=9; 7.5nM: n=13; 10nM: n=22; 12.5nM: n=20; 25nM: n=15). The first point of each kinetic curve was taken and plotted as a function of the concentration as previously explained. Fitting the values with Hill equation allows calculating a K_D value, which is in agreement with previous results obtained on cells. Only the low affinity K_D could be accessed.

Investigating fluorescence intensities at lower concentrations of ligand in native vesicles were not analyzed because of low signal to noise ratio.

A similar experiment was performed using flow cytometry analysis over a broader range of concentrations. Native vesicles preparation was aliquotted and incubated with increasing concentrations of SP-Cy5 on ice to prevent possible internalization. The vesicles were then pelleted by centrifugation and resuspended in cold PBS. Analysis was performed and the median of the results was plotted as a function of the concentration (figure 3.9). Those measurements give similar results to the previous ones. One point at 1 nM was not taken in consideration for the Hill equation fitting. When this point is taken in consideration the K_D value is even lower, and can reflect maybe an average of the two binding affinities seen in cells, but could not be observed in the kinetic measurements.

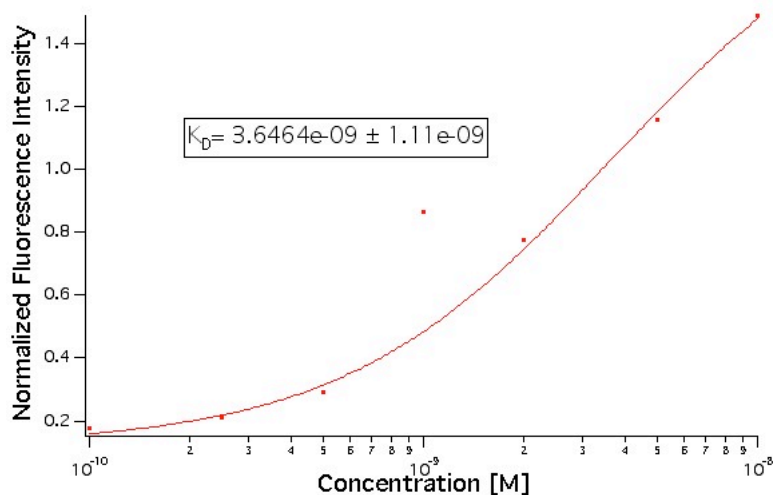


Figure 3.9: Flow cytometry analysis of native vesicles containing the NK₁R-CFP and labeled with different concentrations of SP-Cy5. Median fluorescence intensity of SP-Cy5 signal was normalized by the median fluorescence intensity of NK₁R-CFP. Fit was done with Hill equation. 1 nM was excluded from this fit.

3.3.1.4 Internalization in Native Vesicles

In order to test if native vesicles could perform receptor internalization, experiments were performed with an SP labeled with CyFER, which became only fluorescent when subjected to acidification in early endosomes. Experimental results show that large native vesicles (2-3 μm) can also perform receptor internalization (figure 3.10). These results demonstrate that native vesicles possess all the internalization machinery, such as GRKs and β -arrestin, required to induce receptor desensitization.

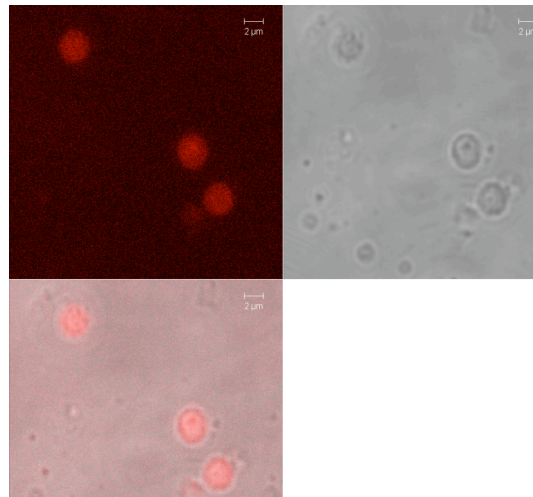


Figure 3.10: Native vesicles expressing the wtNK₁R show efficient labeling with SP-CyFER demonstrating internalization.

Summarizing these results, agonist binding to NK₁R native vesicles could be investigated in cells and in native vesicles despite internalization, mainly by evaluating values from the kinetic curves or by flow cytometry analysis. Membrane cholesterol seems to influence receptor affinity. Native vesicles experiments show that receptor agonist complexes internalize, demonstrating the presence of the endocytotic membrane in native vesicles.

3.3.2 Antagonist Labeling

If receptor internalization would be the major problem in accessing K_D values, the use of antagonist should solve the problem. In our laboratory, a fluorescently labeled antagonist was available, the CP-Cy5. It was used to investigate binding on cells as well as on native vesicles.

3.3.2.1 Cells

As previously done for SP-Cy5, CP-Cy5 was applied to cells at increasing concentrations. Binding affinities were evaluated on an individual cell after sequential ligand applications (figure 3.11). Because antagonist did not induce receptor internalization, we evaluated no longer kinetic data but measured the average fluorescence intensity value per single cell.

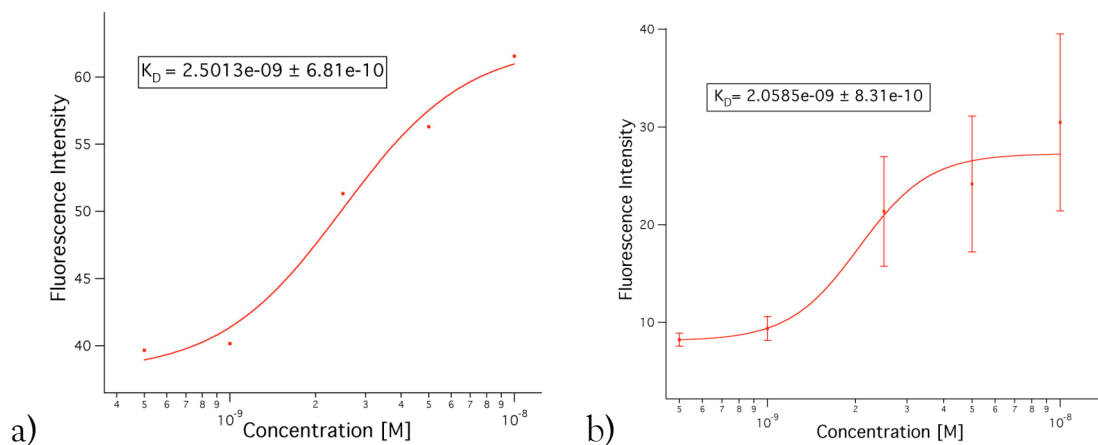


Figure 3.11: Binding of CP-Cy5 on cells expressing the wtNK₁R. (a) shows the fluorescence intensity data evaluated over the entire image comprising many cells. (b) as in (a) but analysis of only 10 ROIs.

Similar experiments performed with NK₁R-CFP yield similar results with similar K_D values. (figure 3.12)

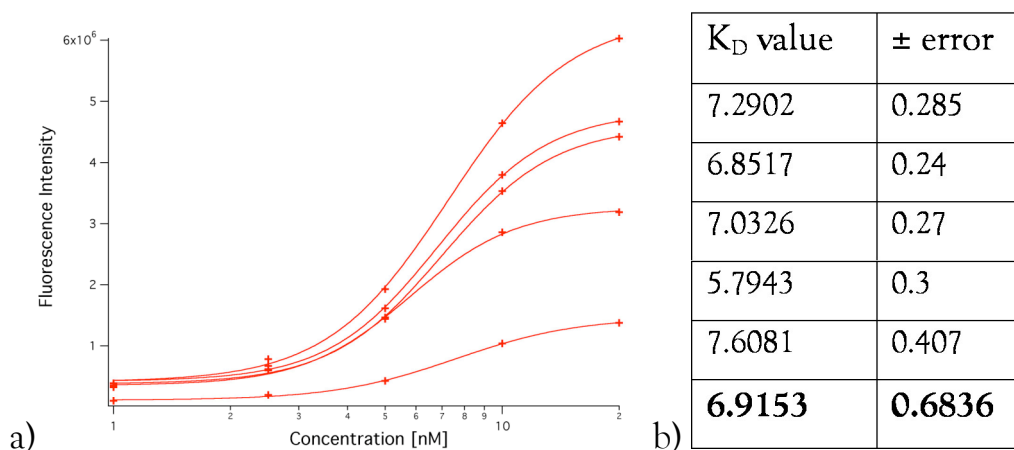


Figure 3.12: HEK cells expressing the NK₁R-CFP labeled with CP-Cy5. (a) Binding points obtained from individual cells fitted with a Hill equation. (b) Individual fits shows in (a) gave individual K_D . Values extracted from the Hill fitting for the diverse curves form top to down, respectively. Last value (in bold) is the average of all.

3.3.2.2 Native Vesicles

The same experiments as performed on cells, demonstrate also efficient sequential labeling. Native vesicles could then be individually analyzed and averaged together. The average numbers are plotted in function of the concentration and fitted with a Hill equation (figure 3.13).

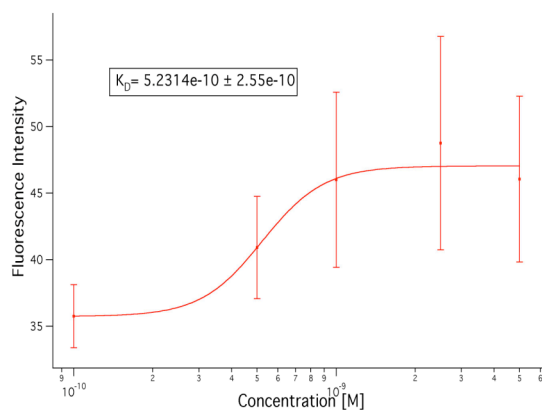


Figure 3.13: Native vesicles containing the NK₁-R-CFP labeled with CP-Cy5. Ligand binding was evaluated on individual vesicles and then averaged. Fitting was done with Hill equation.

Taken together, antagonist binding could be followed in cells and in native vesicles. Quantitative analysis yielded comparable K_D values.

3.4 Conclusion and Outlook

NK₁R-CFP was characterized by binding fluorescently labeled agonist SP-Cy5 as well as fluorescently labeled antagonist CP-Cy5. The results are both investigated by fluorescence microscopy and by flow cytometry. The results are in agreement with previous observations showing two binding affinities for the NK₁R.

Cholesterol depletion had substantial influence on receptor affinity for the agonist indicating the importance of receptor partitioning in membrane microdomains.

The NK₁Rs' ligand binding affinity in vesicles was comparable with the receptor affinities in live cells.

The results demonstrate that the receptor functionality was not affected by native vesicle formation.

Native vesicles also show internalization of desensitized receptors demonstrating that in native vesicles complex signaling machineries are presented and still active.

Taken together, these results confirm that native vesicles serve as artificial cells for GPCRs investigation and downscaling bioanalytics.

Further experiments are required in order to test if two receptor binding affinities could be observed in native vesicles as well as in a single cells. FRET measurements realized with an ACP-NK₁R construct would probably provide further information.

3.5 Material and Methods

Confocal Microscopy

A day prior to experiment, microscope cover glasses (\varnothing : 25 mm; thickness 0.15 μm from Mentel-Glaser) were previously washed with ethanol and placed in 6 wells plates under a laminar flow. Cells were splitted with Trypsin/EDTA and seeded at 300000 cells/ml with DMEM F-12 culture medium + 10% FCS. At the day of the experiment, glass slides were mounted on a metallic support and covered with cell growth medium. Just before recordings, the medium was removed and replaced by typically 250 μl of PBS⁻ (Dubelco, Invitrogen). Ligands were added to PBS⁻ from stock solution in ethanol. These solutions were vortexed for 5s before application to cells (1:1 in relation to the volume of sample). Sometimes cells were seeded on 8-wells LabTek chambers (NUNC) for labeling experiments.

For particular experiments, glass slides were coated with fibronectin (Sigma-Aldrich) to improve cells adherence.

Confocal microscopy was performed using a Zeiss LSM 510 with the adequate set of filters for such wavelengths (HFT 458; HFT488/543; HFT488/543/633; NFT 570; LP 475; BP 505-550; LP650).

Plate Reader

Plate Reader experiments were performed with a “Flexstation” (Molecular Devices).

Cells were splitted the day prior to experiment and seeded at 350000 cells/ml on 96 multi-wells plates (Wallac). At the day of the experiment, ligands

were added to 96 multi-wells plates (Wallac) at a concentration of twice than the desired concentration. Cell medium was replaced by PBS⁻ prior to the experiment. The fluorescence measurements were performed while adding cell suspension to the buffer in the microplates. Raw data was extracted and analysed with IgorPro software.

Flow Cytometry

For flow cytometry measurements, cells were collected, resuspended in PBS⁻, aliquoted and stored on ice. Cells were incubated with ligands at the desired concentrations for 30 min. Cells were then pelleted, supernatant discarded, and resuspended in fresh ice cold PBS⁻. Aliquots were maintained on ice until analysis.

Flow Cytometry measurements were performed at the Flow Cytometry Core Facility at EPFL using a CyAn ADP analyser from Beckman Coulter. Results were analyzed with Summit software (Dako).

Chapter 4

The next sections will focus on the importance of μ CP in bioanalytics for example to position receptors, miniaturize nuclear magnetic resonance measurements using planar microcoils, to immobilize functionalized nanoparticles on surfaces as biomolecular recognition tools, or to immobilize native vesicle to investigating transmembrane signaling.

4. Surface Functionalization by Micro-Contact Printing

Within the framework of computer chip production novel technologies were developed to microstructure a flat silicon surfaces (Gates, Xu et al. 2005), which are meanwhile used in many different field such as bioanalytics. One of the best known examples is photolithography, which uses a photoresistive mask to microstructure silicon surfaces. Thereby a silicon master is produced which serves as a template to produce a polymer stamp for soft lithography. Soft lithography involves the use of elastomers, such as polydimethylsiloxane (PDMS). They are cast as a liquid on the master and after curing they transform in an elastic polymer that can be peeled away easily from the master. Their structure is of course the negative replica of the master. The development of soft lithography enables the reproduction of numerous microstructures at low cost and their application for micro-contact printing (μ CP), microchannel production, or even formation of optical elements (Xia, Kim et al. 1996). PDMS offers a number of optimal properties after curing: (i) the polymer has a low surface energy, which

facilitates to remove it from the master and deposit it to other solid surfaces; (ii) it is optically transparent at wavelengths above 300 nm; (iii) it is thermally stable up to 150°C; (iv) it is chemically inert.

μ CP is widely used to micropattern solid surfaces with biopolymers, proteins or DNA/oligonucleotides. Thereby the PDMS stamp is inked by a solution of the biopolymer of interest, then the excess of the solution is removed and the rest forms a thin film on the PDMS structure. When the stamp is placed in contact with another solid surface, usually glass, the protein for example covering the contact area is transferred to the support. Examples are the micropatterned deposition of proteins, such as fibronectin or collagen, providing a specific interaction with integrins, or polylysine providing positively charged surfaces (Yeung, Lauer et al. 2001) for cellular adhesion (Cuvelier, Rossier et al. 2003; Rozkiewicz, Kraan et al. 2006). Combined with complementary cell-repellent surface micropatterns it is possible to control cell growth (Suh, Seong et al. 2004) or cell-cell contact formation (Chang, Brewer et al. 2006) with micrometer precision. The growth of cells on micropatterned or microstructured surfaces is of importance to permit study of intercellular interaction and communication (Kam, Shain et al. 2001; Lauer, Vogt et al. 2002; Vogt, Lauer et al. 2003; Vogt, Brewer et al. 2005). μ CP also provides interesting possibilities for co-culturing different cell types (Fukuda, Khademhosseini et al. 2006) to investigate complex intercellular communication modulated by release of signaling, such as neurotransmitters. Immobilization of cells or cell fragments on micropatterned surfaces, in combination with microfluidic networks opens novel ways to develop biosensors or bioanalytical devices (Cuvelier, Rossier et al. 2003). Hurdles have to be overpassed to realize such devices (i) non-specific interactions which could lead to unspecific cell adsorption must be avoided; (ii) unspecific adsorption of proteins from the culture media, or freshly synthesized by cells has

to be suppressed.

In this context, the extracellular surface of a living cell has to be considered. A live cell typically synthesizes different sugars that are attached to the extracellular side of plasma membrane proteins and lipids. The sugars surrounding the cellular membrane, especially present in endothelial cells, form the glycocalyx (Reitsma, Slaaf et al. 2007; Weinbaum, Tarbell et al. 2007), which has two major functions. They form a repellent barrier against other cells and they interact with many different extracellular matrix proteins, cell adhesion molecules, growth factors and even receptors.

In our laboratory, arrays of artificial vesicles were immobilized on micropatterned surfaces and were as individual entities to control and observe biochemical reactions in closed containers (Stamou, Duschl et al. 2003; Bolinger, Stamou et al. 2004). The immobilization techniques used were based on the specific interaction between biotin and streptavidin, neutravidin or avidin. Such interactions are among the strongest between molecular with a ΔG^\ddagger of 24.8 kcal/mol (Hyre, Le Trong et al. 2006). The three biotin-binding proteins have a similar structure composed of four subunits each presenting one binding site for biotin. They differ mainly by their isoelectric point, which is 5, 7 and 10.5 for streptavidin, neutravidin and avidin, respectively. Thus it is possible to choose a particular protein according to the surface charge one would like to reach on the sensing surface. Non-specific protein adsorption was reduced by adjusting the surface charge of the liposomes, accordingly via the lipid composition, and by adding about 0.5% of poly(ethylene glycol) (PEG) comprising lipid. PEG is known to reduce unspecific protein absorption (Satomi, Nagasaki et al. 2007).

4.1 Immobilization of Liposomes for NMR Measurements

Results in this section were obtained in collaboration with Dr. Klaus Ehrmann from Microsystems Design Group of Prof. Popovic at EPFL. Here will focus on the precise positioning of a sample at planar microcoils. Details on the technical aspects of micro-NMR are described elsewhere (Ehrmann, Gersbach et al. 2006).

Downscaling analysis is of interest in many diverse fields and was explored here for NMR. Conventional NMR typically performed in sample volumes of a million to microliters using tubes or capillaries placed in a solenoidal coil. Prof. Popovic's laboratory at the EPFL developed planar microprobes (figure 4.1), comprising microcoils embedded in a SU8 polymer. With these microcoils it is possible to record high resolution NMR spectron of small sample volumes.

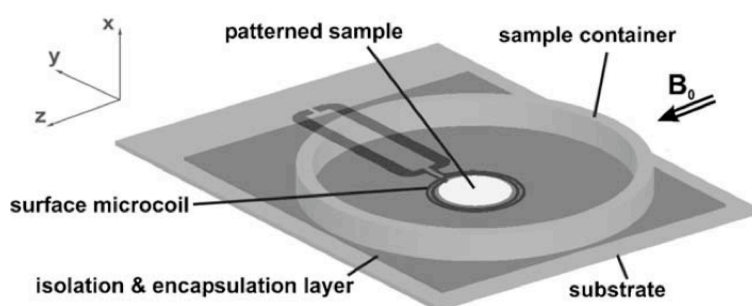


Figure 4.1: NMR microcoil probe embedded in a SU8 polymeric support. The sample container is made of PMMA.

The sample has to be positioned exactly in the center of the microcoil, where magnetic field (B_1) is homogenous, in order to reach high sensitivity. Here liposomes were immobilized in the center of the coil to confine the chemical sample precisely inside the liposome. Neutravidine was shown to have a better

affinity to SU8 than the other investigated proteins (BSA-biotin, streptavidin, avidin and neutravidin). Direct stamping of neutravidin provides an adhesive surface able to immobilize biotinylated liposomes (figure 4.2). The biotin-avidin recognition was tested to immobilize liposomes on the polymer SU8 surface. No surface passivation of SU8 was required as the unspecific absorption of liposomes was quite low.

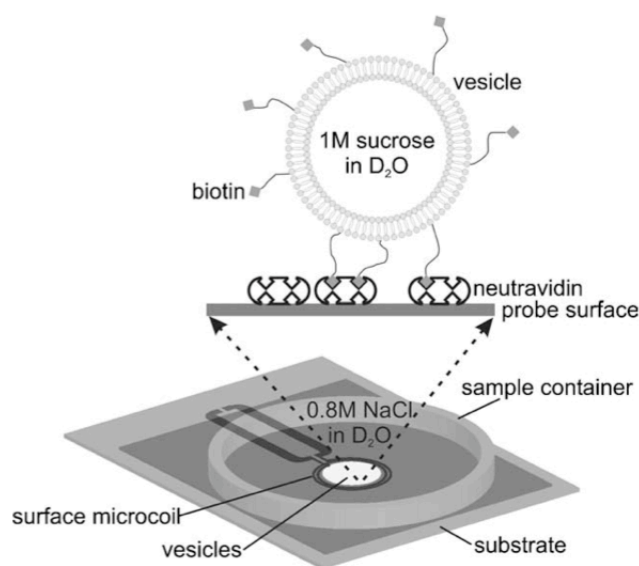


Figure 4.2: Experimental concept of liposomes immobilization on a neutravidin monolayer stamped on a SU8 substrate surface.

To test the influence of immobilization pattern on the sensitivity of the measurements, liposomes were immobilized according to three different pattern areas (figure 4.3). To achieve precise positioning, a micromanipulator was required to handle stamps inked before with neutravidin. In figure 4.3a, the liposomes were homogeneously distributed on the surface. In figure 4.3b avoided liposome were excluded from the area above the microcoil turns, where the B_1 -field was very inhomogeneous. In figure 4.3c, liposomes were only immobilized in the central region of the microcoil, where the B_1 -field shows highest homogeneity. The liposomes contained a solution of 1M sucrose in deuterated PBS. They were dialyzed against an iso-osmotic solution of 0.8 M sodium chloride in deuterated

PBS.

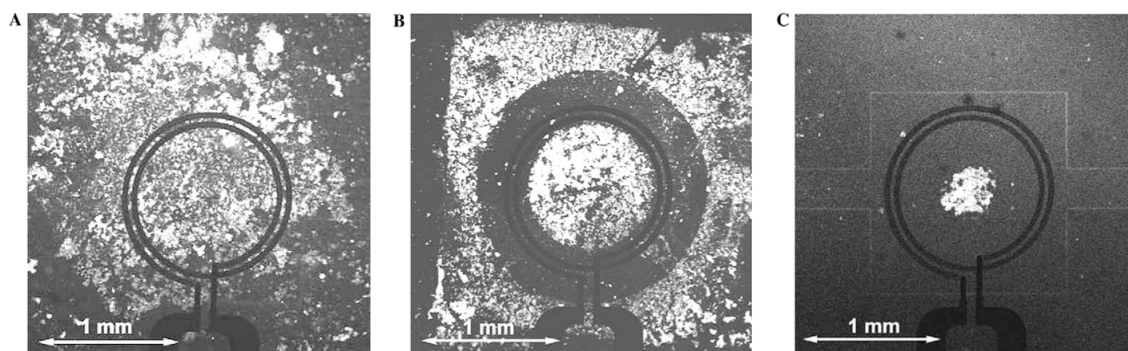


Figure 4.3: Liposomes immobilized via biotin-neutravidin interaction. Three patterned areas (A: homogenous; B: avoiding immobilization above coil; C: centered to microcoil) were used to test the influence of patterning on the measurement sensitivity. The diameter of the patterned area inside the microcoil was 920 μm in B and 440 μm in C. Liposomes contained 0.1% of a rhodamine labeled lipid in order to be visualized by fluorescence.

Figure 4.4 shows an NMR spectrum of ^1H -glucose taken with the microcoils. The biggest peak in the sucrose spectrum originates from the resonance of the H-6 protons of the glucose ring and the two protons in the fructose ring. This major peak is located at 3.8 ppm. A second peak appears at 5.4 ppm and is related to the anomeric proton in the sucrose molecule. This sucrose spectrum was obtained after immobilization of liposomes at the center of the microcoil.

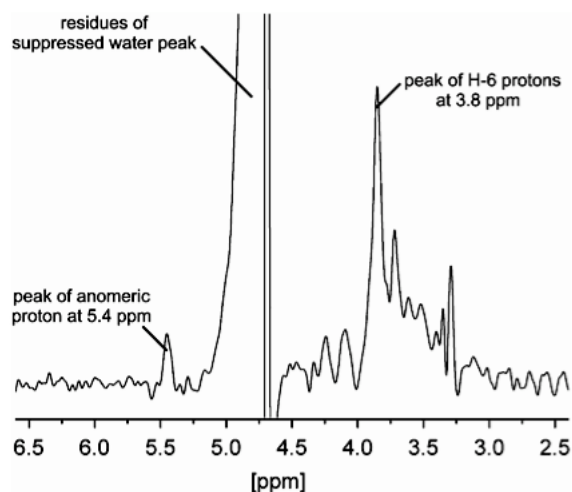


Figure 4.4: ^1H spectrum of sucrose confined in liposomes immobilized at the center of the microcoil. The signal to noise ratios of the H-6 peak and the anomeric proton are 9 and 2 respectively after 512 acquisitions without signal treatment. The original free induction decay (FID) data is multiplied by a Lorentz-Gauss weighting function, giving rise to a Gaussian lineshape. The baseline is corrected.

To test spin excitation uniformity, the signal to noise ratio of the H-6 proton peak was taken at each excitation time after 512 acquisitions. In a completely homogenous B_1 -field, the nutation curve follows a sinusoidal function. In an inhomogeneous B_1 -field, the superposition of different rotation frequencies results in a loss of sinusoidal behavior for high excitation times. Measured and modeled nutation curves from these patterned areas (figure 4.5) demonstrated that sample positioning was of major importance for the obtaining of spin excitation uniformity in regions of higher B_1 -field homogeneity. Performance characteristics are resumed in table.

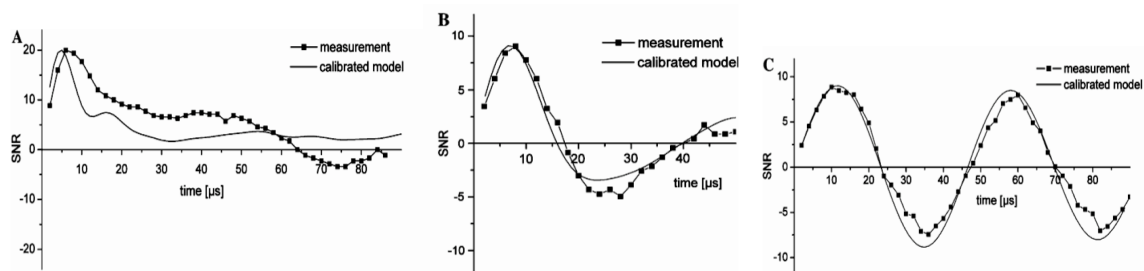


Figure 4.5: Measured and modeled nutation curves of the H-6 proton of sucrose confined in liposomes for the three pattern areas.

	Detection volume (nL)	Measured LW (Hz)	Measured SNR ($n_{acq} = 512$)	Measured $S@450^\circ/S@90^\circ$ [%]
Water in sample container	900	4.3	4700 ($n_{acq} = 1$)	—
Sucrose (H-6 peak) in vesicle—pattern (A)	1.9	15	20	(30) ^a
Sucrose (H-6 peak) in vesicle—pattern (B)	1.0	15	9	10
Sucrose (H-6 peak) in vesicle—pattern (C)	1.2	15	9	90

^a Pattern (A) does not show sinusoidal behavior and therefore $S@450^\circ/S@90^\circ$ cannot be taken as a reliable indicator for spin excitation uniformity.

Table 4.1: Performance characteristics of the NMR spectrum of sucrose in surface immobilized liposomes to pure water as a reference.

These results demonstrate the downscaling of NMR analysis to picoliter volumes using a microcoil probe. The improvement of the spin excitation uniformity, when the sample is immobilized in the center of the microcoil, is due to the homogenous B_1 -field. The signal to noise ratio is in the range of conventional solenoidal coils and demonstrating that NMR experiments with extremely low sample quantities are feasible. This technique opens new possibilities for NMR analysis.

4.2 Nanoparticles for Surface Functionalization

In order to visualize micropatterns obtained by μ CP, we used highly fluorescent and photo-stable streptavidin-coated quantum-dots (QDs) (Lin, Cui et al. 2003; Baumle, Stamou et al. 2004) (figure 4.6), enabling long term imaging (Katz and Willner 2004). Hybridization of complementary oligonucleotides was

used to test the functionality of streptavidin-coated QDs. One strand was biotinylated and its complementary was fluorescently labeled with Alexa 654, whose fluorescence showed a different fluorescent than the QDs. Arrays of 2 μm dots of streptavidin-coated QDs monolayers were microcontact printed on glass. The μCP QDs were incubated with the biotinylated oligonucleotides first, and after several washing steps necessary to remove the excess of unbound oligonucleotides, hybridization with the complementary oligonucleotides was performed (1 nM in PBS around 60°C to ensure a good annealing) (figure 4.7). Fluorescence intensities demonstrating that oligonucleotide hybridization was performed by perfect annealing.

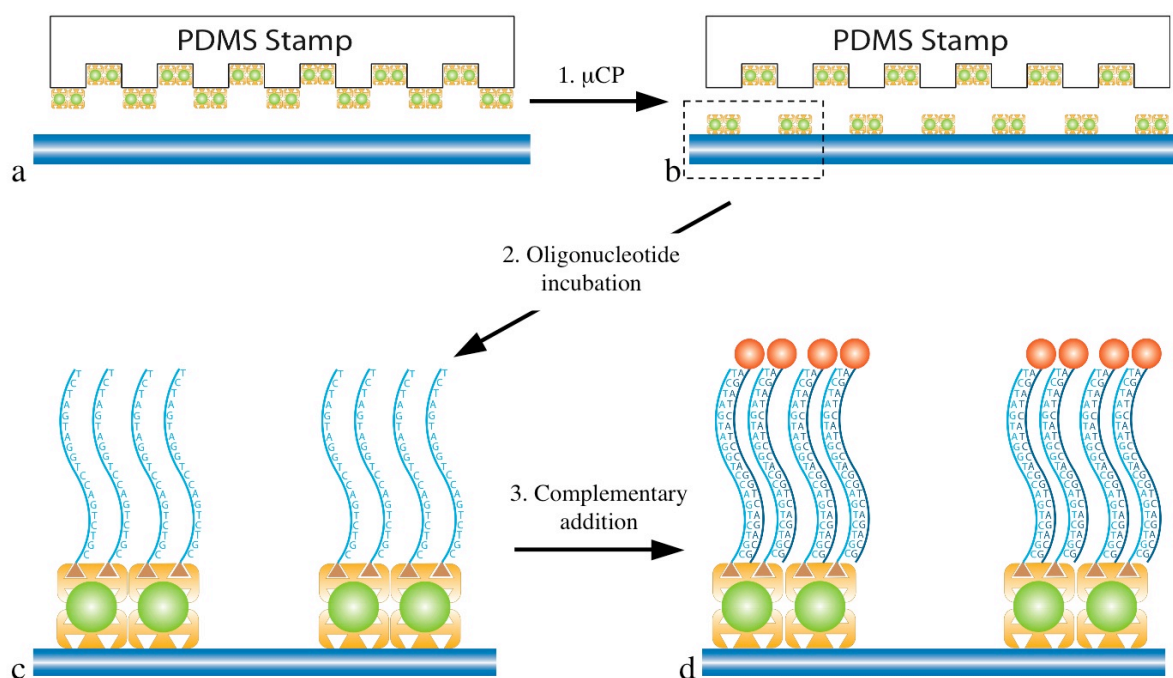


Figure 4.6: Scheme of oligonucleotides hybridization after μCP of streptavidin-coated QDs on glass surface.

As negative control, two experiments were performed. (i) Micropatterned streptavidin was first incubated with free biotin, then with biotinylated oligonucleotides and subsequently with labeled complementary strand. (ii) The

micropatterned streptavidin was incubated with the biotinylated oligonucleotides for hybridization with an identical non-labeled strand; after extensive washing, a complementary fluorescently labeled oligonucleotide was added. Both experiments show no fluorescent micropatterns. These experiments demonstrate that hybridization occurs specifically and that no unspecific interaction with streptavidin or with the oligonucleotides can be detected. The images of the micropatterns from the two different fluorescence channels superpose nicely showing that extensive arrays can be performed with efficient hybridization (figure 4.7).

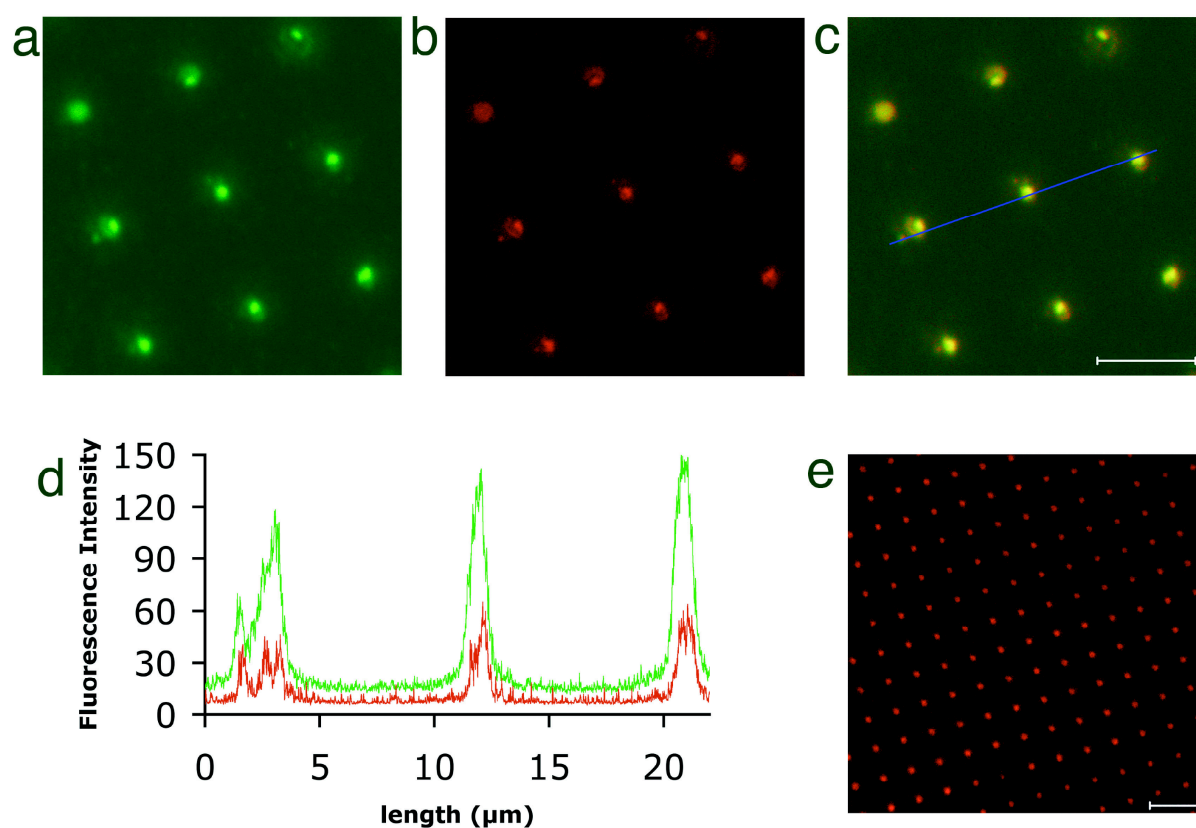


Figure 4.7: (a) Arrays of fluorescent QDs coated with streptavidin obtained by μ CP on a glass slide (ex: 488 nm; em > 560 nm). (b) same array as before, now after new hybridization of complementary labeled oligonucleotide (ex: 633; em: 648). (c) Superposition of both channels shows perfect colocalization. (d) Fluorescence intensities profile of green and red fluorescence channels obtained from a line seen

across the micropatterns (c). (e) Enlarged QD array. Scale bar represents 10 μm in panel (a - c) and 20 μm in (e).

Plotting the ratio of both fluorescence intensities, obtained from the depicted hybridization experiment, shows a homogenous ratio distribution in the central area of the spot. Some deviations are only observed in the lateral area of the spots, where ratio demonstrates to not be well correlated (figure 4. 8).

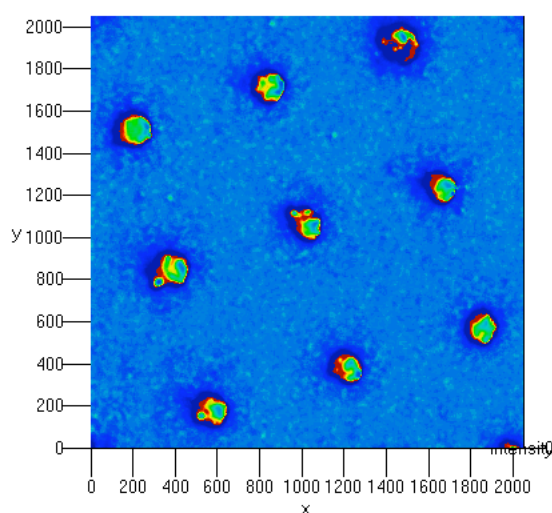


Figure 4.8: Ratio plotting of both fluorescence intensities demonstrates a good homogeneity at the center of the spot (green color), demonstrating a correlation of both signals.

These extended arrays would provide sensitive means to detect DNA hybridization below the nanomolar range. The sensitivity to detect QDs could be further improved by excitation in the UV. Our arrays provide a general platform, without requiring the use of double labeled strands as used on the past resulting in reduction of costs, for DNA screening in gene expression assays (Niemeyer

2004), for medical diagnostics applications (Niemeyer 2004). These arrays could also be used to immobilize liposomes or native vesicles with the advantage to follow the efficiency of μ CP and directly follow the specific attachment from colocalization.

4.3 Immobilization of Native Vesicles in Micro-Arrays

Downscaling bioanalytics to the (sub)micrometer scale offers interesting opportunities for screening purposes. Micro-arrays of native vesicles offer attractive capabilities in fundamental research as efficient platform for investigating the function of membrane proteins, for example by screening, for investigating signaling cascades and their regulation, for biosensor development or even for tissue engineering. Native vesicles could then be analyzed as individuals or as ensembles. In the course of the following experiments native vesicles turned out to be far more difficult than for the case of artificial vesicles (shown in section 4.1). This reflects the higher complexity of native vesicles that contain a high concentration of many different proteins as well as a glycocalyx. In the following section, strategies are developed to immobilize native vesicles with high spatial precision on glass surfaces.

4.3.1 Immobilization Via Biotin-Streptavidin Interaction

(1) The first approach to form microarrays of native vesicles uses the specific interaction between biotin and streptavidin (see section 4.1). Here protocols had to be developed to biotinylate the surface of native vesicles. The strategy was to use biotinylated lipids in detergent micelles, below the CMC

(critical micelle concentration) of the micelles and thereby insert the biotinylated lipids in plasma membrane of life cells. The lipid used contains a short aliphatic spacer between its head group and the biotin to increase both the distance of biotin from the cell surface and the mobility of biotin. This spacer was optimized for efficient interaction with streptavidin. The protocol for lipid insertion in lipidic membranes was previously established in our laboratory. To test the insertion of such lipid on HEK cells, a lipid mixture 1:1 of DHPE-biotin with a fluorescently labeled lipid analog, DHPE-Oregon Green (DHPE-OG), was used. Subsequent labeling with a fluorescent streptavidin demonstrated efficient insertion even in the small cellular filipodia (figure 4.9). Fluorescently labeled lipids were observed after 60 minutes also inside the cells, demonstrating that they enter via endocytic routes. Biotinylated lipids are probably also subjected via the same internalization route but could not be accessed by streptavidin and thus were not labeled. This also shows that cell viability is not affected by this lipid insertion procedure. Thus the surface of living cells can be biotinylated prior to the formations of native vesicles. Alternatively native vesicles can be biotinylated in a similar way after their production.

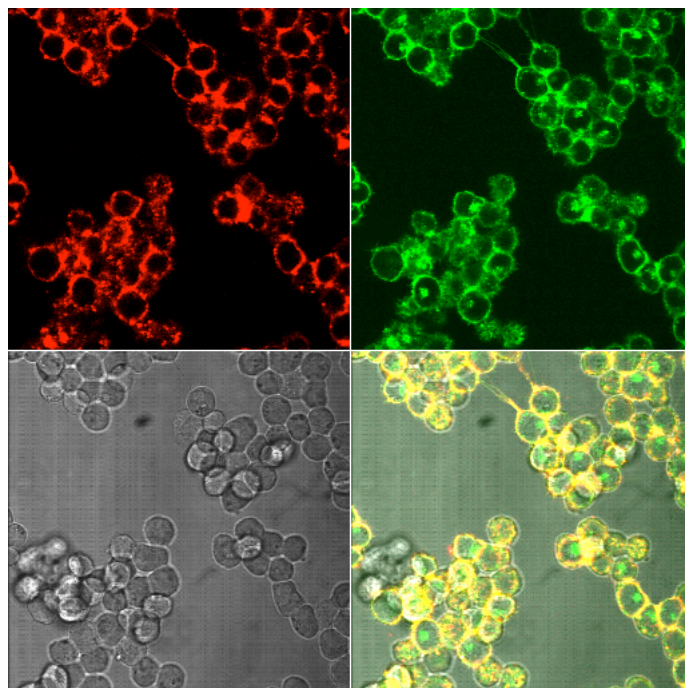


Figure 4.9: A 1:1 mixture of biotinylated and fluorescently labeled lipids was added to a culture of live HEK cells and then incubated for one hour. DHPE-OG (green) incorporates into the cellular plasma membranes. Subsequent labeling with streptavidin-Alexa 568 (red) is demonstrated by perfect colocalization at the cellular membrane (yellow). In the same image DHPE-OG shows been incorporated into the cells following endocytic pathways and can be seen only green in the colocalization (green spots inside the yellow cells).

This procedure outlined before offers the advantage that the inserted, biotinylated lipids remain mobile in the plasma membrane and can thus form multiple attachment sites when placed in contact to a streptavidin-coated surface.

(2) Another biotinylated lipid was tested, the PE-PEG₂₀₀₀-biotin, in order to avoid unspecific attachment of native vesicles to the solid support. It carries a polymeric PEG chain which should suppress unspecific binding of the vesicles to the solid support. This lipid can be solubilized in ethanol and a simple addition (1000 x dilution) to a native vesicle preparation is sufficient for its incorporation.

The overall ethanol concentration always remained below 1‰ to avoid undesirable effects on native vesicles integrity. This lipid inserts in the plasma membrane as DHPE-biotin and shows efficient binding of fluorescently labeled streptavidin.

(3) Another biotinylation procedure was investigated using acyl carrier protein fusions (ACP) (George, Pick et al. 2004). Here, labeling occurs via the recognition of a specific sequence by the enzyme PPTase (phosphopantetheine transferase) and subsequent ligation to a substrate, which is a coenzyme A-labeled moiety (figure 4.10). This moiety can be a biotin or a fluorescent label. The major advantage of this procedure is that a particular protein on the cell or native vesicle surface can be labeled selectively, which can give rise to the realization of more specific arrays. This protocol presents the disadvantage of requiring a sufficient expression level and perfect membrane localization.

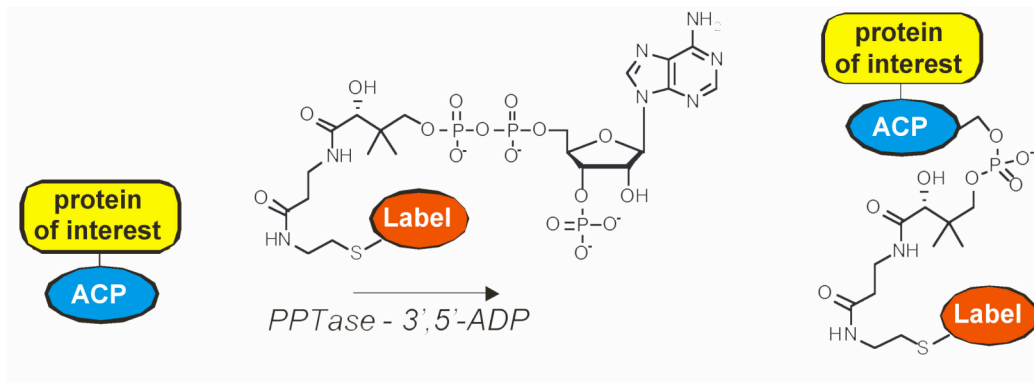


Figure 4.10: ACP-labeling with the fusion protein of interest and his modified substrate by PPTase enzyme. This modified substrate can be a biotin (Meyer, Martinez et al. 2006).

(4) Biotinylation procedure tested the reactive compound NHS-biotin (N-Hydroxysuccinimide-Biotin), which reacts with primary amine groups on proteins

or lipids at pH 7-9. This labeling gives rise to covalent attachment of biotin at cell or vesicle surfaces.

In fact native vesicles can interact strongly in all described procedures a major problem remained that the native vesicles showed relatively high unspecific binding to all the different investigated surfaces, such as those coated with bovine serum albumin (BSA) streptavidin, neutravidin or avidin, with or without a previous biotinylation step (figure 4.11). The use of PE-PEG₂₀₀₀-biotin shows similar results.

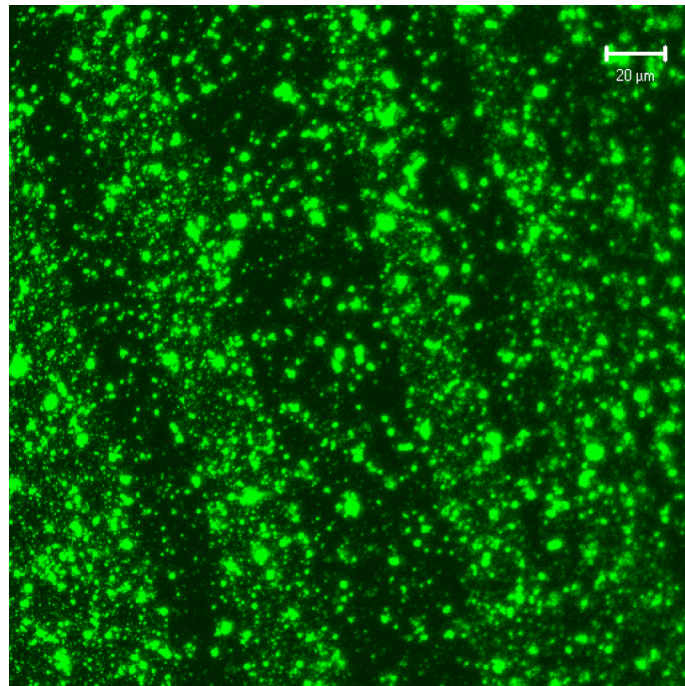


Figure 4.11: Testing unspecific binding of native vesicles. BSA-biotin was first stamped by μ CP, the non-stamped areas were coated with BSA and finally incubated with streptavidin, which specifically bind on BSA-biotin stamped regions. Native vesicles expressing EGFP-NK₁R biotinylated with DHPE-x-biotin were immobilized on the surface. Although native vesicles showed a higher affinity to bind to the streptavidin printed areas, there is relatively high unspecific binding to the BSA even.

As streptavidin, neutravidin and avidin can differently tune surface apparent electrical charge, this shows that electrostatic forces do not dominate native vesicles interactions with surfaces. Despite unspecific and probably due to glycocalyx (Mehrishi and Bauer 2002), such interactions were strong enough to maintain native vesicles immobilized even after extensive washing steps. Besides these interactions, native vesicles can interact also with adhesive expected surface such a poly-L-lysine (PLL), mainly by electrostatic interaction or/and membrane direct insertion. Specific adhesive interactions can also be achieved by lectins (Zheng, Peelen et al. 2005), such as wheat germ agglutinin (WGA) or concanavalin A, by interactions with membrane surface sugars. In fact, HEK cells demonstrate efficient surface labeling with fluorescently labeled lectins (figure 4.12).

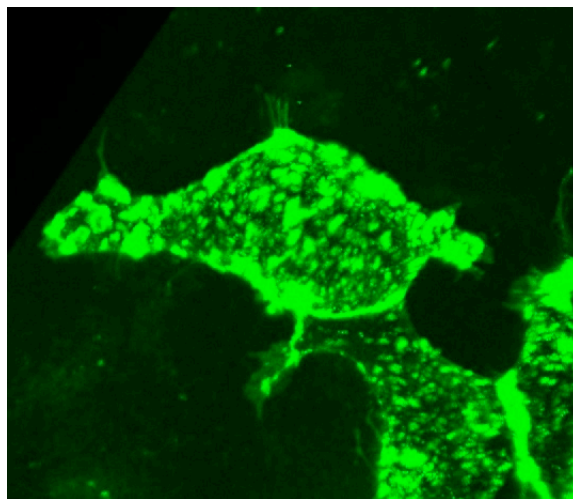


Figure 4.12: HEK cells labeled with a lectin mixture (1:1 WGA-A488 and concanavalin A-FITC) demonstrates high plasma membrane sugar content. Image extracted from an Imaris Software 3D reconstruction from confocal data.

Taken together, the results of this section show that native vesicles can interact with different surfaces both specifically and unspecifically. Cells as well as native vesicles can be efficiently biotinylated with various methods and show good recognition for streptavidin stamped surfaces accompanied by a high unspecific binding. The remaining challenge is then to find efficient repulsive surface treatments in order to suppress unspecific binding.

4.3.2 Suppression of Unspecific Attachment

To solve the problem of unspecific binding of native vesicles on the glass surface, several strategies for surface treatments have been investigated. There are several published reports to avoid non-specific protein adsorption to surfaces. PEGylated polylysine was reported (PLL-g-PEG) to suppress unspecific protein adsorption (Csucs, Michel et al. 2003; Rossetti, Reviakine et al. 2004). The PLL-PEG copolymer offers the possibility to adjust during synthesis the PEG-content, which allows to control the surface density of grafted PEG chains. The length of PEG chain can also be tuned. Here we tested only one type of such polymer, PLL₂₀₀₀₀-g[3.4]-PEG₂₀₀₀, resulting in an inefficient suppression of unspecific adsorption of native vesicles. This could be explained by a non-ideal grafting ratio or an unadapted ionic strength of the medium. All experiments were performed with physiological PBS-buffer and variation of the ionic strength of the medium was not envisaged.

Another recently reported deposition method termed decal-transfers or light stamping lithography (Park, Seo et al. 2006), allows the creation of patterns by deposition of PDMS. PDMS stamps are put in contact with the surface of a solid support and activated by UV light irradiation for at least 2 min. This reaction induces a strong adhesion of the PDMS to the surface, in this case glass.

When the stamp is physically peeled off from glass, a micropatterned hydrophobic layer of PDMS remains, and did not avoid unspecific attachment of native vesicles.

Finally the following protocol gave good results to produce repulsive surfaces for native vesicles, was the deposition of artificial vesicles composed of DPPC (1,2-Dipalmitoyl-sn-glycero-3-phosphocholine (16:0) PC)). Once produced such liposomes were extensively sonified above the melting temperature in order to form extremely small unilamellar. When placed in contact to a glass surface, they cover it creating non-adherent regions with good resistance to native vesicles deposition. This favorable technique was then used to coat the non-stamped regions besides BSA-micropatterns, in order to create repulsive surfaces. In this approach, each step could be separately followed by fluorescence microscopy using labeled molecules (figure 4.13). First BSA-biotin micropatterns were formed by μ CP, and the non-stamped areas were completed by adsorbing DPPC vesicles labeled with a C₁₈-Cy5. A photobleaching experiment demonstrates a good coverage of areas even those where BSA-biotin was previously stamped. Further incubation with streptavidin-fluorescein shows good colocalization, demonstrating that biotin remains accessible even in the presence of DPPC vesicles TM. This tends to demonstrate that the artificial vesicles do not rupture to form a bilayer but probably conserve their spherical shape. This is the result of using vesicles below the lipid phase transition. A further labeling with biotin-Alexa546 demonstrates that streptavidin remains fully active and accessible for subsequent attachment. Similar experiment realized with DOPC artificial vesicles, clearly demonstrates that the use of a lipid above the lipid phase transition, induces formation of a lipid bilayer able to recover BSA-Biotin stamped surfaces and impairing furthermore accessibility of the streptavidin.

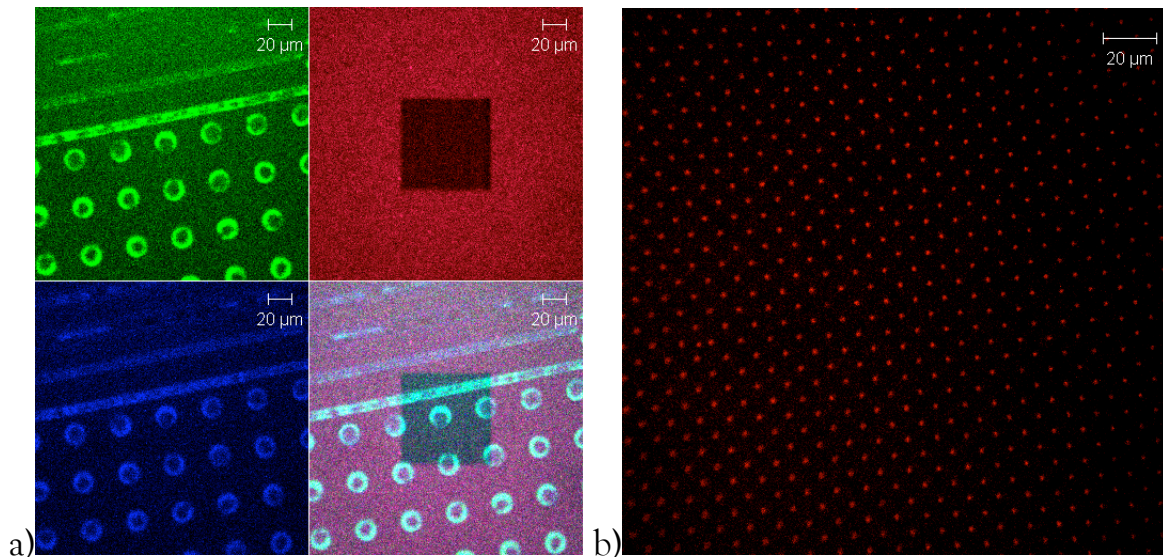


Figure 4.13: (a) shows the diverse steps of creation of 3D assemblage. BSA-biotin was previously stamped on glass surface by μ CP. The backfilling was realized with DPPC artificial vesicles labeled with C_{18} -Cy5 (red). The photobleaching step can be seen as a darker square. Streptavidin-fluorescein (green) could still bind to stamped BSA-biotin with good colocalization. A last incubation with Biotin-Alexa546 (blue) demonstrates that streptavidin remains fully accessible. (b) shows extensive pattern arrays created by similar protocol.

In summary, the first approach using PLL-g-PEG did not suppress unspecific vesicles adsorption and was therefore not further investigated. The protocol using adsorption DPPC vesicles protocol provided an interesting result to form native vesicles arrays with high contrast to the surface background. Unfortunately, biotinylated native vesicles do not demonstrate to be extensively immobilized on such kind of patterns, probably due to sterical hindrance of the glycocalyx. Such results remain surprising and further investigation should be applied to clarify such non-interaction. The diverse combinations between biotinylation protocols and recognition molecules were not fully investigated and still deserve some further investigations.

4.3.3 COMB Polymer for Suppressing Unspecific Vesicles Adsorption

COMB polymer, kindly provided by Prof. Chilkoti, was reported to avoid cell attachment for extensive time period in culture conditions (Ma, Hyun et al. 2004). This copolymer is composed of a poly(methyl methacrylate) backbone (PMMA), extensively modified with hydroxy- poly(oxyethylene) methacrylate (HPOEM) and poly(oxyethylene) methacrylate (POEM) side chains (figure 4.14), thus called combinatory polymer.

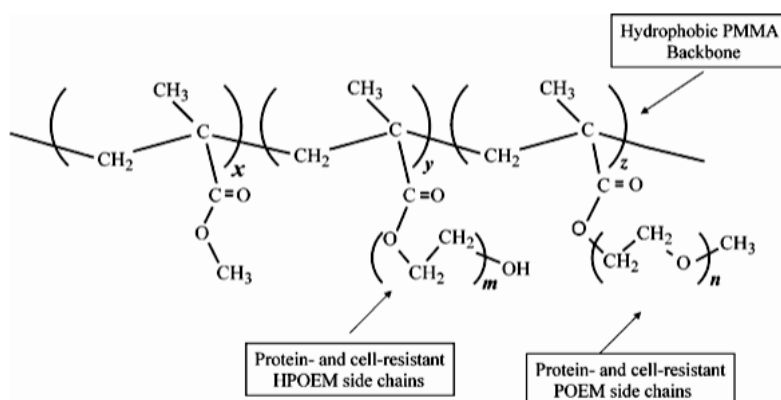


Figure 4.14: COMB polymer structure.

The PDMS stamp was first spin-coated with this polymer and then contacted to a glass plate. The glass can be incubated before with a protein or polymer of interest. A backfill with the protein of interest after COMB polymer stamping is also possible. Native vesicles demonstrate to be best immobilized on BSA, fibronectin or concanavalin A after washing steps. Native vesicles immobilization on BSA might be due to van der Waals forces. Concanavalin A interacts with native vesicles via cell surface sugars and fibronectin through specific integrin receptors probably present in the membrane of native vesicles.

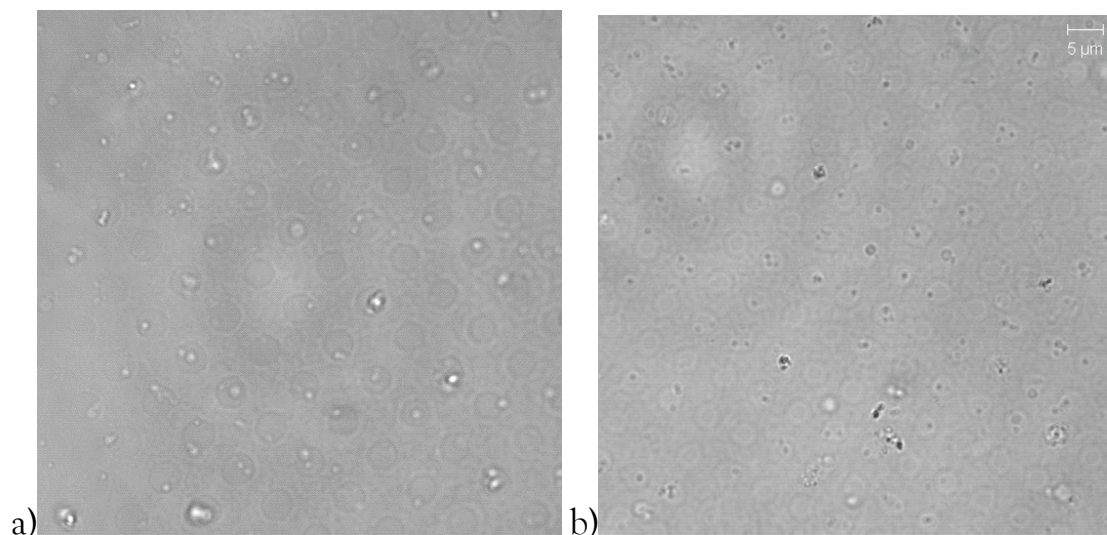


Figure 4.15: Native vesicles were extensively immobilized on proteins even after successive washing steps. (a) μ CP COMB polymer structured surface backfill with BSA, leading to unspecific adsorption of native vesicles. (b) μ CP COMB polymer structured surface backfilled with concanavalin A, leading to specific attachment by cell surface sugar recognition

When such kinds of arrays were filled with native vesicles expressing fluorescently labeled proteins, such as EGFP-NK₁R, fluorescent arrays could be obtained (figure 4.16).

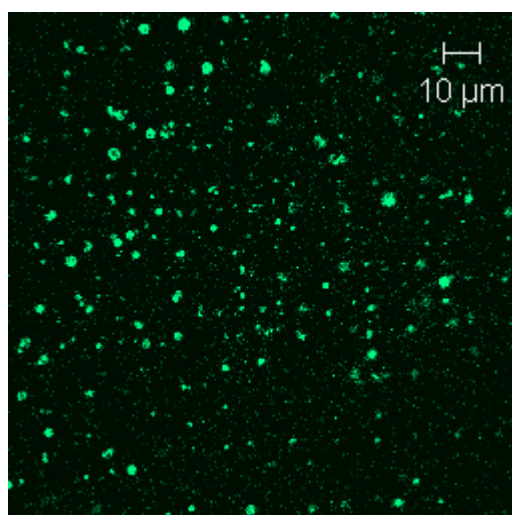


Figure 4.16: Native vesicles expressing EGFP-NK₁R immobilized on a BSA incubated surface on which an array was created by deposition of COMB polymer.

A similar experiment using native vesicles containing CFP-5HT₃R yielded immobilized vesicles on the COMB polymer array backfilled with fibronectin. To these native vesicle arrays it was possible to bind specifically first 5 nM GR-Cy5, the 5HT₃R antagonist, and a further increase can be observed after a second 20 nM addition. The receptor found GR-Cy5 could be replaced in a competition, experiment by adding excess of quipazine in presence GR-Cy5, a 5HT₃R partial agonist as monitored by a concomitant decrease of fluorescence. Such recordings were monitored by confocal microscopy and both signals from receptor and ligand were constantly recorded on two separated channels. Analysis of 13 native vesicles by hand made regions of interest (ROIs) and with one ROI without any vesicle to settle the background value. The averaged data are presented in figure 4.17. The time course of the fluorescence intensity fitted by an exponential equation: $y = y_0 + A \cdot \exp^{-invTau \cdot t}$.

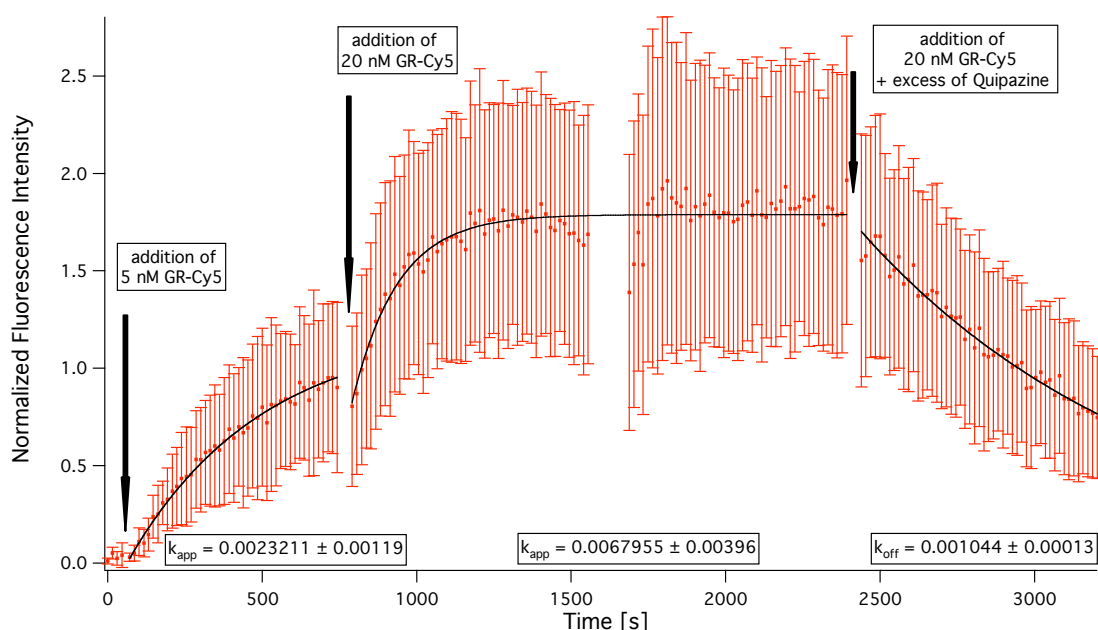


Figure 4.17: Average of 13 native vesicles measurements. Native vesicles expressing the 5HT₃R-CFP were successively labeled with 5 and 20 nM GR-Cy5 and finally competition was achieved with an excess of quipazine.

$k_{app} = k_{on} \times [Ligand] + k_{off}$, where k_{app} and k_{off} were obtained from the fitted data by the equation: $y = y_0 + A \exp^{-invTau-1}$, in the association and dissociation phase, respectively. k_{on} was then calculated and gives the K_D values of 4.09 ± 3.83 nM and 3.63 ± 2.54 nM in relation to k_{app} of 5 and 20 nM, respectively. The real K_D value of GR-Cy5 is of 15 nM and the obtained value is thus in the order of magnitude expected. Other reports performed with radioligand binding or GR-Fluorescein demonstrates lower K_D values (Miller, Weisberg et al. 1992; Tairi, Hovius et al. 1998), closer to the obtained result. These results tend to demonstrate that microarrays of immobilized native vesicles are suited to characterize the function of membrane proteins quantitatively.

4.3.4 Hyaluronic Acid for Suppressing Unspecific Vesicles Adsorption

Hyaluronic acid (HA) is one of the major constituents of the extracellular matrix and is known to be an excellent repulsive surface to suppress cellular adhesion (Richert, Lavallo et al. 2004; Fukuda, Khademhosseini et al. 2006). Spin coated HA on glass surface allows additional μ CP of PLL on top, resulting in surface microstructuring. Here we micropatterned PLL-FITP. Native vesicles labeled with C_{18} -Cy5 demonstrate a very good specificity for PLL stamped regions with almost no unspecific bonding (figure 4.18). When the stamped PLL region is sufficiently large, several vesicles can bind to it. This protocol allows the creation of large arrays.

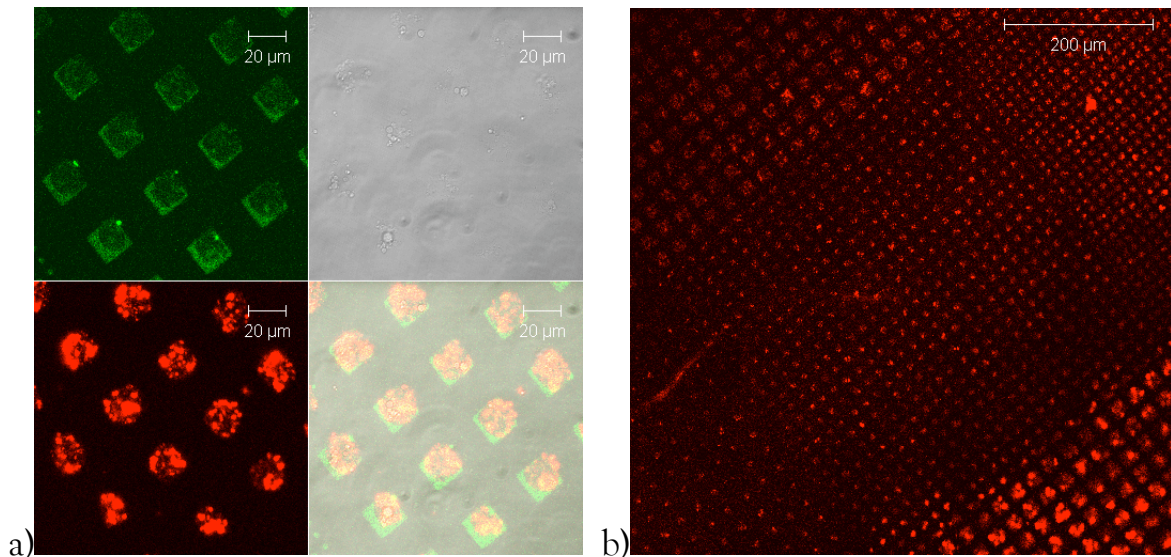


Figure 4.18: (a) Glass surface spin-coated with HA polymer and then μ CP with PLL-FITC. Further incubation with native vesicles labeled with C_{18} -Cy5 demonstrates very specific attachment. (b) Extended arrays of native vesicles created by this protocol.

Native vesicles can be immobilized on glass slides in form of large arrays. Such immobilized native vesicles produced from HEK expressing the α_{1B} -adrenergic receptor were investigated for their function to bind the adrenergic receptor antagonist Prazosin-Bodipy 558/568. The binding of the fluorescent antagonist to individual vesicles was monitored by fluorescence microscopy and the averaged fluorescence time-trace from 27 vesicles delivered his signal to noise kinetic data of the ligand-receptor interactions (figure 4.19).

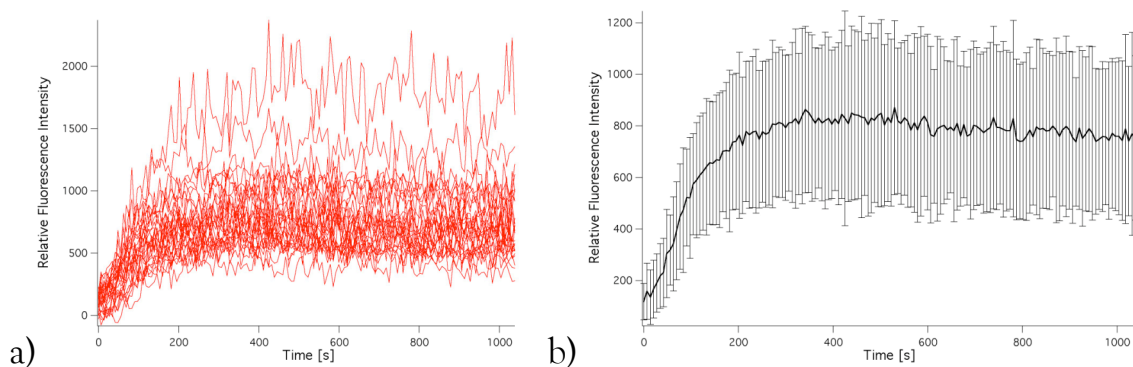


Figure 4.19: Native vesicles derived from HEK cells expressing the α_{1B} -adrenergic receptor were immobilized on a glass slide and investigated by fluorescence confocal

microscopy. (a) Fluorescence (exc. 514 nm, em. 568 nm) versus time on individual vesicles after addition of 100 μM of Prazosin-Bodipy 558/568 shown as traces of X vesicles. (b) Fluorescence intensity versus time trace (black bold line) obtained from a normalized sum of all traces presented in (a) with errors bars representing standard deviations at each time. All traces have been background corrected.

The protocol described at the end of this section finally yielded the best immobilization results and might be used further to produce extended native vesicles arrays. In combination with microfluidics, such arrays provide a generic platform to screen the function of cell surface receptors in a highly parallel manner.

4.4 Conclusions and Outlook

In this chapter we used μCP to micropattern surfaces of lass slides for different applications.

(i) Miniaturized NMR measurements.

In order to miniaturize NMR experiments using micrometer-sized magnetic coils on glass supports, it is essential to entrap the solution to be analyzed in proper micrometer sized containers. We used micrometer-sized lipid vesicles as sample containers. The lipid vesicles filled with the analyte solution, here a sucrose solution, were then immobilized on the surface of the NMR probe-head which was a glass slide comprising the magnetic microcoil on its surface. The vesicle immobilization yielded a sufficient sucrose concentration confined in a densely packed layer of vesicles in the counter of the NMR microcoil probe. The

total amount of sucrose was downscaled to 1.4 nl considered on the ensemble of the immobilized vesicles.

(ii) DNA/oligonucleotide microarrays

Microcontact printed QDs demonstrate to be an efficient approach to visualize surface functionalization, which might be useful for native vesicle further immobilization. They can probably also serve as donor for a FRET pair for labeled proteins immobilized through biotin interactions. The hybridization of oligonucleotides at the concentration of 1 nM demonstrates efficient signal to noise acquisition and further experiments should be realized to test the lowest detection barrier.

The use of single labeled oligonucleotides opens possibilities the possibilities of cost reduction for standard DNA/RNA screening protocol.

(iii) Native vesicles arrays

The developed protocols for producing native vesicles arrays open possibilities of developing biosensors, screening for unknown ligands, or for investigating molecular interactions.

4.5 Material and Methods

Micro Contact Printing (μ CP)

Glass slides were cleaned by several cycles of 15 minutes in an ultrasonic bath (Bandelin Sonorex) : 5x [detergent (1% Hellmanex from Hellma) followed by rinsing with water (MilliQ: resistance $>18 \text{ M}\Omega\text{-cm}$)], 5x [deionized water] and 1x in methanol. They were stored in methanol and dried in a stream of N_2 just before stamping.

PDMS (Sylgard 184 from Swiss-Composite) stamps were produced using a microstructured silicon wafer as a master (produced at the EPFL by F. Vincent), (comprising either circles, squares, lines of 25, 10, 5, 4 and 2 μm sizes). Liquid PDMS was cast on the master and left for 2 hours for gas bubble release and then cured overnight. After detachment from the master, small stamps were cut in pieces of 5 x 5 mm. They were cleaned by sonication for 5 minutes in ethanol and dried under a stream of N_2 for 5 min.

Proteins, such as BSA, BSA-biotin, streptavidin, neutravidin, avidin, concanavalin A-FITC, concanavalin A-Biotin biotin), WGA-Alexa 488, or fibronectin were all purchased from Sigma-Aldrich. PLL was purchased from Sigma-Aldrich. Prof. Marcus Textor at ETHZ kindly provided $\text{PLL}_{20\text{k-g}[3.4]-\text{PEG}_{2\text{k}}}$.

Stamps were incubated for 30 minutes with 0.1 mg/ml and then rinsed with water, dried under N_2 stream and put in contact with the surface (glass or SU8) for a few seconds. The non-contacted glass surface were covered with BSA (1 mg/ml solution for 15 minutes) and washed with water. This was followed by

further incubation with 0.025 mg/ml streptavidin (or related proteins) for 1 min and washing with water, removed and to native vesicles incubation.

COMB polymer (kindly provided by Prof. Ashutosh Chilkoti) was stored at 10 mg/ml in water/ethanol mixture. Hyaluronic acid was purchased from Sigma-Aldrich. Either compound was done spin-coated directly on the glass surface. For μ CP, compounds were spin-coated on the PDMS stamp which was then put in contact with the support surface under slight pressure. Non-contacted glass surface areas were covered with proteins (BSA, fibronectin or concavalin A) by incubation with 1 mg/ml protein solutions for 15 minutes and then washed with water.

Liposome Preparation

The following lipids were purchased from Avanti Polar Lipids, Inc.

DPPC : 1,2-Dipalmitoyl-sn-glycero-3-phosphocholine

DOPG : 1,2-Dioleoyl-sn-glycero-3-[phospho-rac-(1-glycerol)]

DSPE-PEG₂₀₀₀-Biotin: 1,2-Distearoyl-sn-glycero-3-phosphoethanolamine-N-[biotinyl(polyethylene glycol) 2000]

DHPE-TRITC: N-(6-tetramethylrhodaminethiocarbonyl)-1,2-dihexadecanoyl-sn-glycero-3-phosphoethanolamine

For experiments using DPPC, a stock solution of DPPC in chloroform was prepared and aliquoted to glass vials. For liposome preparation, first the chloroform of the DPPC solution was evaporated using a rotavapor (Büchi Rotavapor EL 130) until a uniform lipid film was formed on glass wall, the lipid films were hydrated in water overnight at 4°C. The hydrated lipid sample was sonified with a tip sonifier (Branson Sonic Power Company; Sonifier B-12;

Microtip power: 30) for 3 minutes in a water bath at $\sim 70^{\circ}\text{C}$ and then cooled to RT.

For NMR experiments liposomes were prepared by mixing DOPG, 0.3% of DSPE-PEG2000-biotin, and 0.1% of (DHPE-TRITC) in chloroform. Chloroform was evaporated on a rotavaporator (Büchi Rotavapor EL 130) until a uniform lipid film was formed on glass walls. The lipid film was then hydrated with a 1M sucrose in deuterated PBS overnight at 4°C . Liposomes were filtered to exchange the extravesicular solution to 0.8 M NaCl in deuterated PBS.

Native Vesicles Biotinylation

Native vesicles were prepared as described in chapter 2.

DHPE-x-biotin : (N-((6-(biotinoyl)amino)hexanoyl)-1,2-dihexadecanoyl-sn-glycero-3-phosphoethanolamine) was in CHCl_3 stock solution at 10 mg/ml (purchased from Molecular Probes Invitrogen). n-Octyl- β -D-Glucopyranoside (OGP) (purchased from Anatrace) was in CHCl_3 stock solution at 0.6 M. OGP and DHPE-x-biotin were mixed to reach a final concentration of 187.5 mM and 73.5 μM , respectively. After evaporation of chloroform and hydrating to reach desired lipid concentration and Samples were stored at 4°C . The lipid stock solutions were just before use diluted 45-fold below the CMC of the detergents (OGP $\text{CMC}_{\text{H}_2\text{O}} \sim 18\text{-}20$ mM; $\text{CMC}_{0.1\text{ M NaCl}} \sim 23.4$ mM).

PE-PEG₂₀₀₀-Biotin was applied directly on cell or native vesicles from an ethanol stock solution at 2 mg/ml.

NHS-biotin (purchased from Sigma-Aldrich) was added to a corresponding native vesicle preparation and incubated for 30 minutes before native vesicles immobilization.

ACP labeling

ACP PPTase and Coenzyme A-biotin were kindly provided by Prof. Kai Johnsson at EPFL.

Cells stably expressing ACP-NK₁R receptor were labeled with a solution containing 10 mM MgCl₂, 5 μM Coenzyme A-biotin and 1 μM PPTase in PBS at 37°C for 15 minutes. Cells were washed three times with PBS⁻ at 37°C and native vesicles were then formed. A similar protocol was used for labeling native vesicles, introducing an additional final centrifugation and resuspension step.

Streptavidin-Coated QDs

They were synthesized as described elsewhere (Baumle, Stamou et al. 2004). 4.4 mmol of Cd(ClO₄)₂•6H₂O and 2.9 mmol glutathione were dissolved in 250 mL of N₂-saturated deionized water at a pH of 11.5. After adding 45 mL of a freshly prepared oxygen-free solution of NaHSe (0.05M), the mixture was heated at 90°C for 12 h, cooled to room temperature and dialyzed (dialysis cassettes with 3500 Da cutoff from Pierce) for 3 h against water. The QDs (2.5 mg/mL) were incubated in a 1 μM streptavidin solution. Streptavidin-coated QDs were separated from free streptavidin by ultracentrifugation (13000 rpm, 80 min.); the pellet was dissolved in water and stored at 4°C

PDMS stamps were inked for 40 minutes with 35 μL of a freshly prepared aqueous solution of streptavidin-coated QDs. After rising the stamp with water and drying under a stream of nitrogen, the QDs were microcontact printed on glass. Images of the fluorescent patterns of Q-dots were recorded using a confocal microscope (LSM, Zeiss, excitation at 488 nm, dichroic mirror HFT 488, filter LP 560).

Hybridization of DNA

Oligonucleotides were purchased from Mycosynth. The micropatterned streptavidin QDs were incubated for 15 min with a solution (1 nM, in PBS) of 5'-biotin- GTC GTC GTC GTC TGA CCT GGA TGA TCT GTC GTC GTC GTC-3' at 25°C. After washing with PBS, the glass substrate was incubated at $\sim 60^\circ\text{C}$ with the labeled complementary oligonucleotide 5'-Alexa654-GAC GAC GAC GAC AGA TCA TCC AGG TCA GAC GAC GAC GA-3' (1 nM, in PBS) for 15 min in order to hybridize with the complementary biotinylated oligonucleotide. After thorough washing with PBS, confocal microscopic images of the patterned fluorescently labeled complementary oligonucleotide were recorded (λ_{ex} at 633 nm, dichroic mirror HFT 633, filter LP 650).

Ratio plotting by direct division of the two channels intensities was performed with the instrument software (LSM Examiner).

Chapter 5

This chapter concerns the investigations done with a single optical tweezer. Throughout this chapter this technique allows investigating the production of native vesicles as well as cell membrane properties and leads to make intercellular connections. Such artificially produced intercellular connections finally makes it possible to investigate the chemical synapse in primary cells as well as the electrical synapse in HEK cells by patch clamp techniques.

5. Artificial Cellular Connections With Optical Tweezers

Arthur Ashkin at Bell Laboratory developed optical trapping in 1986 and reported as the first many applications. Optical tweezers are extraordinary tools opening the possibility to immobilize objects in the (sub)micrometer range free in solution via single or multiple laser beams. Since Ashkin's seminal development, optical tweezers were used in many different fields; especially near infrared (NIR) lasers improved substantially the trapping of biological objects, such as viruses (Ashkin and Dziedzic 1987), yeast cell (Grimbergen, Visscher et al. 1993), gametes (Tadir, Wright et al. 1991), mammalian cells (Ashkin and Dziedzic 1989; Steubing, Cheng et al. 1991; Leitz, Weber et al. 1994; Luo, Li et al. 2007), or even intracellular organelles (Weber and Greulich 1992) and chromosomes (Liang, Wright et al. 1993; Vorobjev, Liang et al. 1993), increasing the range of biological applications (Kuo and Sheetz 1992). The major advantage to use NIR laser beams for trapping over visible light is the fact that biological samples do almost not

absorb such wavelengths, thus providing non-invasive means to manipulate the objects and leaving the visible light for fluorescent measurements. Optical tweezers became a tool to manipulate diverse particles from different sizes from atoms (Chu, Bjorkholm et al. 1986) to polystyrene beads, which presently are the most used object for trapping. In fact trapping of polystyrene beads is highly efficient because they show extremely homogenous refractive index, enabling to perform precise optical force measurements of biomolecular interactions (Simmons, Finer et al. 1993; Warrick, Simmons et al. 1993; Kojima, Muto et al. 1997; Dai and Sheetz 1999; Kegler, Salomo et al. 2007). A novel interesting application was recently reported directing axonal guidance by light (Ehrlicher, Betz et al. 2002).

In order to realize 3D optical trapping, the refraction index of the particle must be different to the surrounding medium and a high numerical aperture objective ($NA > 1$) has to be used for focusing laser beam also. Other parameters influence the trapping efficiency such as, the power of the laser, the wavelength used, the beam shape as well as the size of the particle. How these parameters influence trapping efficiency is further discussed. Efficient 3D trapping can only be achieved using a focused laser beam, which passes a high numerical aperture objective and thus creates a diffraction limited focus. Although all wavelengths can be used, longer ones are more appropriate due to the lower absorption by biological tissues. For biological samples typical trapping wavelengths are between 750-1064 nm. The refractive index of the trapped object should be higher than the surrounding medium, typically 1.33 in physiological buffer as PBS. Since living cells, have a refractive index around 1.37 the trapping efficiency is reduced compared to polystyrene beads that have a refractive index of 1.59. Although a broad range of sizes of particles can be trapped, ranging from atoms to μm sized particles, the physical laws responsible for optical trapping are different in

different size regimes. If the particle size is much smaller than the wavelength of trapping the trapping follows the Rayleigh regime theory. When the size particle is larger than the wavelength, the trapping can be explained by Mie regime theory and follows ray geometric optics (Ashkin 1998). For particle whose sizes are similar to the trapping wavelength, the quantification is rather complex.

The more intuitive way to understand optical trapping remains thus the simple geometrical description of light rays. Two media with different refraction indexes crossed by a ray of light induce a change in the momentum of the photons, known as refraction. This change of quantum momentum of light when shined through an object induces an opposite momentum on the object resulting in a net force. When the particle is perfectly centered in the laser beam, the resultant net force is axial and imposes the particle to be pushed in direction of the focal point. When the object is placed below the focal point, the resultant force pushes the particle up (figure 5.1a). By opposition when the object is above, the resultant force pushes it down (figure 5.1b). Thus the object is maintained in an equilibrium position according to the axis of laser beam. If the object is not perfectly centered in the plane perpendicular to the laser beam, the resultant lateral force brings it to the central position (figure 5.1c). Following the same laws an additional force, imposed by reflection, but much weaker in magnitude place the equilibrium position actually slightly above the center of the trapped object. Such a change is so small, only 0.06 times the size of the object (Ashkin 1998) that it is usually neglected. All these forces create a 3D optical trap maintaining the object in an equilibrium focal point.

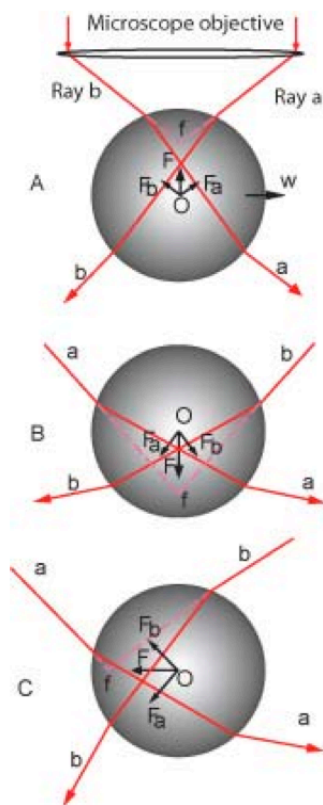


Figure 5.1: Scheme of ray light optics for optical trapping. Only external rays are shown and the resulting forces imposed on the object (for instance a polystyrene bead). A) shows the case where a bead is placed below the focal point. B) shows the case where a bead is placed above the focal point. C) shows the case where the bead is not centered to laser beam and is valid for any deviation in the plane perpendicular to the laser beam.

5.1 Intercellular Communication

Specialized intercellular communication is required in diverse fundamental biological processes and occurs between similar cells in a tissue but also between distinct specialized cells from different tissues. Examples of intercellular specialized contacts can be found at the immunological synapse (Groves 2005), where it controls antigen presentation between macrophages and T cells, at epithelial tight junction of occludins (Madara 1998) (Hopkins, Walsh et al. 2003) (Blasig, Winkler et al. 2006) (Benz, Blume et al. 2008), in many cell types of desmosomes (Maddugoda, Crampton et al. 2007), at the neuromuscular junction (Kohsaka, Takasu et al. 2007), where muscle contractility is provided and principally at neuronal connection through the formation of synapses (Pereda,

Rash et al. 2004), which can be chemical in the synaptic cleft or direct between GAP junctions (Goodenough, Goliger et al. 1996) (Panchin 2005).

The simplest intercellular electrical communication, which occurs through the assembly of a protein family, is realized by the connexins. Such proteins are composed of six subunits, each composed of four transmembrane helices, and usually called connexon. Their extracellular domains can associate with the same protein present in a contacting cell to form a channel, called connexin. This pore opens through the tilt of subunits and permits a bidirectional passage of ions and cytoplasmic molecules up to 1000 Da. Connexins can also assemble in larger ordered patch-like structures by lateral interaction (Kandel, Schwartz et al.).

One of the most essential intercellular connections is the chemical synapse. Such a specialized intercellular chemical communication is extremely localized, occurring in a closed volume, called synaptic cleft. Ligand gated ion channels are responsible for neuronal depolarization. Chemical synapses are unidirectional. The formation of synapses require special membrane proteins (Yamagata, Sanes et al. 2003; Takeichi and Abe 2005; Levinson and El-Husseini 2007; Chen, Liu et al. 2008), which promote the interaction between two cells and maintain in close contact the presynaptic and postsynaptic membrane. During subsequent maturation diverse other membrane proteins (Li and Sheng 2003; Montgomery, Zamorano et al. 2004; Lau and Zukin 2007) and cytosolic proteins are involved (Gerrow, Romorini et al. 2006) (Kim, Futai et al. 2007), from whom cytoskeletal proteins play an essential role in synaptic vesicle delivery (Cingolani and Goda 2008). The neuronal chemical transmission process starts with the fusion of synaptic vesicle at axonal terminations near the target cell, by releasing neurotransmitter into the synaptic cleft. Neurotransmitters finally bind to postsynaptic receptors leading to membrane depolarization and electrical signal

propagation through voltage-dependent channels, called action potential. The mature synapse is a complex network involving many different proteins (figure 5.2).

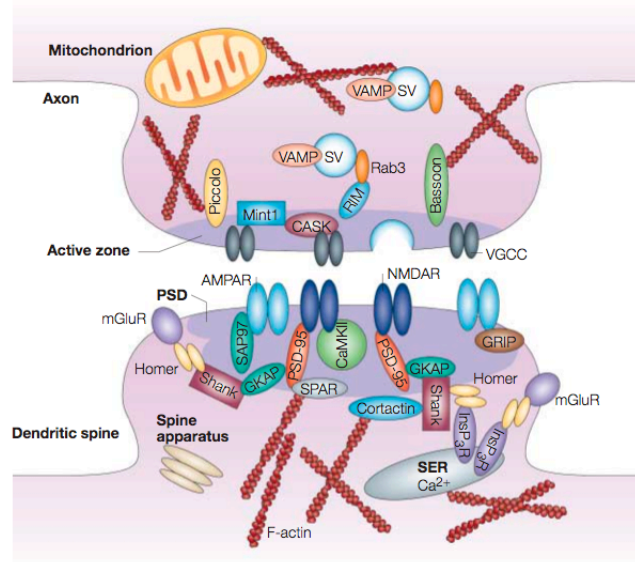


Figure 5.2: Scheme of a mature synapse with a sketch of the complexity of molecular assembly. Image taken from Li Z. and Sheng M. (Li and Sheng 2003)

5.1.1 Primary Cells

Normally intercellular communication can not be achieved with HEK lacking the required specialized proteins of the neuronal cells. Primary cells taken from cellular tissues would be ideally suited for reconstituting synapse formation artificially; this requires dissection of living animals and isolation of neuronal interesting tissues. Due to strict legislation rules concerning the dissection of living animals, we decided to obtain primary afferent neurons by the dissection of dorsal root ganglions (DRGs) from chicken embryos (figure 5.3a) (Florio, Westbrook et al. 1990) (Caffrey, Eng et al. 1992) (Zheng, Walters et al. 2007) (Yang, Yao et al. 2003). Ganglions are distributed symmetrically along spinal medulla and are present at each vertebra. During chicken development, the bigger

DRGs are present in the lumbar part of the spinal column. The collected DRGs can be maintained in culture where they develop axonal growth (figure 5.3b). DRGs can also be dissociated in single cells and seeded on culture dishes. During dissociation, axons were cut and thereby neurons were obtained which display a round morphology. When cells were maintained in culture for a few days, they exhibit new axonal growth.

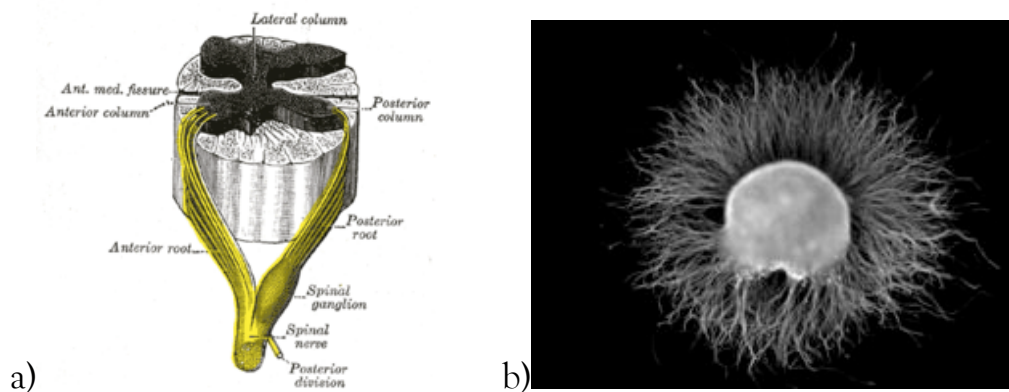


Figure 5.3: (a) cross section of spinal column with a dorsal root ganglion, named spinal ganglion. (b) DRG of chicken after dissection. When maintained in culture under suitable conditions, axonal growth can be observed after immunostaining with anti-neurofilament antibodies.

5.2 Electrophysiology

Intercellular communication is a fast process proceeding in the order of milliseconds. It can be measured by the electrophysiological patch clamp techniques.

Erwin Neher and Bert Sakmann developed the patch-clamp technique in 1976 (Neher and Sakmann 1976) (Hamill, Marty et al. 1981; Neher and Sakmann 1992). This technique requires the use of glass pipettes with a tip

diameter of about 1 μm , containing a metallic electrode. The pipette is placed in contact with the cell membrane to form a seal of very high electrical resistance in the order of gigaohms. After short suction, the cell membrane below the patch ruptures and connects the interior of pipette with the cellular cytoplasm, while the regions of the pipette are still remain sealed with the plasma membrane. This procedure is called whole-cell patch clamp and allows recording the average activity of all the channels present in the cell plasma membrane. The metallic electrode placed inside the pipette is usually connected to an amplifier for recordings electrical currents but can also inject current into the cell, when connected to a current generator. Injection of current allows controlled stimulation of neuronal cells. In our experiment an electrophysiology setup was combined with an optical tweezer to modulate and test neuronal activity. The electrophysiology part comprises two patch pipettes, one for excitation and another for recording (figure 5.4).

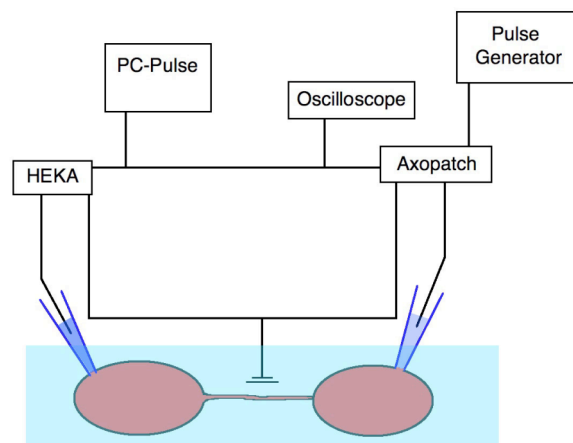


Figure 5.4: Scheme of two cells artificially connected by a thin tether which was formed by a laser tweezer. The patch pipettes are connected to the amplifiers (HEKA and Axopatch), which are connected to the reference electrode and the PC. The Axopatch amplifier is connected to a pulse generator to apply external excitation and to an oscilloscope to visualize the applied pulses.

5.3 Results and Discussion

The goal of next experiments was to study biological relevant applications of laser tweezers. First observations demonstrate that it was possible to trap and manipulate cell membrane with a single laser in order to produce native vesicles from adherent cells. Subsequent experiments show the investigation of tethers formation with a single laser tweezer as well as intercellular connections in between neighboring cells. This last case gives rise to an interesting approach to artificially induce neuronal connection, thus tested in primary cells for chemical synapses and in HEK cells for electrical communication.

5.3.1 Single Vesicle Investigation

If the laser of the optical tweezer is focused to the cell surface, the cell membrane can be pulled away from cell body with the optical trap, giving rise to two distinct membrane forms: (i) If the captured membrane region is small, the tweezer tends to form a membrane tether; (ii) If a larger membrane area is pulled, a vesicle is formed, which remains connected to the cell surface via a tether. If this tether ruptures, a native vesicle is released from the mother cell.

Native vesicles created by an optical tweezer can in turn be placed in contact with solid supports, where they rapidly adhere. Even with the use of cytochalasin that induces membrane blebbing and provides already preformed vesicles, which can be more efficiently pulled and released from cells by optical tweezers, only small quantities can be produced by such procedure. These vesicles are relatively big, more than 1 μm and contain sometimes intracellular components. When

produced from cells expressing the wtNK₁R, they show ligand binding activity to the agonist SP-Cy5 (figure 5.5).

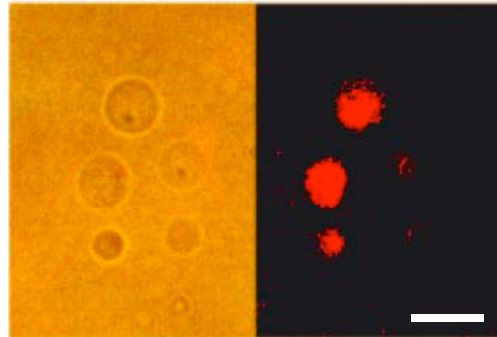


Figure 5.5: Optical micrographs of native vesicles extracted with an optical tweezer from HEK cells expressing the wtNK₁R, and labeled with SP-Cy5. The contrast of right image has been increased for a better clarity. On the left transmission micrograph shows 5 native vesicles extracted by such procedure and placed in contact with the glass surface where they adhere and for a small array. Right image shows the fluorescence micrograph of the same vesicles after SP-Cy5 labeling. Some vesicles demonstrate to contain less receptors. Image contrast was increased for a better visualization. Scale bar represents 5 μ m

This procedure allows isolating cellular membrane vesicles of a particular composition for further analysis.

5.3.2 Artificially Induced Intercellular Contact

A membrane tether can be pulled from a cell over long distances, up to tens of micrometers. Such a tether can be brought into contact with a neighboring cell. Our first experiments were performed with HEK cells (figure 5.6), to investigate the membrane-membrane interaction between the tether and the cell. To visualize tether formation and to investigate whether the laser tweezer

would induce any damage on cell membrane which might lead to leakage, or whether intercellular chemical or electrical communication can be realized after connection, small cytosolic dyes (MW < 1000 Da), such as calcein or fluorescein, were previously loaded on cells cytoplasm.

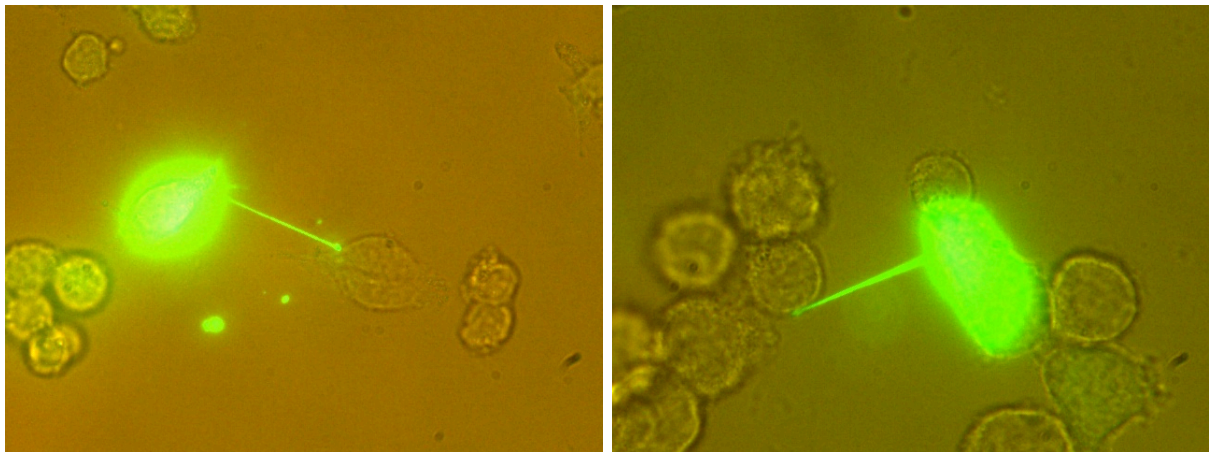


Figure 5.6: Two examples of HEK cells connected by membrane tether formed by pulling with an optical tweezer. The cell to be pulled was previously labeled with calcein in order to visualize tether formation and to test whether if any molecular exchange was possible between the two cellular cytosols.

Results demonstrate that tether can be efficiently pulled from one cell and connected to a neighboring one. Some seconds after connection establishment, the laser trap could be shut down. The connection remains stable and the integrity of cell membrane was not affected. The used of cytosolic dyes tend also to demonstrate that passage of dye between the two cells was not possible and that the fusion of the two contacted cell membranes does not occur. Such experiments lead to investigate with laser tweezer more interesting intercellular contacts reported in the next sections.

5.3.3 Neuronal Communication in Primary Cells

As demonstrated previously, since membrane pulling by an optical tweezer did not require any external support, such as polystyrene beads, the cell membrane at the end of the tether is left free for further interaction for example for the formation of artificially controlled cell-cell contact. A totally new sort of experiments can thus be conceived, opening the possibility to investigate intercellular communication. This section will focus on experiments investigating intercellular communication after laser tweezer induced artificial connections.

Chicken embryos were sacrificed between day 14 to 18 after fertilization and dorsal root ganglions were collected and dissociated in form of single neurons. When cells were maintained in culture for a few days, they exhibit new axonal growth and efficient interconnection, leading to the formation of a complex network (figure 5.7). They have also tendency to associate and form small patches of cells.

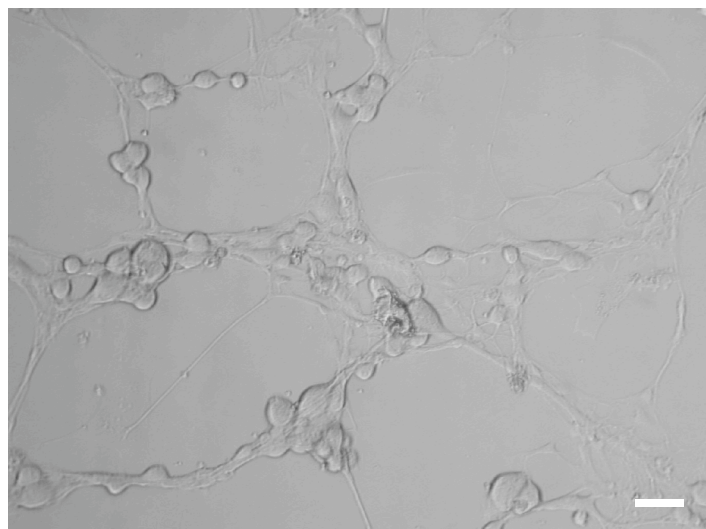


Figure 5.7: After a few days in culture single cells form new patches and axonal growth form a complex network, as seen in the optical micrograph. Scale bar represents 10 μm .

Many of the cultured neurons show normal electrophysiological responses when electrically stimulated and measured by the patch pipettes (figure 5.8). Single cells are able to trigger action potential(s) after initial current stimulation or even without any stimulation by spontaneous activation.

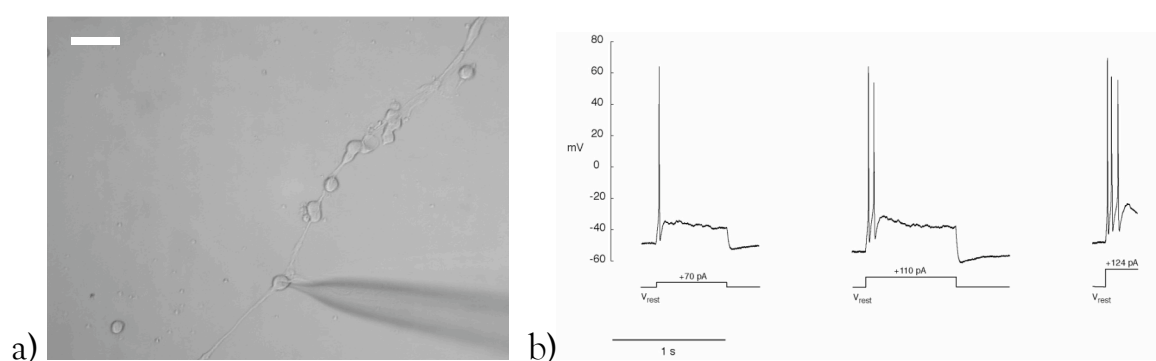


Figure 5.8: (a) After dissociation and maintenance in culture for a few days, patch clamp measurements were performed on DRG neurons. (b) Typical action potentials after current stimulation. Scale bar represents 20 μm .

In a typical experiment where artificial connection was realized between two cells via a tether with an intercellular molecular exchange is showed in figure 5.9. After an excitatory pulse of 500pA applied to the first patch cell that was connected through a tether to a neighboring cell, an electrical response was observed on the second cell. Both cells display depolarization through voltage sensitive ion channels, but due to the very short delay of time of the response, which is almost instantaneous, this communication can't be considered as a chemical transmission, which response is expected to be delayed at least for a few milliseconds.

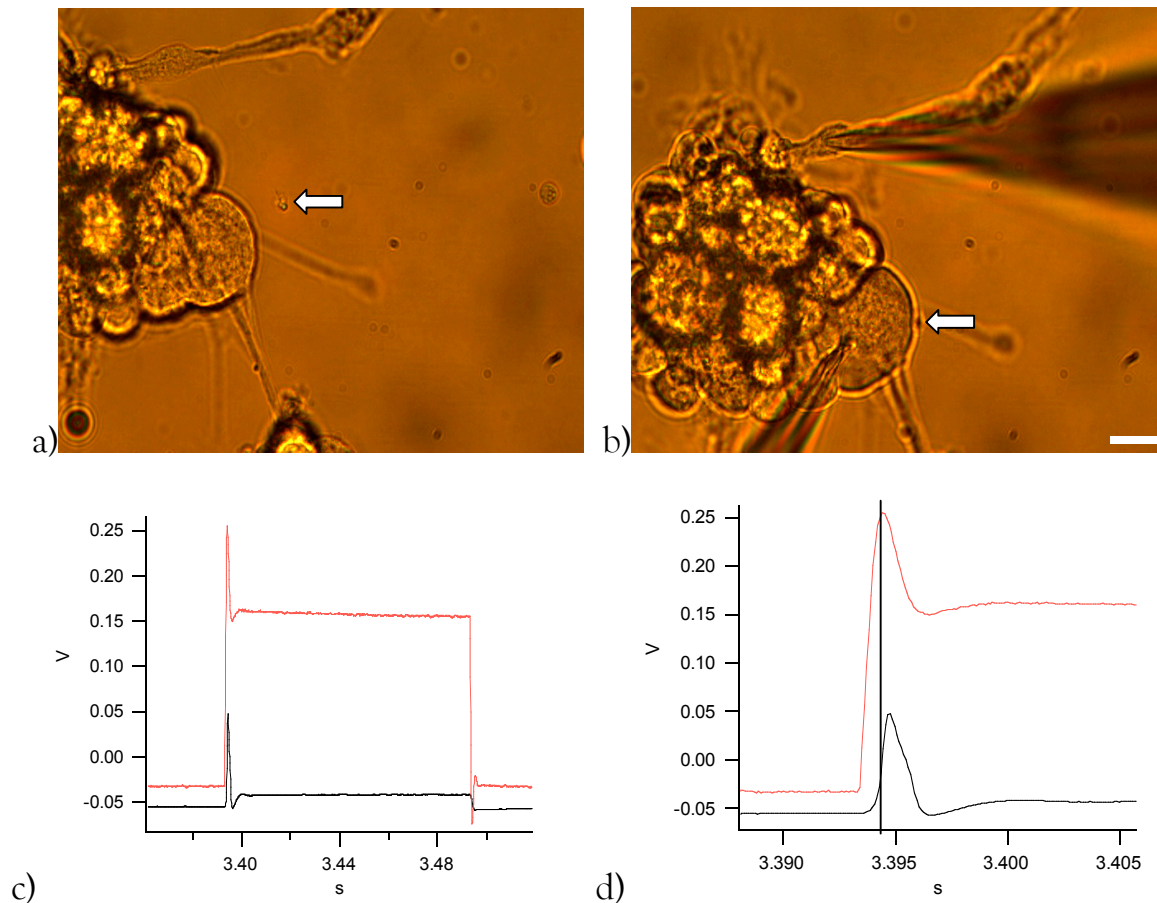


Figure 5.9: Neuronal cells from dissociated from chicken embryos after 4 days in culture. (a) Tether extension before connection (the arrow indicates optical trap). (b) The two patch pipettes after connection (the arrow indicates the contact point between the two cells). (c) Patch clamp recording: 500pA excitation pulse with a duration of 500 ms (red trace) applied to the first cell evokes an electrical response (black trace) in the second cell. (d) Magnification showing almost no response delay. Scale bar represents 10 μm .

Moreover, when a negative excitation pulse was applied, an electrical negative response was measured (figure 5.10). Since chemical transmission is unidirectional and don't lead to an opposite response, these results demonstrate probably that the electrical transmission occurs through connexins from gap junctions. Such an electrical communication was abolished after tether rupture and no electrical response could anymore be detected on the response trace of the

second cell. As a second negative control a 2 nA pulse, 4 times larger than the previous one, was applied after retracting the excitatory patch pipette that remains in solution. The patch pipette was at comparable distance of the second cell, which remained clamped. This demonstrates that direct excitation through the patch pipette can't induce the electrical response observed on the second cell.

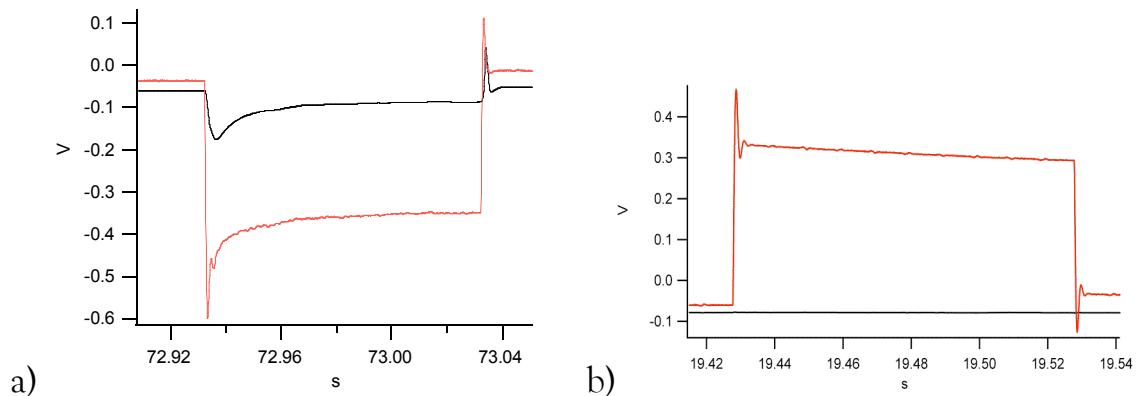


Figure 5.10: (a) Patch clamp trace recording: applying a negative 500 pA excitation pulse with a duration of 100 ms (red trace) an electrical response (black trace) is measured in the second cell demonstrating a bidirectional transmission. (b) The response after rupture of the tether demonstrates the abolishment of electrical response.

Connexin proteins are usually present in glial cells, where they induce intercellular electrical transmission; these proteins were reported to occur in other neuronal and non-neuronal cell lines (Belluardo, Mudo et al. 2000; Wellershaus, Degen et al. 2008). Previous results show that such electrical transmission occurs through gap junctions, probably between two glial cells. The presence of such cells in culture could not be excluded after isolation and dissociation of DRGs.

Despite the establishment of several interneuronal artificial connections, we never succeeded to see synaptic transmission. This disappointing result can be

explained by several factors. First, even after establishing a membrane-membrane contact, several other steps are required until the maturation of the synaptic button. As previously introduced, the maturation of a synaptic button requires the assembly of a complex signaling complex, leading to the delivery of synaptic vesicles at the membrane vicinity. Such a process, usually occurs at physiological temperature, may take place over a longer time range (several hours) than our typical experimental sessions. Furthermore our setup, did not allow a total control of the temperature; at lower temperature the diffusion of proteins could be slowed down, thus requiring even longer time periods for synapse formation. Second, neuronal transmission usually occurs between two distinct cellular regions, synaptic boutons present along the axon of the first cell and dendrites of the second cell. Most of the connections were realized from cell body to cell body, specially when cells were recently plated and possess a round morphology. Third, the extraction of tethers from axons, starting directly from axonal membrane or from preformed not yet connected boutons, appears to be very challenging. When successful, such tethers couldn't reach long distances, because they became extremely rigid after a few seconds, impairing further extension and subsequent connection, probably due to the very high content of cytoskeletal filaments. The use of cytochalasin to decrease membrane tension was avoided, but remains a possibility to be tested. Fourth, synapses can be of two opposing types, excitatory or inhibitory. This property can probably not be controlled when an artificial connection is established. Fifth, according to discussions we had with colleagues working on electrophysiological recordings on hippocampal brain slices, the percentage of synapses leading to synaptic transmission is only about 10%. Sixth, recent reports (Holm, Sundqvist et al. 1999) also demonstrate an influence of optical trapping on function of cells even if they are not damaged. Finally, a neuron is usually highly connected up to a thousand of contacts by surroundings neighboring cells, which can be neurons or glial cells. They are able to integrate

several inputs arriving at the same time, giving rise to a positive or no response. The question remains if a single input is sufficient to give a chemical neuronal response? All these considerations lead to the conclusion that artificial reconstitution of chemical transmission between neurons is a complex problem, which is difficult to realize by simple intercellular connections.

5.3.4 Artificial Electrical Synapses between HEK Cells

In parallel to chemical synapse, which complexity is high, a simpler neuronal communication can be investigated, the electrical synapse formed by connexins. Thus the formation of artificial electrical synapses seems to be a more feasible experiment.

Moreover, it can be performed in HEK cells after transient transfection with connexin 36 (Cx36). The electrical synapse can be realized from any cellular membrane region as connexin proteins can laterally freely diffuse. Their tendency to form larger connexin patches might lead to a larger current. HEK cells transiently expressing connexin 36 were maintained in culture for 2 days after transfection to reach high expression level. During such period connexin patches assemble, forming functional connection between contacting cells and current passage can be recorded by patch clamp measurements (figure 5.11): As expected a bidirectional communication could be observed; current clamp measurements demonstrate a current flow proportional to the applied excitation. Negative controls realized on non-transfected HEK cells show no electrical passage between cells in contact (results not shown).

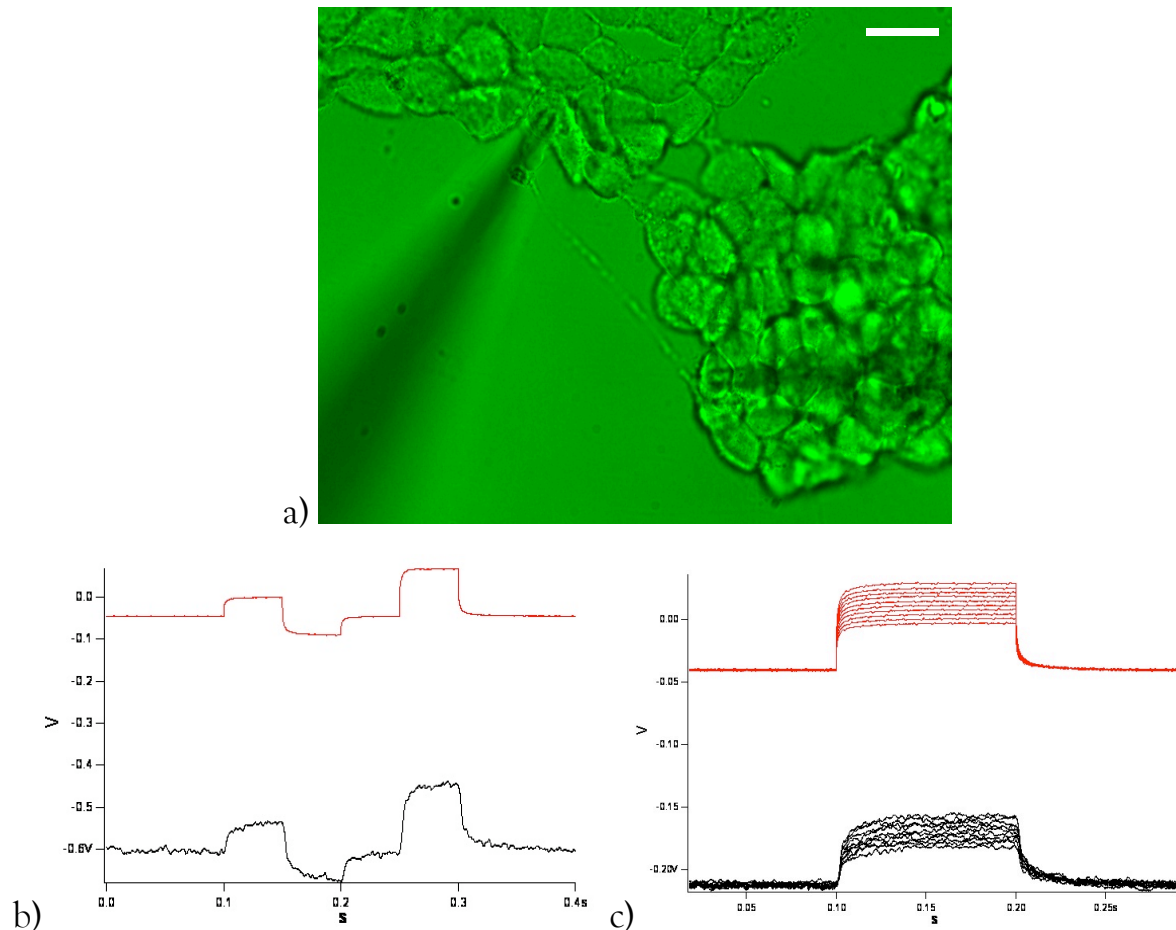


Figure 5.11: HEK cells expressing the Cx36 investigated by patch-clamp experiments. (a) Connection of two cells with the patch pipettes in shadow. (b) A patch clamp recording of positive and negative excitatory pulses (red trace) and the corresponding response observed on the second cell (black curve). Positive and negative response proves the bidirectional passage of current. (c) Electrical responses obtained on the same cells as used for (b) now on current clamp measurements with increasing stimulation giving rise to larger responses. Scale bar represents 10 μm .

In a second experiment, HEK cells expressing Cx36 have been artificially connected by a tether. A significant passage of current was observed a few minutes after the connection was established (figure 5.12), demonstrating the association of connexons into functional connexin pores. This passage is bidirectional as expected. The amplitude of the current recorded in the second cell is smaller than

those observed between naturally connected cells, due probably to a higher resistance of the long and thin tether or to smaller connexin patches.

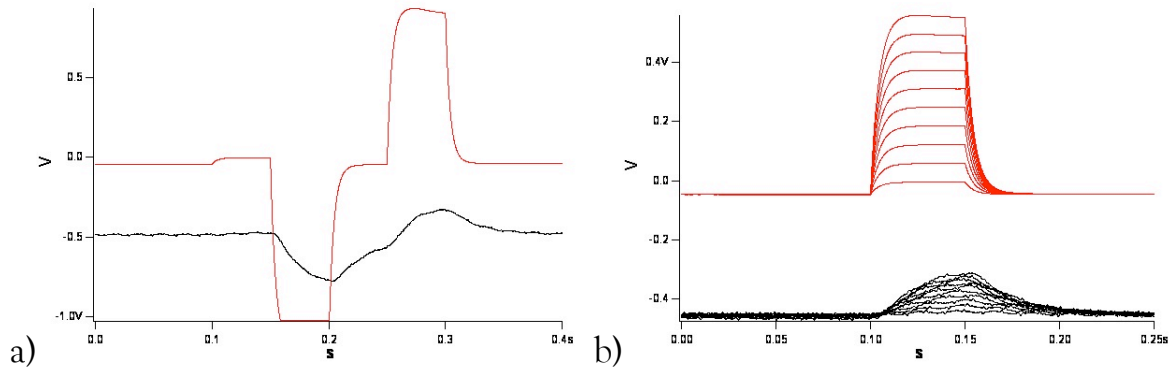


Figure 5.12: (a) A patch clamp recording of two cells expressing Cx36 and connected by a tether demonstrating the bidirectional passage of current (black trace) after stimulation (red trace). (b) Increasing flow of current (black) according to excitation steps (red).

These experimental results show that functional electrical synapses can be formed between two cells artificially connected using an optical tweezer.

5.4 Conclusions and Outlook

In this chapter we have demonstrated that optical tweezers enable to pull efficiently cellular plasma membranes from different cell types without using polystyrene beads as support. This procedure allows producing native vesicles by isolating fractions of plasma membranes from cells containing functional cell surface receptors. Furthermore, this approach can be made to produce long plasma membrane tethers to connect neighboring cells. First trials to form

chemical synapses were unsuccessful and are still under progress. However, optical tweezer assisted connections are enabled to generate electrical synapses in primary cells as well as in cells transiently expressing connexins.

Artificially induced intercellular connections can provide an interesting tool to investigate connexins physiology. With some improvements, such as a better control on experimental conditions (temperature, patch stability) neuronal chemical connection might also be realized. Such achievement could provide new possibilities in order to understand fundamental processes in synaptogenesis and intercellular communication.

5.5 Material and Methods

Laser Tweezer

The laser tweezer beam was generated by a Ytterbium vanadate laser (J-Series/BL10:106 Q from Spectra Physics; emission of 1064 nm; P_{\max} of 3W). The beam is aligned by a couple of mirrors and expanded by a couple of lenses. Two lasers are used for fluorescence excitation: an Argon laser (532R-AP-A01 from Melles Griot; emission of 488 nm and P_{\max} of 5mW) and a helium-neon laser (05-LHP-171 from Melles Griot; emission of 633 nm and P_{\max} of 15mW). A dichroic mirror (16-MBF-453 from Melles Griot) combines the two fluorescent beams. The beams are then aligned by a couple of mirrors and expanded by a couple of lenses. Finally the fluorescent excitation beams are coupled to the IR beam by a dichroic mirror (Laseroptik, Germany) and all of them overfill the back aperture of the objective (Zeiss C-Apochromat W 63X/1.2 Korr UV-Vis-IR) of the microscope (Zeiss Axiovert 100)

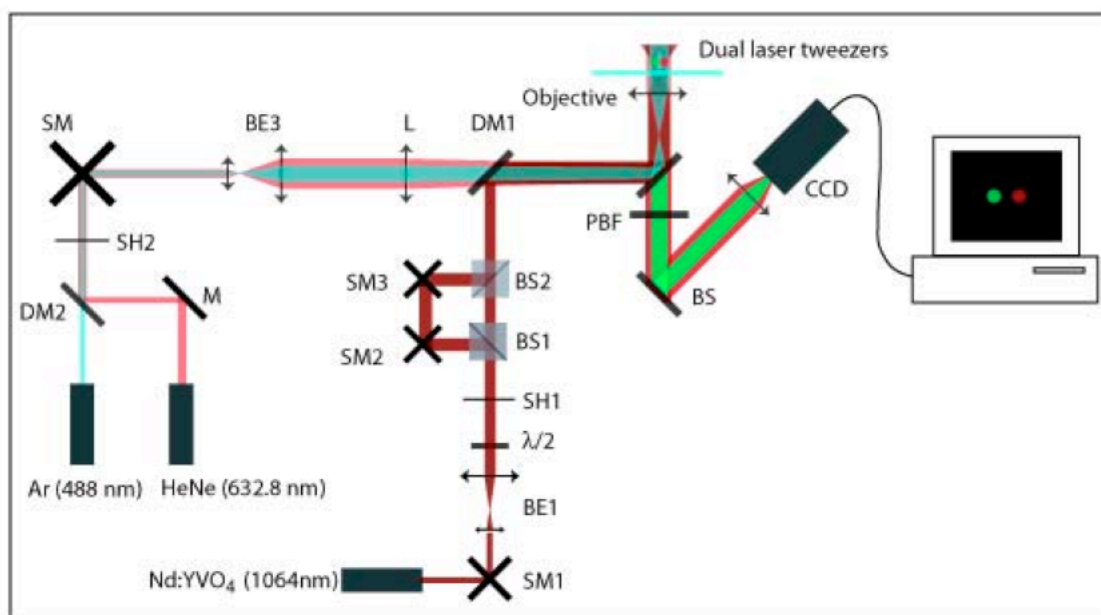


Figure 5.13: Scheme of the single laser tweezer setup. A simplified version of such setup was used for artificially forming inter-cell connections. Two laser beams for

fluorescence excitation and a IR laser beam for trapping were uniaxially aligned and expanded to overfill the back aperture of the microscope objective. The IR beam is focused by the microscope objective creating a laser tweezer (trap). Essential parts: M (mirror); DM (dichroic mirror), SM (scanning mirror), BE (beam expander), PBF (passband filter), L (lens).

Electrophysiology

The electrophysiology setup allows excitation and recording by two patch pipettes in the whole-cell configuration. Patch pipettes were made of glass capillaries (CB105F-8P from Science Products GmbH) in a pipette puller (P-87 from Sutter Instrument CO.). The first patch pipette was connected to a patch clamp amplifier (EPC9 from HEKA; sample recording at 10 kHz with a filtering at 1 kHz) and computer controlled by Pulse software (company). The second patch pipette was connected to a patch clamp amplifier (Axopatch 200B from Axon Instruments; sample recording at 10 kHz with a filtering at 1 kHz). The Axopatch amplifier was coupled to a pulse generator (SMP-310 from Bio-Logic SAS) and to an oscilloscope. The ground electrode was connected to both amplifiers. Both traces were recorded simultaneously via Pulse software.

External bath solution contained 147 mM NaCl, 12 mM Glucose, 10 mM HEPES, 2 mM KCl, 1mM MgCl₂, 2 mM CaCl₂ and was adjusted with NaOH to pH 7.4. Patch pipettes were filled with a solution containing 145 mM KCl, 5 mM EGTA and 10 mM HEPES adjusted with KOH to pH 7.4.

Culture of Primary Cells

Fertilized chicken eggs were incubated at 37°C in constant humidity conditions around 50%. Eggs were turned regularly 1 time per day. Chicken

embryos were sacrificed between day 14 to 18 after fertilization and dorsal root ganglions (DRG) were collected by dissection. DRG were transferred to PBS medium and an equivalent volume of 0.25% trypsin solution was added. They were maintained at 37°C for 15 minutes. The trypsin was inhibited by the addition of a similar volume of DMEM + 10% FCS medium (Invitrogen). Mechanical shear forces dissociated DRG by gently passages (up to 20 times) through a glass Pasteur pipette, whose tip was previously flamed. At the end of the procedure single neurons were obtained and seeded on glass slides. The surface of the glass slides was previously coated with a solution of 10 µg/ml of laminin (Sigma-Aldrich) for 10 minutes, rinsed three times with PBS and once with DMEM. They were maintained in culture in DMEM + 10% FCS supplemented with 10 ng/ml of nerve growth factor-7S (Sigma-Aldrich). Patch clamp measurements were performed the same day after cell attachment up to five days after plating.

Expression of Connexin 36

HEK cells were transiently transfected with connexin 36 (generously provided by Prof. Paolo Meda at CMU of Geneva) following Effecten (Qiagen) transfection protocol. Per ml of medium 0.1 µg of DNA is diluted in 50 µl of EC buffer. 0.8 µl of enhancer solution is added, vortexed for 10 s and stored at maximum for 5 minutes. Then 1 µl of Effecten solution was added, vortexed for 10 s, stored for 10 minutes and applied to cells. Prior to experiments cells were maintained at 37°C in culture medium DMEM + 10% FCS for 36 to 48 hours to reach a high expression level.

Fluorescent HEK cells

In order to visualize tether formation and test for dye passage in between cells after laser tweezer induced connection HEK cells were loaded with 50 nM calcein AM (Sigma-Aldrich) for 30 minutes at 37°C, washed three times with PBS and collected. They were mixed with non-labeled cells and seeded on glass slides.

Chapter 6

This chapter reports on the accomplishment of a lab-on-chip assay using native vesicles. It describes the experimental approaches to the development of this bioanalytical platform. The investigations required the use of different techniques, such as microfluidics and the development of new designs, dielectrophoresis and the potential of producing, trapping and separating particles or on laser tweezers, which lead finally to the assembly of a multi-tweezer setup. Finally, the demonstration of the labeling of the trapped native vesicles with multi-tweezers in a microfluidic channel.

6. Lab-on-chip for Investigating Native Vesicles

For a few decades the downscaling of manufacturing technologies initially developed for informatics has opened new possibilities in research and medicine making them step into the micrometer world. George Whitesides developed soft lithography using new polymers (Whitesides, Ostuni et al. 2001), leading to the manufacturing of precise structures at low cost. This miniaturization makes possible the parallelization of reactions on a few square centimeters (Becker and Gartner 2000). Combined with emerging detection techniques, the use of microfluidics channels (Beebe, Mensing et al. 2002) allows studying chemical or biophysical reactions within nanoliters or even smaller reaction volumes, to detect pathogens for health or environmental purposes and to open new horizons for screening applications (Waggoner and Craighead 2007). It was hence rightfully

termed “miniaturized total chemical analysis systems” (μ -TAS). The integration of several laboratory functions in such devices created the term lab-on-chip, where all these improvements found applications as diverse as DNA micro-arrays (Anthony, Brown et al. 2001), immunological and biochemical screening assays, polymerase chain reaction (PCR) (Zhang, Xu et al. 2006; Beer, Wheeler et al. 2008) or even single cell analysis (Bao, Wang et al. 2008). Another microfluidic application based on micromachining, microelectromechanical systems (MEMS), whose pioneer was Kurt Peterson at IBM, uses the deposition of thin metal films on microfluidics walls. These devices integrating electrodes that can be used for recordings or manipulate objects (Ziaie, Baldi et al. 2004).

In order to perform lab-on-chip assays with native vesicles, the most elegant approach would be to produce them from one (or a few) cell(s) directly on the chip device. Then proceed with purification if required, immobilize them on an array, and subsequently analyze their responses by fluorescence microscopy when exposed to a specific chemical compound. No available μ -TAS or MEMS allows performing such a challenging experiment and its realization was soon found to require a new combination of technologies. In order to gain time and to understand the whole process of vesicle formation better, we finally broken it up into the following main steps: production, purification, immobilization and analysis of native vesicles. Several technologies were tested to find the most appropriate ones to reach such individual goals. Production of native vesicles was performed in single microfluidic channels, purification and immobilization using MEMS devices. In order to efficiently immobilize native vesicles in microfluidic channels, a new experimental setup was developed based on multiple optical tweezers (figure 6.1). The miniaturized bioanalytical platform requires also appropriate microfluidic configurations allowing efficient labeling of the vesicles

and their membrane proteins. This chapter describes the experimental approaches to the development of this bioanalytical platform.

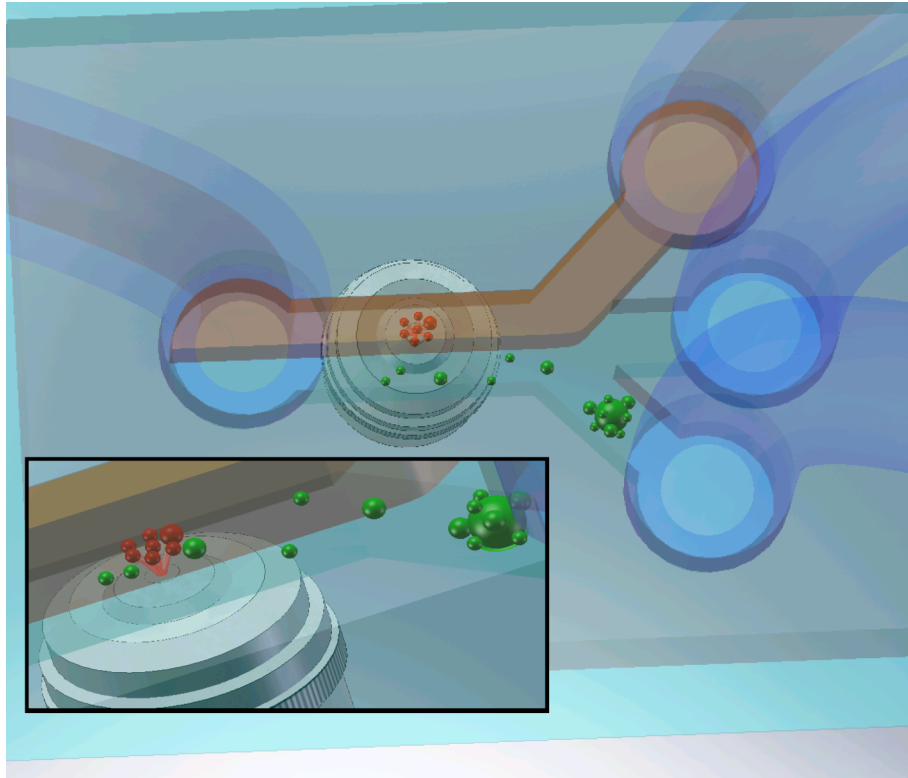


Figure 6.1: Schematic illustration of a labeling assay on native vesicles as realized in section 6.4 (top view). A PDMS block comprising microfluidic channels (gray) is bound on a glass slide (light blue), and connected to microfluidic tubes (blue). External syringe pumps control a pressure driven flow. Only two laminar flows are depicted: the upper one contains a fluorescently labeled ligand and the lower one cytochalasin B, required for native vesicle production. A cell blebbing vesicles is shown in green and native vesicles trapped by the laser tweezers are shown in red. The trapped vesicles can be labeled when moving to the label solution (insert).

6.1 Microfluidics for Production of Native Vesicles

There are several possibilities to control the flow of solution in the microchannels. When using external syringe pumps, the solution flow is driven by

pressure. In microchannels, the fluid behavior differs from macroscopic fluid dynamics. Besides others (Beebe, Mensing et al. 2002), two parameters are of particular importance: (i) in microfluidics, the Reynolds number, which characterizes the flow turbulence, is low in comparison to macroscopic fluids and hence the flow can be considered as laminar. This physical property dictates that two flows running in parallel in the same channel will not mix by turbulence but only by diffusion across the boundaries between the laminar flows. (ii) Due to a higher surface to volume ratio, the surface tension at the edges of the channel is increased. Consequently the flow velocity profile is inhomogeneous and becomes parabolic (Kuricheti, Buschmann et al. 2004), with a higher velocity in the middle than at the edges of the channel (figure 6.2). These two physical properties have important consequences on the next experiments proposed and their implications will be further discussed.

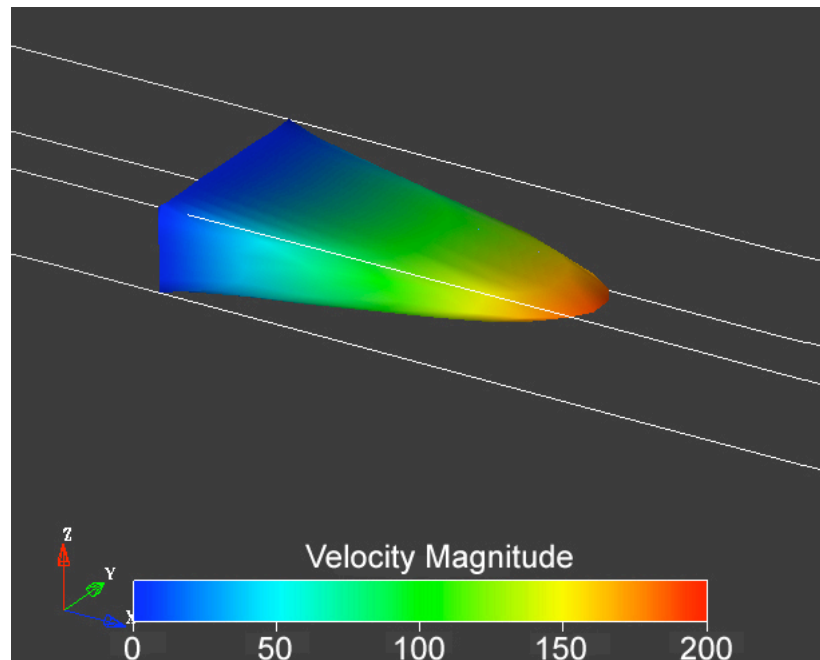


Figure 6.2: Flow velocity profile in a microchannel with aspect ratio 2:5 under pressure driven conditions. Velocity is assumed to be zero at channel walls. Image results from a calculation using Coventorware software. Extracted from Basic Microfluidic Concepts from the homepage of Prof. Paul Yager's group.

(<http://faculty.washington.edu/yagerp/microfluidictutorial/basicconcepts/basicconcepts.htm>)

6.1.2 Adherent Cells

As previously discussed, native vesicles are ideally suited to downscale bioanalytics below the single cell level. Their size makes them the smallest autonomous, biological relevant container appropriate to perform lab-on-chip experiments. The first step, native vesicle production, was tested in a single microfluidic channel. Cells were first attached to the bottom surface of the microchannel and then treated with cytochalasin B to induce blebbing, i.e. native vesicles. Native vesicles detach from cells under a constant flow, which can be visualized by fluorescence microscopy when the flow is stopped (figure 6.3). Together with vesicles, cells occasionally detach from glass surface.

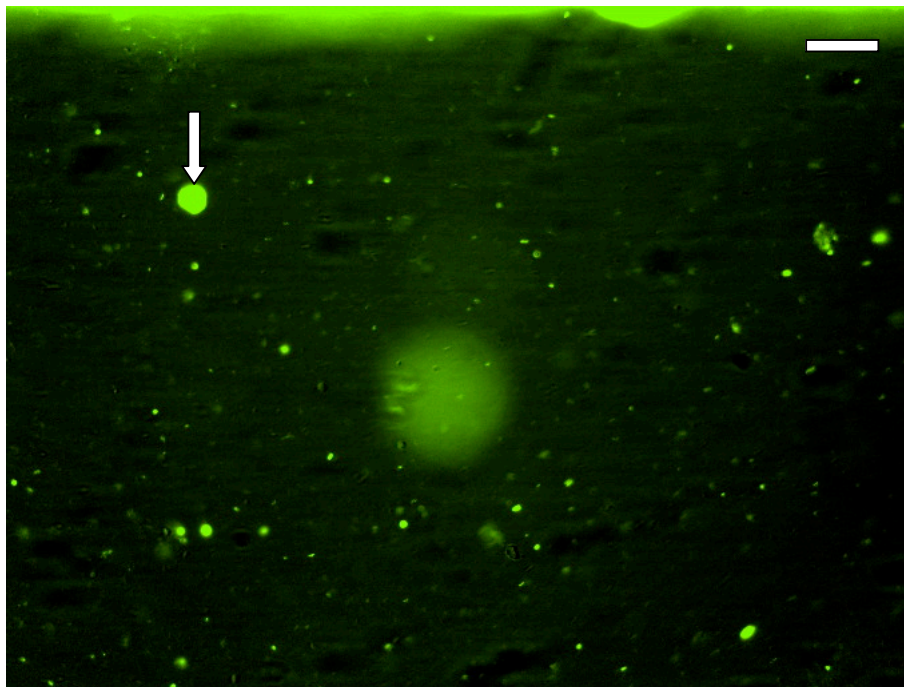


Figure 6.3: Native vesicles were produced in a microchannel from adherent HEK cells expressing β -arrestin-YFP by application of cytochalasin B. The flow is able to

detach them from their mother cells. After the flow is stopped native vesicles (small green spots) as well as cells (arrow) are observed. Scale bar represents 10 μm .

When vesicles are produced from single cells, some remain attached to their mother cell. If the vesicle is not totally closed, a tether will remain, connecting the vesicle to its mother cell. The shear force created can be sufficient to elongate such a tether, rendering it slim enough for the membrane of the tubule edges to collapse and finally induce the total closure of the vesicle. In this case the vesicle can separate from its mother cell without rupture or leakage.

When remaining attached stronger shear forces should be created to induce their separation. Shear forces are dependent of flow velocity and the surface exposed to the flow and then in direct relation to vesicle size. Thus the chance to detach a large vesicle is higher than to detach a smaller one. Another non-obvious aspect is the position of the vesicle and the cell in relation to the flow direction (if the vesicle is in front or behind the cell). Flow velocities in the range of 1-1000 $\mu\text{m/s}$ were applied to release them, but due to the parabolic profile of the flow at the proximity of channel edge, the flow velocity and proportionally the shear forces applied on the particle were weak too. The release of native vesicles remaining attached to the cell requires the use of higher flow velocity up to 1.4 $\mu\text{l/s}$ (which is in the range of mm/s) with switching between forward-backward flows (figure 6.4). Experimental evidence shows that in some cases, the difficulties to detach native vesicles from its mother cell were not only due to the low experimental shear forces, but also due to additional factors, such as a strong membrane-membrane interaction induced either by glycoproteins or by the presence of electrical charges on the cell surface. The major disadvantage is that at such flow rates, optical trapping is no longer possible, which in turn

requires more complex microfluidic platform in order to combine production and trapping. On the other hand the switching between forward-backward flows represent an advantage, element allowing to maintain all the produced vesicles in the same volume, without any dilution, as it would occur in a directed permanent flow.

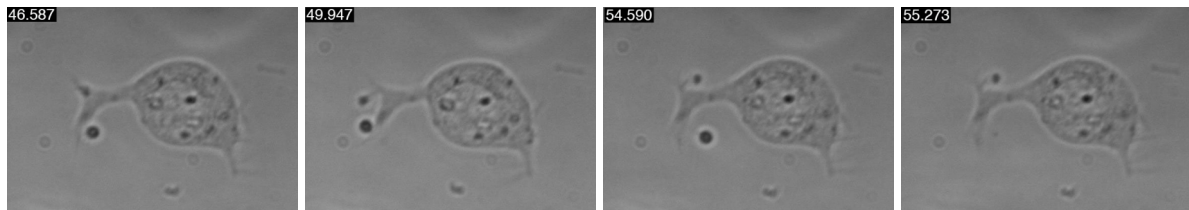


Figure 6.4: Sequence of images depicting on an NG108 adherent cell the formation of native vesicles after cytochalasin B application. Shear forces created by switching between forward-backward flows detach the native vesicles from their mother cell.

Native vesicles can thus be separated from cells directly by shear forces created by flow velocity. Cells with strong adhesion to the surface are most appropriate. Coating the surface of the microfluidic channel with poly-lysine or fibronectin, can increase cell adhesion.

6.1.2 Single cells in suspension

Negative dielectrophoresis was used to produce native vesicles from single cells in suspension in a microfluidic channel. The experiment was performed in a Evotech[®] Cytocon 400 setup which consists of a MEMS device connected to a fluidic control system to manipulate objects ranging from 5 to 25 μm (Muller, Pfennig et al. 2003). For manipulating cells/vesicles in inhomogeneous

alternating electrical field the particles do not require net surface charges. Dielectrophoresis exploits the difference in polarizability between the medium and a particle in suspension in a uniform electric field. When an electrical field of a given frequency is applied between the two electrodes, a dipole moment is created in the particle. This dipole moment is a function of the particle volume, the strength and the frequency of the electrical field. This electrical dipole moment created at the particle induces a force perpendicular to the electrodes moving the particles along the electrical field (positive dielectrophoresis or pDEP) or away from it (negative dielectrophoresis or nDEP).

The MEMS devices, also termed chips, integrate different electrode shapes and configurations (Schnelle, Muller et al. 1999) symmetrically on the top and at the bottom of the channel. The shape of the electrical field allows manipulating objects in diverse manners. Various combinations of electrodes have been realized: deflectors, composed of two electrodes which will push particles according to their orientation; funnels which are double deflectors, composed of four electrodes, which will focus objects at the middle of the channel; 3D cage electrode array (Schnelle, Muller et al. 2000) composed of four electrodes placed on the top of the channel and four other at the bottom; zigzag or hook electrodes, which retain and immobilize particles due to the creation of a barrier opposing the solution flow.

The 3D cage electrode is based on the following principle: alternating phase shift between the electrodes rotates and thus creates an AC cage field able to trap particles. Adjustable modes of phase shifts produce a controlled movement of the trapped particles, such as rotation around a single axis (spinning), rotation on a single plan or stretching. These modes allow orientating the trapped object and are susceptible to create centrifugal forces on the particle

or even increase shear forces created by the flow, if the positioning of the object is optimized to this effect. Although not developed to handle small objects such as native vesicles, this setup was tested to verify if it was possible to handle them and if these different modes are able to separate native vesicle from the trapped mother cell.

The following experiment was performed: single cells are trapped in the 3D cage array and subjected to cytochalasin B. In some cases the flow was sufficient to release vesicles from the cell, but usually at such high shear forces cells tend to escape from the cage electrodes, before native vesicles could be separated.

Another approach consists in imposing additional rotational movements, which can be a spinning movement or a circular displacement in the horizontal plane. Thus imposed rotational movements were tested to expel the native vesicles at the beginning of the blebbing process from the trapped cell (figure 6.5). Unfortunately also this approach did not achieve a satisfactory separation of native vesicles from their mother cells, probably because the main resultant dielectrophoretic forces push cells and vesicles towards the center of the cage, maintaining them together and finally increasing membrane-membrane interactions along the time.

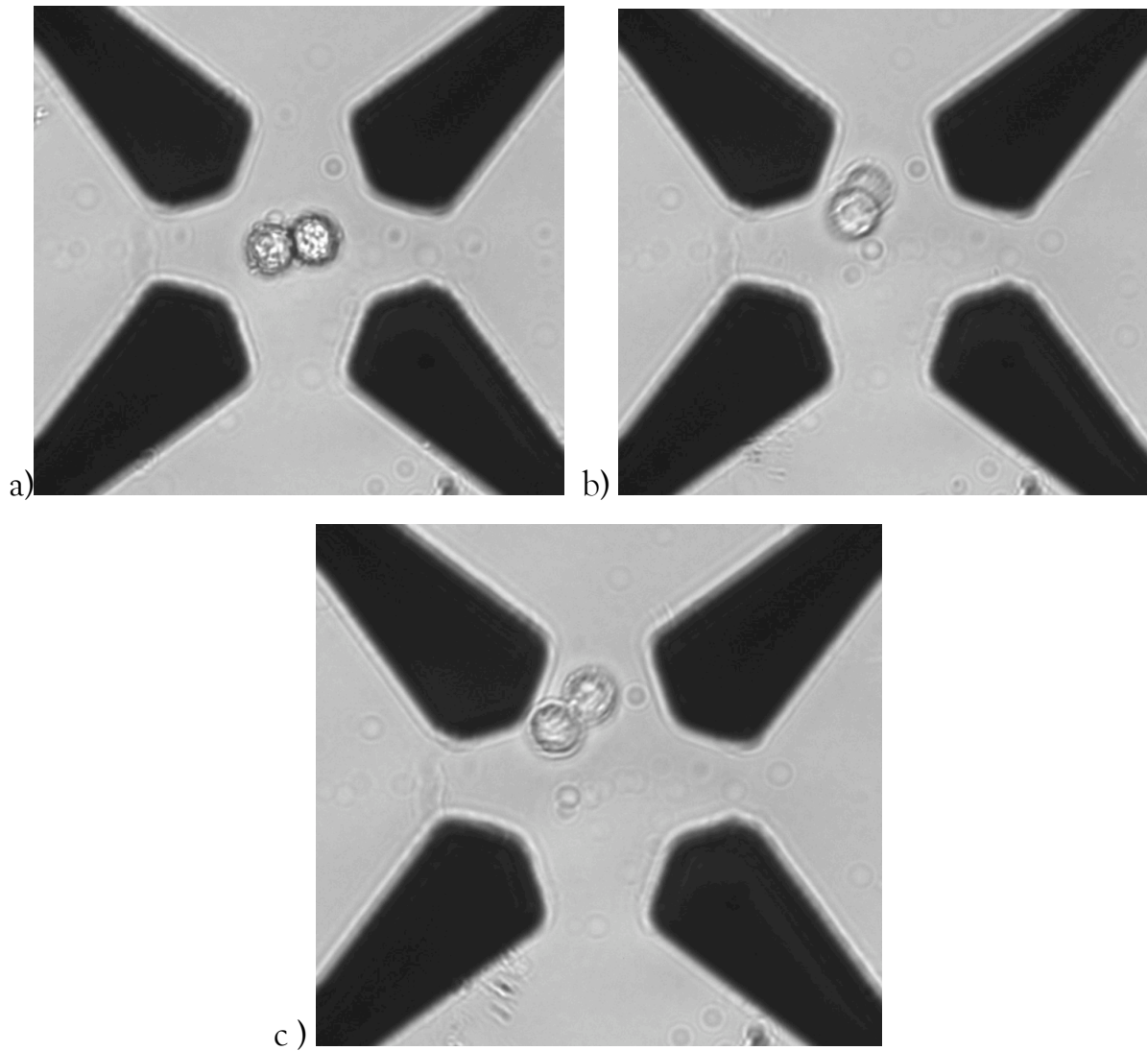


Figure 6.5: Microscopic micrographs showing a time series of two HEK cells exposing native vesicles at their surface (at times: a: 52 s; b: $t = 167$ s; c: $t = 196$ s). The imposed rotational pattern creates forces, which allows the separation of vesicles from their mother cell. Such forces are pointing to the center of the cage and have a tendency to cluster all the objects, rendering difficult the final separation.

Instead of using a cage electrode, single cells can also be maintained in hook electrodes. Additional forces can here be imposed by briefly increasing the power applied to the electrodes resulting in an increased total force imposed to

the cell. This additional force promotes the formation and the release of native vesicles by flow induced shear forces (figure 6.6).

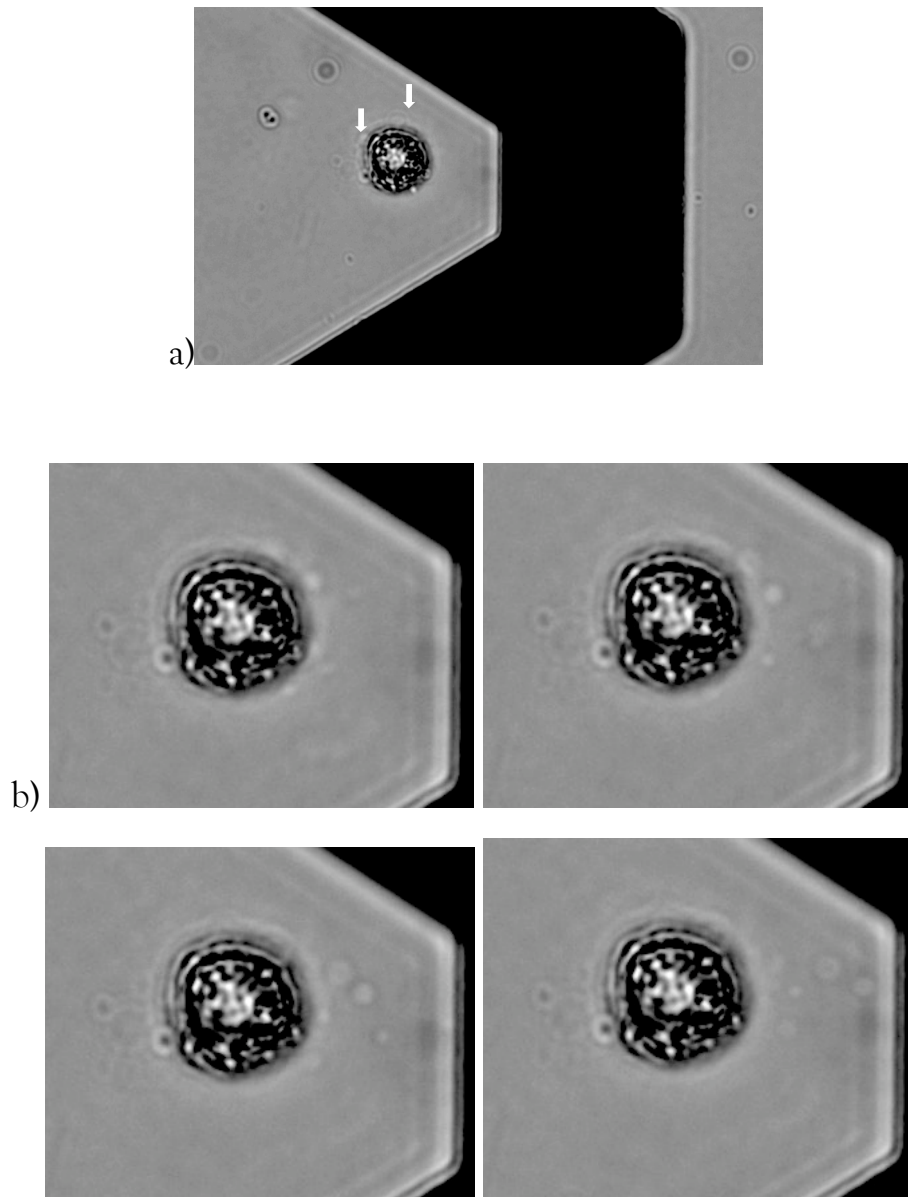


Figure 6.6: (a) shows a single cell trapped in a hook electrode in the Evotech microfluidic chip Loader blebbing native vesicles after cytochalasin treatment. (b) The four lower images are extracted from a movie showing native vesicles release from the cell (at times: 23s; 24s; 25.5s; 26.5s, respectively) after additional pressure created by increase of power applied to the electrodes.

To summarize, despite demonstrating that native vesicles can be produced from a selected cell in suspension, this approach shows low yield of vesicle production in a microfluidic channel. As described previously in section 5.3.1, laser tweezer can also be used directly to pull cell membrane and induce formation of native vesicles. However, despite the possibility to produce with a laser tweezer single native vesicles from an adherent desired cell, this approach can not be applied to produce large numbers of native vesicles. Overall the best results are obtained with cells attached to the surface of the channel, yielding sufficient number of native vesicles for further analysis.

6.2 Purification

Whether native vesicles are produced in bulk solutions or from adherent cells in a microchannel, the final preparation contains cell bodies but also cellular fragments that may disturb further experiments. Thus an additional purification step was performed prior to surface immobilization and further analysis. To test if the purification can be performed in the same microfluidic device as the one used for production of native vesicles, a MEMS setup was tested.

6.2.1 Electrophoresis

Electrophoresis is based on electrostatic forces actions on electrically charged particle in an electrical field. Because they enclose part of the cytoplasm of the mother cell and the membrane possesses the same composition, native vesicles can be considered as small artificial cells comprising net electrical negative charge. Under these conditions, electrophoresis can induce a net movement of

native vesicles. We performed an experiment using a simple microfluidic device with electrodes placed at the extremities of the microchannel. Biological particles, like native vesicles or cells, can be displaced in a stopped flow by electrophoresis (figure 6.7). This demonstrates that intact native vesicles possess a net negative charge similar to the live cell from which they are prepared. Other contaminating aggregates present in solution can be displaced in the opposite direction probably due to an overall positive net charge. This behavior could be used to purify the native vesicle preparation.

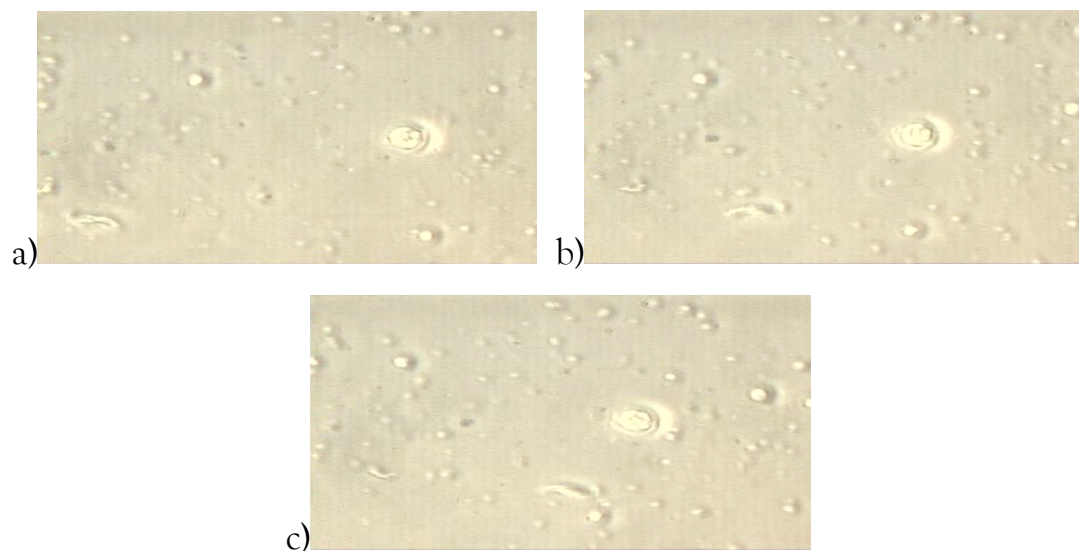


Figure 6.7: Sequential time series (a: $t = 25s$, b: $t = 37s$, c: $t = 44s$) The microscopic images depict vesicles and cells in a microchannel being displaced in one direction while some fragments migrate to the opposite direction.

6.2.2 Dielectrophoretic Depletion (DEPD)

Dielectrophoresis depends on the third power of the particle radius (Schnelle, Muller et al. 1999) offering the possibility to separate biological particles according to their size. In our case, dielectrophoretic effect is achieved via two parallel electrodes, one placed at the top and another at the bottom of the

microfluidic channel. In this configuration, the space between the two electrodes acts as an electrical barrier. At a particular angle α (optimally $\alpha = 45^\circ$) between the electrodes and the solution flow the particles are displaced by the dielectrophoretic force (F_{nDEP}) (figure 6.8). The size of displacement results from a superimposition of two forces: i) the nDEP which is proportional to the third power of the radius of the particle, and ii) the Stokes force originating from the friction of the particle with the solvent and scaling with the medium and the square power of the radius of the particle. In a typical experiment, 3 parameters can be adjusted to separate particles according to their size: electric field strength, oscillation frequency of electric field and flow speed of fluid. This separation method is termed dielectrophoretic depletion (DEPD), and was used in the present work to separate cells from native vesicles or native vesicles according to their sizes.

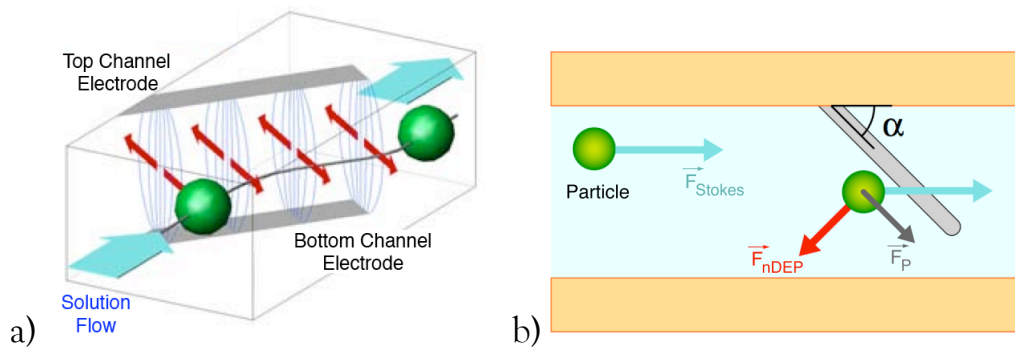


Figure 6.8: (a) Schematic representation of a biological particle (green) in a micro-flow (blue arrow indicates flow direction) before and after passing the dielectrophoretic barrier exerted by two parallel electrodes (grey bars) on the top and on the bottom of the microfluidic channel. The grey lines between the two electrodes indicate the electrical field and the bulk red arrows the dielectrophoretic force F_{nDEP} acting on the green particle. (b) Cross section through the microfluidic channel showing the action of F_{nDEP} and the Stokes force F_{Stokes} and the resulting force component F_{p} on the green particles, which also indicated the direction of movement. Images from Urban Seger's Ph.D. Thesis (EPFL TH 3610) and adapted to present case.

Cells can be efficiently separated from native vesicles according to their size and their capacity to become dipolar (figure 6.9). The limitation of this approach for our particular application turns out to be the speed of the flow, which can not be maintained very high (up to $100 \mu\text{m/s}$), constraining the use of this technique to small sample quantities, but in perfect range to combine it with optical trapping. On the other hand, small sample quantities is a big advantage, allowing to work with few or even single cells in the context of primary cells of which only a limited number is available.

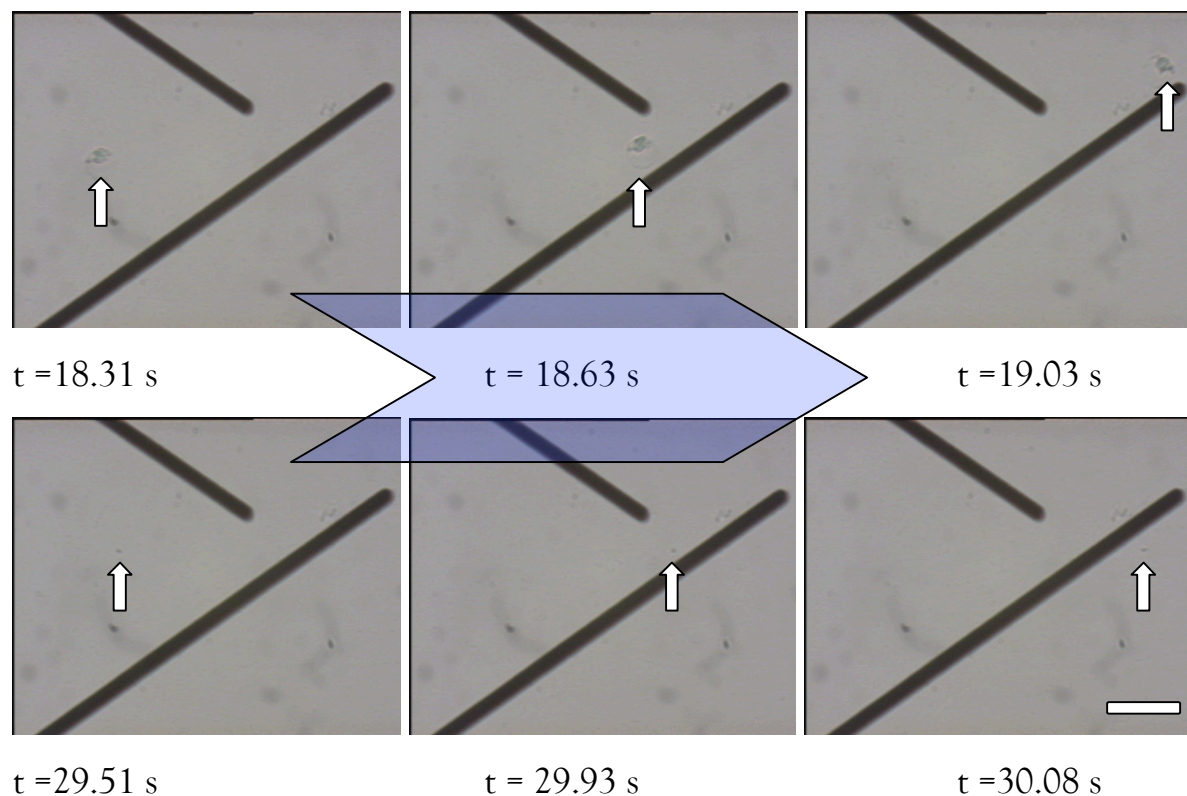


Figure 6.9: Separation of cells from native vesicles by DEP. Here, biological objects are repelled from the electrode according to their sizes. A cell is efficiently pushed away (upper panels) and native vesicles can flow through (lower panels). White arrows indicate relative positions at times. At the present magnification the small native vesicles are difficult to detect. Large blue arrow indicates flow direction. Scale bar represents $20 \mu\text{m}$.

Similar DEP experiments were performed using previously purified native vesicles preparations to separate them according to their size. Unfortunately, the range of size difference was too small to create a sufficient difference of polarization for separation. The use of a curved electrode across the channel might solve this problem by increasing the influence on the size of the particle in the separation process. Unfortunately these setups could not be tested because the appropriate chip configuration was not available.

6.3 Immobilization of vesicles by Negative Dielectrophoresis

The immobilization of native vesicles was tested using the Evotech setup. We used zigzag electrodes placed across the channel; this allowed to trap the objects and to expose them to potentially interacting compounds for screening purposes. This electrode configuration turned out to trap native vesicles efficiently (figure 6.10). Under certain conditions of electrodes versus vesicles sizes positive dielectrophoresis can occur, leading to the accumulation of vesicles at the edges of the channel at close proximity or directly on the electrodes, which finally disturbs the electrical field and decreases the efficiency of the separation. Despite larger Stokes forces exerted on the vesicles originating from the increased flow speed (up to mm/s), the forces created by the dielectrophoretic barrier are sufficient to maintain vesicles trapped while exchanging bulk solutions. The major disadvantage of the zigzag electrodes, which were originally developed to trap cells, is the fact that only 4 vesicles at a time can be trapped and analyzed.

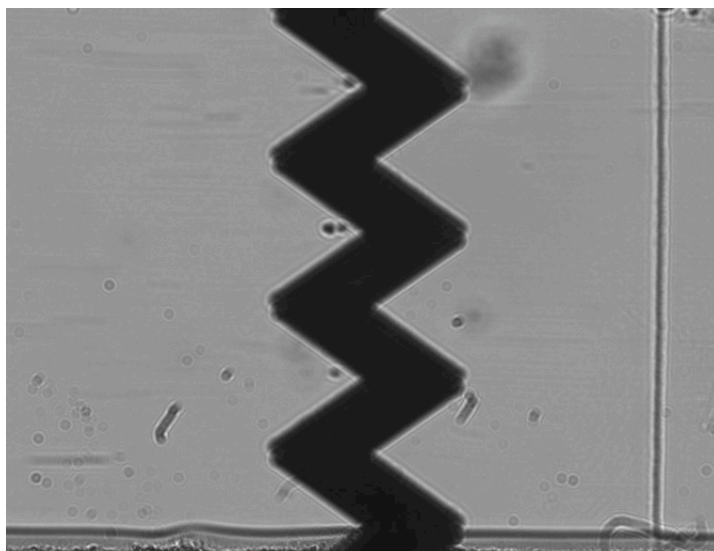


Figure 6.10: Zigzag electrode in a microfluidic chip (Evotech Loader) demonstrating trapping of native vesicles in the presence of a constant flow of solution (1 mm/s). The trapping zones are localized on the edges of the zigzag electrode. In the present case a too high concentration of native vesicles was used yielding accumulation of vesicles at each electrode edge.

6.4 Parallel Analysis with Laser Multi Tweezers

Previous experiments using a single focus laser tweezer have demonstrated that cells and cell fragments could be trapped efficiently, allowing the development of a novel bioanalytical platform. First, a home-build setup was designed to trap native vesicles in a multi array format (figure 6.19a). This setup exploits single IR beam, which is expanded and then passes through an array of microlenses and reproduces thus an 2D array of laser tweezers after crossing the lens of the microscope (figure 6.19b). The 2D array focused by the microscope lens, gives rise to a pseudo 3D trapping. This setup allows trapping and moving native vesicles in a microfluidic chip when flow velocities remain under 100 $\mu\text{m/s}$. This flow limitation avoids displacement of native vesicles from their optical traps by shear forces (figure 6.11).

The multiple laser tweezers offers major advantages in comparison to other existing techniques: (i) it is the fastest and most efficient technique to immobilize native vesicles and also allows the fastest exchange of sample.

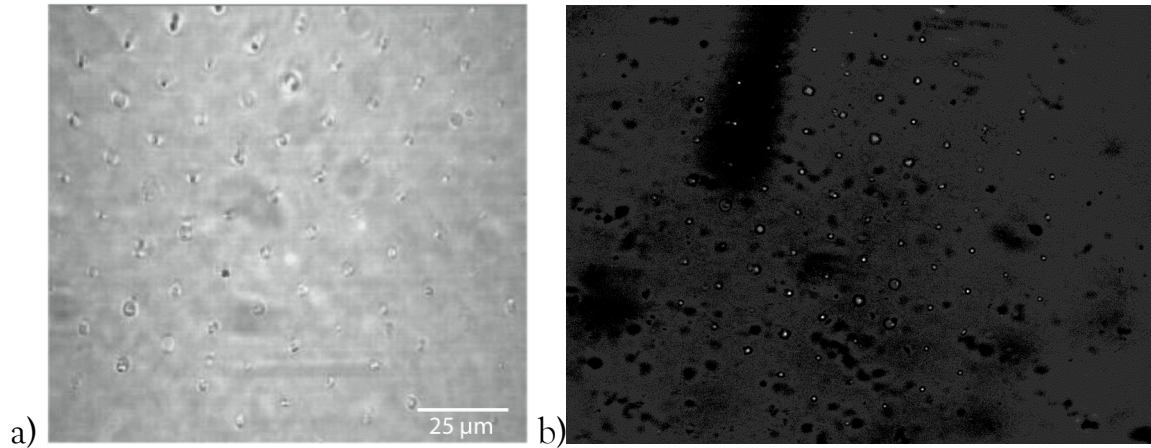


Figure 6.11: Trapping of native vesicles produced from HEK cells by multiple laser tweezers in a microfluidic channel. The two images are from two independent experiments. (a) Native vesicles can fill almost all available traps demonstrating an excellent efficiency of trapping. (b) Contrast and luminosity of right image has been adjusted for better clarity.

(ii) Due to the enormous number of trapped vesicles a reliable statistical analysis can be performed. Native vesicles expressing wtNK₁R previously labeled with SP-Cy5 can be trapped and fluorescence intensity can be measured.

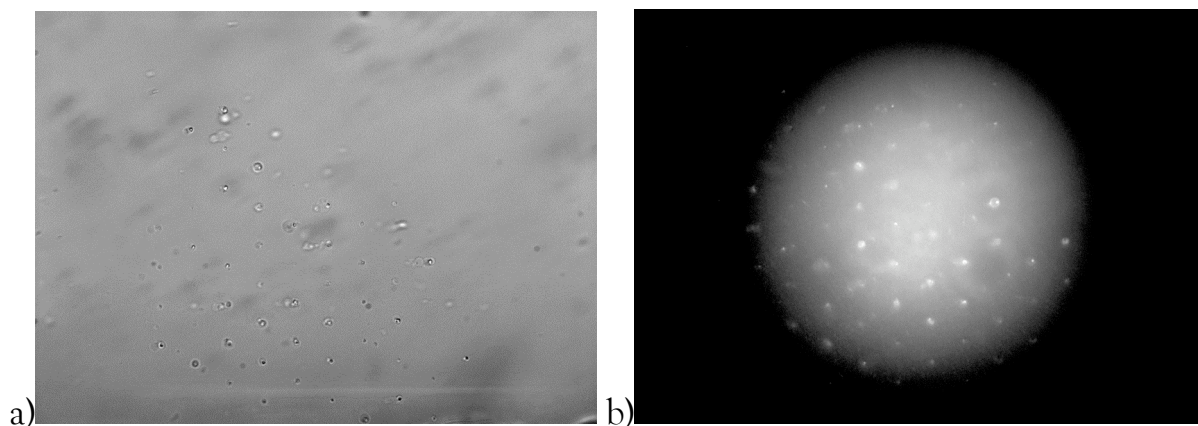


Figure 6.12: Native vesicles trapped by multiple optical tweezers in a microfluidic channel. The vesicles contain in their plasma membranes wtNK₁R labeled with 50

nM SP-Cy5. (a): Transmission micrograph; (b): Fluorescence micrograph as an average of 5 images from a time series.

(iii) Another interesting aspect of this technique is the possibility to follow the time course of a reaction in the trapped object. Using for example two parallel laminar flows within the microchannel (figure 6.1), it is possible to label native vesicles within seconds by lateral displacement of the sample from a buffer to a reaction flow. This experiment was accomplished with trapped native vesicles produced from cells expressing wtNK₁R labeling the vesicles with the NK₁R antagonist CP-Cy5 (figure 6.13). After correcting for background fluorescence and photobleaching, the time course of the labeling reaction could be resolved.

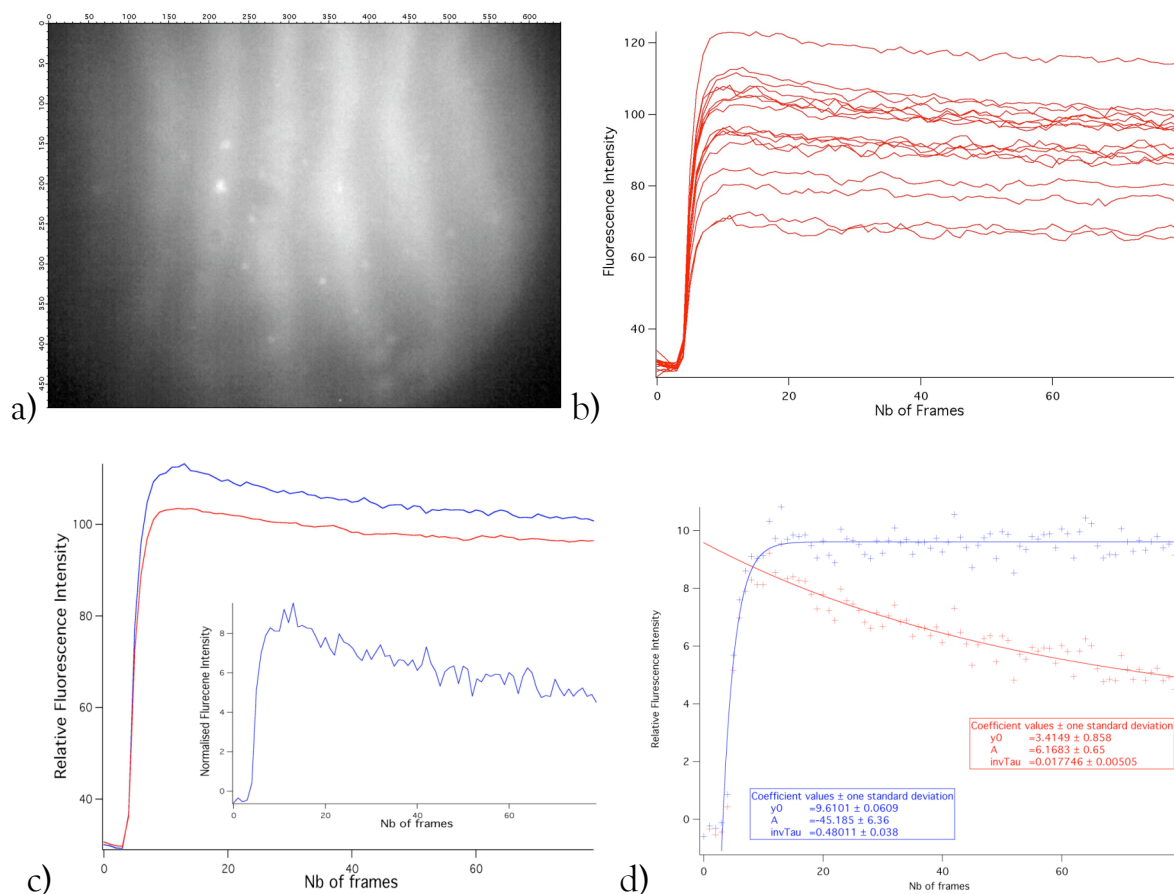


Figure 6.13: (a) Transmission micrograph of native vesicles expressing wtNK₁R and labeled with CP-Cy5 antagonist trapped by a multiple laser tweezer in a

microfluidic channel. (b) Fluorescence versus time traces of individual vesicles of the multi-laser tweezer trapped multiarray during binding of CP-Cy5. The intensity traces are not yet corrected for background and photobleaching. (c) As an example, it is possible to access a kinetic curve (red curve) and after background (red curve) correction (insert). (d) Photobleaching correction demonstrating the efficient recording. Mathematical analysis was performed with IgorPro software.

Our multiple tweezer/microfluidic chip platform offers the possibility to select a desired particle after analysis. This is achieved by using a second single laser tweezer beam tuned at a different wavelength, to remove the desired particle from the trapped vesicle multiarray and move it out of the array, transferring it to a parallel flow of buffer where subsequent manipulations can be performed. The platform can be also used for other unicellular organisms, such as yeast or bacteria.

6.5 New Lab-on-chip Designs

In order to fully exploit the potential of the native vesicles in our biochip platform for broad bioanalytical applications, it became clear within the course of our work that special, novel microfluidic chips should be developed to integrate all steps from production to analysis of native vesicles according to the following requirements: First, the flow velocity of the solution required to induce separation of native vesicles from adherent cells should be 2 to 3 orders of magnitude higher. Second, the flow velocity should be low enough to maintain native vesicles trapped in the array. Third, if adherent cells are grown inside the microfluidic channel and the bioanalytical assay is performed in this same channel,

background fluorescence arising from cells can be deleterious to perform fluorescence recordings on the vesicles.

Therefore, it is obvious that production and trapping can not be easily realized in the same channel and that the simplest microfluidic configuration require two separated channels, one for vesicle production and the other one for trapping and analyzing the vesicles. The simplest configuration fulfilling such requirements is called H design (figure 6.14), comprising two parallel major channels. The first channel is used for cell cultivation and native vesicles production, where switching between forward-backward high-velocity flows will induce separation of native vesicles from the cells. Using a pressure driven flow the vesicles can be pushed trough a connecting channel into the second channel, where optical trapping will be performed at lower flow velocity. An independent inlet provides additional control on the flow, maintaining an isolated flow profile and providing separate application of compounds in proximity of the vesicle trapping area without contacting the cells. Different compounds or compound concentrations can be applied sequentially. Adequate dimensions are in a few centimeter range for the primary channel length and as short as one centimeter for the secondary channel, both with a width of 200 μm and a height of 25 μm . These dimensions are smaller than conventional microfluidic systems but probably more appropriate to handle native vesicles.

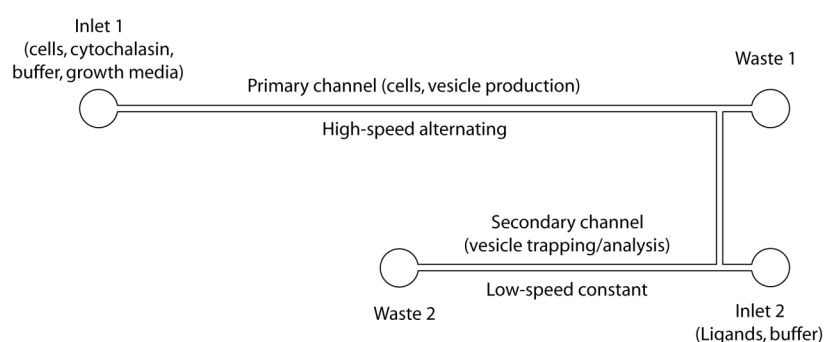


Figure 6.14: Microfluidic chip with H configuration composed of two separated channels: The primary channel is for cell growth and native vesicle production and

comprises waste outlet. It is connected by an intermediary channel to the secondary channel, where bioassays can be performed.

In order to perform bioanalytical assays at different concentrations in a single microfluidic channel, two other chip designs were tested. The first consists of a cross channel configuration (figure 6.15). In this case, a particular ligand concentration is adjusted along the micro-mixer channel to finally enter the crossing channel where the sample solution is also entering from the opposite side, thus creating a region, where the two flows are counterbalanced. The opposing flows are evacuated through the crossing channel. The two counterbalanced flows form a well defined interface, where vesicles can be trapped and moved from the buffer to the reagent solution. The crossing channel is of smaller dimension thus increasing the flow velocities to the waste and decreasing the diffusion across the interface at the two fluids, hence avoiding a significant change of the reagent concentration in the corresponding fluid. The length of the micro-mixer is of a few centimeters to ensure a perfect mixing of the solutions. The main advantages of this design are the control of the reagent concentration and the fast exchange to the reagent solution.

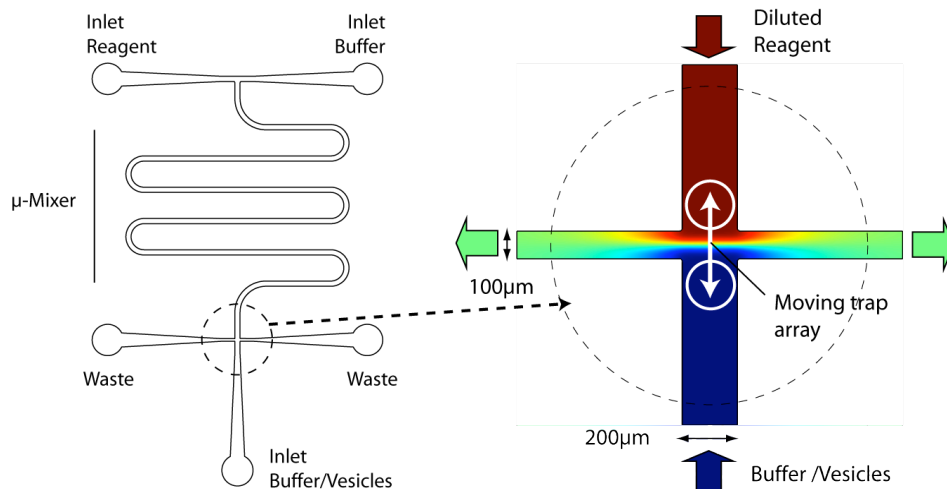


Figure 6.15: Cross-channel chip design. The right panel is a magnification of the cross section showing the simulated diffusion region with an assumed diffusion

constant for the reagent of $5 \cdot 10^{-10} \text{ m}^2/\text{s}$, performed with COMSOL Multiphysics software. Colors are indicative to show diffusion reagent profile.

The second alternative to perform bioanalytical assays at different concentrations in a single microfluidic channel makes use of a Y shape channel with two different branch widths, generating in the mixing region a smooth concentration gradient, created by the diffusion of the reagent along the length of the channel (figure 6.16). The smaller channel (200 μm width) provides a concentrated solution of reagent and the larger channel (800 μm width) conveys a solution of free buffer containing the sample of interest to the mixing area. For parallel laminar flows, the concentrated solution of reagent diffuses across the interface between the two fluids and creates a gradient of concentration along the length of the main channel (3 cm). Varying the flow velocity of the reagent solution allows adjusting the profile of concentration gradient. The disadvantage of this last design is that reagent diffusion is difficult to model; the concentration gradient at the mixing region was to be measured experimentally, e.g. by fluorescence techniques.

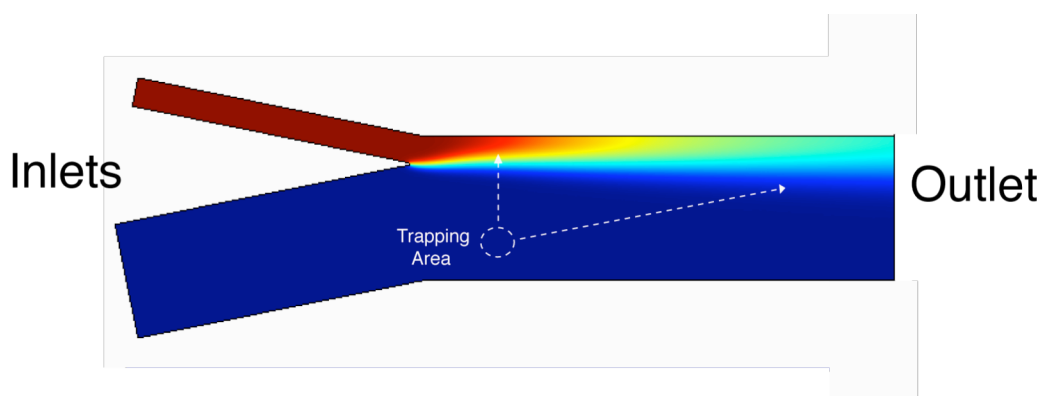


Figure 6.16: Scheme of the Y chip design with a simulated diffusion region with an assumed diffusion constant for the reagent of $5 \cdot 10^{-10} \text{ m}^2/\text{s}$, performed with COMSOL Multiphysics software. Colors are indicative to show diffusion reagent profile. The trapped vesicle array (circular area) can be moved (arrows) to high

concentration (moving directly upwards) or to lower concentration regions (moving first to the right). The lowest concentration could be reached further along channel length.

These H and Y microfluidic configurations were tested for labeling of vesicles. The vesicles have been produced separately. The final design for an optimal lab-on-chip platform probably requires a combination of the H chip and the Y shape microfluidics. These chips are produced in collaboration with the CSEM and are currently under investigations.

6.6 Conclusions and Outlook

Different steps for a bioanalytical chip platform have been investigated independently with different technologies. We demonstrated that each step from production, purification, and immobilization to the analysis of native vesicles can be performed within a single microfluidic platform.

In MEMS devices, production of native vesicles from a single cell in suspension was demonstrated, with subsequent possibility of immobilization. However, in regard of the electrode sizes, which were conceived for trapping larger objects, such chips do not allow performing immobilization of high number of native vesicles.

Production of native vesicles from adherent cells in a microfluidic channel was demonstrated and presents the advantage of a larger production scale required to multiplexing bioanalytics.

Dielectrophoresis depletion, performed with MEMS chips, demonstrated to be an appropriated technique to achieve efficient separation of native vesicles from cells in a permanent flow and can be achieved at a speed in the order of magnitude required for subsequent laser trapping.

The development of the multi-tweezers setup demonstrates to be, for the moment the most appropriated technique to perform large-scale immobilization of biological objects. When coupled to microfluidics and fluorescence detection in a standard microscope, efficient labeling of native vesicles could be achieved, demonstrating that immobilization and on-line measurements can be performed together. This setup presents the major advantage to be able to perform fast rounds of labeling by facilitated sample exchange, opening the possibility of multiplexing bioanalytics.

However, to achieve complete lab-on-chip assays on this setup still calls some improvements, especially in microfluidics designs. In order to combine all individual steps into a lab-on-chip device, this general investigation finally demonstrates the probable requirement of a combination of several technologies in a proper device design.

Native vesicles appear to be the most appropriated biological objects to be combined to laser multi-tweezers trapping technology. This step in miniaturization downscales analysis under the single cell analysis offering a clear reduction in cost. The development of this new setup opens diverse possibilities for screening purposes for GPCRs or ionic channels as well as in situ hybridization offering a new technology for medical diagnosis, or even for environmental analysis and screening.

6.7 Materials and Methods

Microchannel Fabrication

PDMS (Sylgard 184) microchannels were produced using metal master. Liquid PDMS was cast on to the master, left for 2 hours to release gas bubbles, and afterwards cured overnight. After detachment from the master, the microchannels comprising side of the PDMS block was treated with oxygen plasma for 30 seconds and then attached to a clean glass slide surface. The PDMS block was occasionally exposed to UV light irradiation for 30 minutes, leading even to stronger attachment to glass slides.

Evotech Cytocon 400 microchip analysis system

Evotech Cytocon 400 System is composed of the following components:

- 1) Microscope Zeiss 200 M equipped with mercury lamp illumination and adequate set of optical filters for the fluorophores DAPI, GFP, YFP, Cy3, Cy5. The microscope is controlled using Metamorph software (Molecular Devices).
- 2) Syringe Pump: (SP210w Infusion) from World Precision Instruments computer controlled with Swith Software (Evotech Technologies).
- 3) Syringes (25 ul or 50 ul) from Hamilton.
- 4) Tubes, adaptators and connections from Upchurch Scientific.
- 5) Generator system (Evotech Technologies): Voltage V_{out} : 0-25 V; Frequency: 300 Hz - 18 MHz computer controlled with Swith Software
- 6) Chips : DFC, Sorter and Loader.
- 7) Cytocon-Buffer II, conductivity = 0.3 S/m.

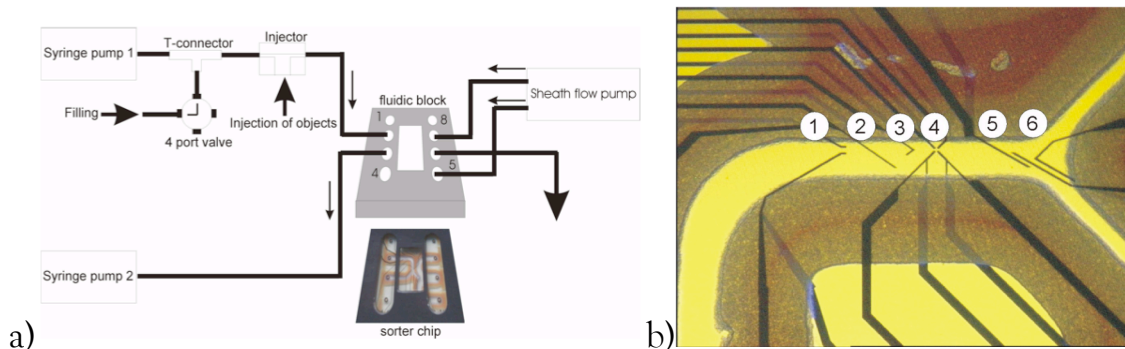


Figure 6.17: (a) Scheme of fluidic connections for Sorter chip. (b) Sorter chip integrates the following combination of electrodes functions: 1) funnel, 2) deflector 3) hook, 4) cage, 5) switch and 6) hence.

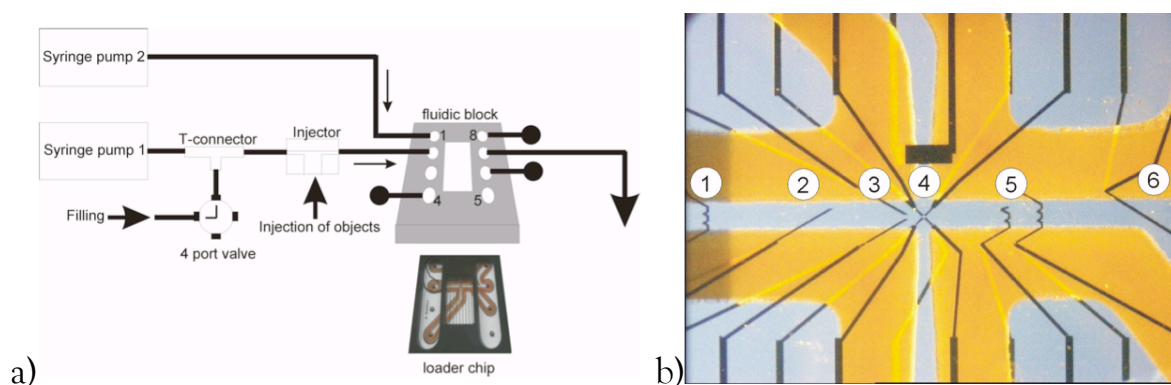


Figure 6.18: (a) Scheme of fluidic connections for Loader chip. (b) Loader chip integrates the following combination of electrodes: 1) and 5) zigzag, 2) deflector 3) funnel, 4) cage and 6) switch.

Cells were resuspended in Cytocon II buffer, introduced into the microfluidic channel via the injector and trapped by electrodes (cages, hook or zigzag) at a standard frequency of 1 MHz, with typical applied voltage 6-10 V with flow solution at 1200 $\mu\text{l/s}$. Such values were slightly adjusted according to particular requirements. For rotational modes a second imposed frequency was in between 100 kHz -4 MHz.

Dielectrophoretic Depletion (DEPD)

Native vesicle preparations were introduced into microchannels in PBS⁻ buffer. Flow speed of solution ranged from 50 to 200 $\mu\text{m}/\text{s}$. Voltages applied to electrodes were between 6 to 12 V at a frequency from 800 kHz to 1 MHz.

Multiple laser tweezers

The multiple optical tweezers array was generated with a single collimated laser beam produced by Ytterbium fiber laser (IPG Photonics; Em: 1064 nm; P_{max} : 10W). A diode (Bookam Technology UC9XX; Em: 974 nm; P_{max} : 100mW) controlled by a galvanic mirror was used for sorting purpose. The principal beam was passing through a microlenses array (Süss MicroOptics), creating an array of 100 converging beams, which were focused through a high-NA water-immersion objective (Zeiss C-Apochromat W 63X/1.2 Korr UV-Vis-IR) via the entry port of an inverted microscope (Zeiss Axiovert 100). Fluorescence excitation was generated by two He-Ne lasers (Polytech GmbH; Em: 543 nm; P_{max} : 0.5 mW and Em: 633 nm; P_{max} : 2 mW) entering the microscope dichroic mirror (Chroma). Fluorescence images were collected by a color CCD camera (PCO Pixelfly Standard 205xs VGA). PDMS microfluidic chip is bound to a glass slide placed on a motorized xy microscope table (Märzhäuser) and connected to fluidic tubes. During experiment two laminar flows were maintained. Native vesicles preparations run on the first flow, where they are trapped. Once trapped, they are moved to the labeling solution (SP-Cy5 or CP-Cy5) by displacing the motorized stage.

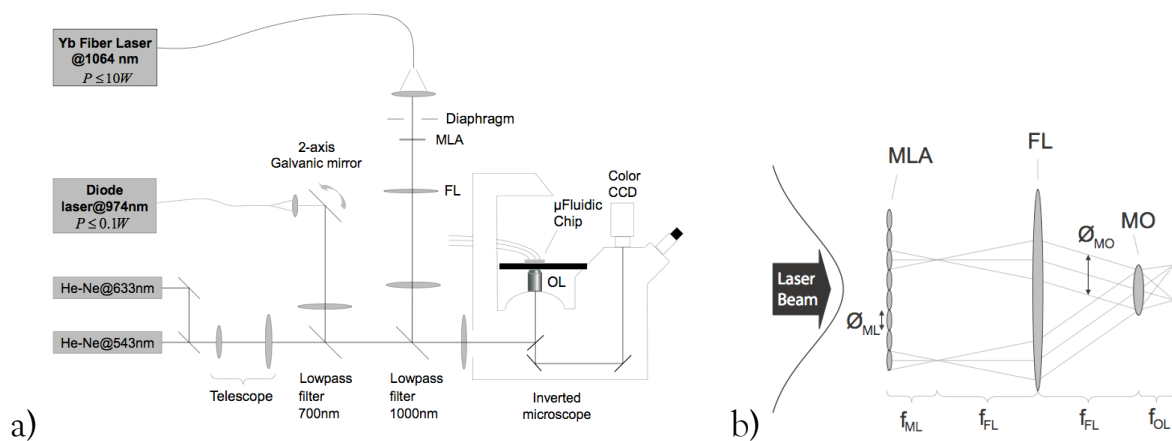


Figure 6.19: (a) Scheme of the complete multi-tweezer array setup. (b) Illustration of the creation of multiple tweezers array when the laser beam crosses successively the microlens array (MLA), field lens (FL) and microscope objective (MO).

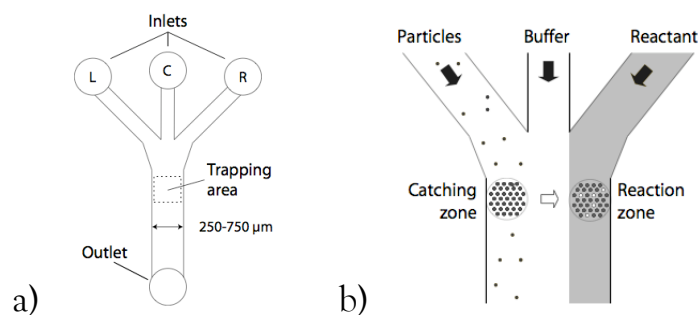


Figure 6.20: The microchannel structure is depicted in (a). The laminar flow and the experimental concept were illustrated in (b).

Bibliography

- Alves, I. D., D. Delaroche, et al. (2006). "The two NK-1 binding sites correspond to distinct, independent, and non-interconvertible receptor conformational states as confirmed by plasmon-waveguide resonance spectroscopy." *Biochemistry* **45**(16): 5309-18.
- Amara, A. and D. R. Littman (2003). "After Hrs with HIV." *J Cell Biol* **162**(3): 371-5.
- Anthony, R. M., T. J. Brown, et al. (2001). "DNA array technology and diagnostic microbiology." *Expert Rev Mol Diagn* **1**(1): 30-8.
- Ashkin, A. (1998). "Forces of a single-beam gradient laser trap on a dielectric sphere in the ray optics regime." *Methods Cell Biol* **55**: 1-27.
- Ashkin, A. and J. M. Dziedzic (1987). "Optical trapping and manipulation of viruses and bacteria." *Science* **235**(4795): 1517-20.
- Ashkin, A. and J. M. Dziedzic (1989). "Internal cell manipulation using infrared laser traps." *Proc Natl Acad Sci U S A* **86**(20): 7914-8.
- Azzi, M., P. G. Charest, et al. (2003). "{beta}-Arrestin-mediated activation of MAPK by inverse agonists reveals distinct active conformations for G protein-coupled receptors." *Proc Natl Acad Sci U S A* **100**(20): 11406-11411.
- Baba, T., K. Udaka, et al. (2003). "Actin-rich spherical extrusion induced in okadaic acid-treated K562 cells by crosslinking of membrane microdomains." *J Histochem Cytochem* **51**(2): 245-52.
- Babst, M., D. J. Katzmann, et al. (2002). "Escrt-III: an endosome-associated heterooligomeric protein complex required for mvb sorting." *Dev Cell* **3**(2): 271-82.
- Bacia, K., P. Schwille, et al. (2005). "Sterol structure determines the separation of phases and the curvature of the liquid-ordered phase in model membranes." *Proc Natl Acad Sci U S A* **102**(9): 3272-7.
- Bao, N., J. Wang, et al. (2008). "Recent advances in electric analysis of cells in microfluidic systems." *Anal Bioanal Chem* **391**(3): 933-42.
- Barnes, W. G., E. Reiter, et al. (2005). "beta-Arrestin 1 and Galphaq/11 coordinately activate RhoA and stress fiber formation following receptor stimulation." *J Biol Chem* **280**(9): 8041-50.
- Baumle, M., D. Stamou, et al. (2004). "Highly fluorescent streptavidin-coated CdSe nanoparticles: preparation in water, characterization, and micropatterning." *Langmuir* **20**(10): 3828-31.
- Becker, H. and C. Gartner (2000). "Polymer microfabrication methods for microfluidic analytical applications." *Electrophoresis* **21**(1): 12-26.
- Beebe, D. J., G. A. Mensing, et al. (2002). "Physics and applications of microfluidics in biology." *Annu Rev Biomed Eng* **4**: 261-86.
- Beer, N. R., E. K. Wheeler, et al. (2008). "On-chip single-copy real-time reverse-transcription PCR in isolated picoliter droplets." *Anal Chem* **80**(6): 1854-8.
- Belluardo, N., G. Mudo, et al. (2000). "Expression of connexin36 in the adult and developing rat brain." *Brain Res* **865**(1): 121-38.
- Bennett, M., S. M. Onnebo, et al. (2006). "Inositol pyrophosphates: metabolism and signaling." *Cell Mol Life Sci* **63**(5): 552-64.
- Benz, P. M., C. Blume, et al. (2008). "Cytoskeleton assembly at endothelial cell-cell contacts is regulated by alphaII-spectrin-VASP complexes." *J Cell Biol* **180**(1): 205-19.

- Bernstein, B. W. and J. R. Bamburg (2004). "A proposed mechanism for cell polarization with no external cues." Cell Motil Cytoskeleton 58(2): 96-103.
- Berridge, M. J., M. D. Bootman, et al. (2003). "Calcium signalling: dynamics, homeostasis and remodelling." Nat Rev Mol Cell Biol 4(7): 517-29.
- Berrier, A. L. and K. M. Yamada (2007). "Cell-matrix adhesion." J Cell Physiol 213(3): 565-73.
- Bettache, N., L. Baisamy, et al. (2003). "Mechanical constraint imposed on plasma membrane through transverse phospholipid imbalance induces reversible actin polymerization via phosphoinositide 3-kinase activation." J Cell Sci 116(Pt 11): 2277-84.
- Binder, W. H., V. Barragan, et al. (2003). "Domains and rafts in lipid membranes." Angew Chem Int Ed Engl 42(47): 5802-27.
- Blasig, I. E., L. Winkler, et al. (2006). "On the self-association potential of transmembrane tight junction proteins." Cell Mol Life Sci 63(4): 505-14.
- Bolinger, P. Y., D. Stamou, et al. (2004). "Integrated nanoreactor systems: triggering the release and mixing of compounds inside single vesicles." J Am Chem Soc 126(28): 8594-5.
- Caffrey, J. M., D. L. Eng, et al. (1992). "Three types of sodium channels in adult rat dorsal root ganglion neurons." Brain Res 592(1-2): 283-97.
- Caroni, P. (2001). "New EMBO members' review: actin cytoskeleton regulation through modulation of PI(4,5)P(2) rafts." Embo J 20(16): 4332-6.
- Carter, S. B. (1967). "Effects of cytochalasins on mammalian cells." Nature 213(73): 261-4.
- Chang, J. C., G. J. Brewer, et al. (2006). "Neuronal network structuring induces greater neuronal activity through enhanced astroglial development." J Neural Eng 3(3): 217-26.
- Charras, G. T., M. Coughlin, et al. (2008). "Life and times of a cellular bleb." Biophys J 94(5): 1836-53.
- Charras, G. T., C. K. Hu, et al. (2006). "Reassembly of contractile actin cortex in cell blebs." J Cell Biol 175(3): 477-90.
- Chen, X., H. Liu, et al. (2008). "Structural basis for synaptic adhesion mediated by neuroligin-neurexin interactions." Nat Struct Mol Biol 15(1): 50-6.
- Chou, Y. H., O. Skalli, et al. (1997). "Intermediate filaments and cytoplasmic networking: new connections and more functions." Curr Opin Cell Biol 9(1): 49-53.
- Chu, S., J. E. Bjorkholm, et al. (1986). "Experimental observation of optically trapped atoms." Phys Rev Lett 57(3): 314-317.
- Cingolani, L. A. and Y. Goda (2008). "Actin in action: the interplay between the actin cytoskeleton and synaptic efficacy." Nat Rev Neurosci 9(5): 344-56.
- Cooper, S. (2002). "Minimally disturbed, multicycle, and reproducible synchrony using a eukaryotic "baby machine"." Bioessays 24(6): 499-501.
- Csucs, G., R. Michel, et al. (2003). "Microcontact printing of novel co-polymers in combination with proteins for cell-biological applications." Biomaterials 24(10): 1713-20.
- Cunningham, C. C. (1995). "Actin polymerization and intracellular solvent flow in cell surface blebbing." J Cell Biol 129(6): 1589-99.
- Cuvelier, D., O. Rossier, et al. (2003). "Micropatterned "adherent/repellent" glass surfaces for studying the spreading kinetics of individual red blood cells onto protein-decorated substrates." Eur Biophys J 32(4): 342-54.
- Dai, J. and M. P. Sheetz (1999). "Membrane tether formation from blebbing cells." Biophys J 77(6): 3363-70.
- Denker, S. P. and D. L. Barber (2002). "Ion transport proteins anchor and regulate the cytoskeleton." Curr Opin Cell Biol 14(2): 214-20.

- Denker, S. P., D. C. Huang, et al. (2000). "Direct binding of the Na-H exchanger NHE1 to ERM proteins regulates the cortical cytoskeleton and cell shape independently of H(+) translocation." Mol Cell **6**(6): 1425-36.
- Didichenko, S. A., C. M. Fragoso, et al. (2003). "Mitotic and stress-induced phosphorylation of HsPI3K-C2alpha targets the protein for degradation." J Biol Chem **278**(28): 26055-64.
- Disanza, A., A. Steffen, et al. (2005). "Actin polymerization machinery: the finish line of signaling networks, the starting point of cellular movement." Cell Mol Life Sci.
- Ehrlicher, A., T. Betz, et al. (2002). "Guiding neuronal growth with light." Proc Natl Acad Sci U S A **99**(25): 16024-8.
- Ehrmann, K., M. Gersbach, et al. (2006). "Sample patterning on NMR surface microcoils." J Magn Reson **178**(1): 96-105.
- Flanagan, M. D. and S. Lin (1980). "Cytochalasins block actin filament elongation by binding to high affinity sites associated with F-actin." J Biol Chem **255**(3): 835-8.
- Florio, S. K., C. D. Westbrook, et al. (1990). "Transient potassium currents in avian sensory neurons." J Neurophysiol **63**(4): 725-37.
- Fong, A. M., R. T. Premont, et al. (2002). "Defective lymphocyte chemotaxis in beta-arrestin2- and GRK6-deficient mice." Proc Natl Acad Sci U S A **99**(11): 7478-83.
- Fong, T. M., R. R. Huang, et al. (1992). "Localization of agonist and antagonist binding domains of the human neurokinin-1 receptor." J Biol Chem **267**(36): 25664-7.
- Fong, T. M., H. Yu, et al. (1992). "The extracellular domain of the neurokinin-1 receptor is required for high-affinity binding of peptides." Biochemistry **31**(47): 11806-11.
- Fukuda, J., A. Khademhosseini, et al. (2006). "Micropatterned cell co-cultures using layer-by-layer deposition of extracellular matrix components." Biomaterials **27**(8): 1479-86.
- Garrus, J. E., U. K. von Schwedler, et al. (2001). "Tsg101 and the vacuolar protein sorting pathway are essential for HIV-1 budding." Cell **107**(1): 55-65.
- Gates, B. D., Q. Xu, et al. (2005). "New approaches to nanofabrication: molding, printing, and other techniques." Chem Rev **105**(4): 1171-96.
- Gaus, K., S. Le Lay, et al. (2006). "Integrin-mediated adhesion regulates membrane order." J Cell Biol **174**(5): 725-34.
- Geiger, B. (1983). "Membrane-cytoskeleton interaction." Biochim Biophys Acta **737**(3-4): 305-41.
- George, N., H. Pick, et al. (2004). "Specific labeling of cell surface proteins with chemically diverse compounds." J Am Chem Soc **126**(29): 8896-7.
- Gerrow, K., S. Romorini, et al. (2006). "A preformed complex of postsynaptic proteins is involved in excitatory synapse development." Neuron **49**(4): 547-62.
- Gether, U. (2000). "Uncovering molecular mechanisms involved in activation of G protein-coupled receptors." Endocr Rev **21**(1): 90-113.
- Goodenough, D. A., J. A. Goliger, et al. (1996). "Connexins, connexons, and intercellular communication." Annu Rev Biochem **65**: 475-502.
- Grashoff, C., I. Thievensen, et al. (2004). "Integrin-linked kinase: integrin's mysterious partner." Curr Opin Cell Biol **16**(5): 565-71.
- Grimbergen, J. A., K. Visscher, et al. (1993). "Isolation of single yeast cells by optical trapping." Yeast **9**(7): 723-32.
- Groves, J. T. (2005). "Molecular organization and signal transduction at intermembrane junctions." Angew Chem Int Ed Engl **44**(23): 3524-38.
- Gruenberg, J. and P. LBPA (2003). "Lipids in endocytic membrane transport and sorting." Curr Opin Cell Biol **15**(4): 382-8.

- Hagmann, J., M. M. Burger, et al. (1999). "Regulation of plasma membrane blebbing by the cytoskeleton." J Cell Biochem 73(4): 488-99.
- Hall, A. (1998). "Rho GTPases and the actin Cytoskeleton." Science 279(5350): 509-14.
- Halloran, M. C. and M. A. Wolman (2006). "Repulsion or adhesion: receptors make the call." Curr Opin Cell Biol 18(5): 533-40.
- Hamill, O. P., A. Marty, et al. (1981). "Improved patch-clamp techniques for high-resolution current recording from cells and cell-free membrane patches." Pflugers Arch 391(2): 85-100.
- Heuillet, E., J. Menager, et al. (1993). "Characterization of a human NK1 tachykinin receptor in the astrocytoma cell line U 373 MG." J Neurochem 60(3): 868-76.
- Heydorn, A., B. P. Sondergaard, et al. (2004). "A library of 7TM receptor C-terminal tails. Interactions with the proposed post-endocytic sorting proteins ERM-binding phosphoprotein 50 (EBP50), N-ethylmaleimide-sensitive factor (NSF), sorting nexin 1 (SNX1), and G protein-coupled receptor-associated sorting protein (GASP)." J Biol Chem 279(52): 54291-303.
- Hicke, L. (2001). "A new ticket for entry into budding vesicles-ubiquitin." Cell 106(5): 527-30.
- Higgs, H. N. and T. D. Pollard (2001). "Regulation of actin filament network formation through ARP2/3 complex: activation by a diverse array of proteins." Annu Rev Biochem 70: 649-76.
- Holm, A., T. Sundqvist, et al. (1999). "Mechanical manipulation of polymorphonuclear leukocyte plasma membranes with optical tweezers causes influx of extracellular calcium through membrane channels." Med Biol Eng Comput 37(3): 410-2.
- Honda, A., M. Nogami, et al. (1999). "Phosphatidylinositol 4-phosphate 5-kinase alpha is a downstream effector of the small G protein ARF6 in membrane ruffle formation." Cell 99(5): 521-32.
- Hopkins, A. M., S. V. Walsh, et al. (2003). "Constitutive activation of Rho proteins by CNF-1 influences tight junction structure and epithelial barrier function." J Cell Sci 116(4): 725-742.
- Huang, R. R., D. Huang, et al. (1995). "Conformational compatibility as a basis of differential affinities of tachykinins for the neurokinin-1 receptor." Biochemistry 34(50): 16467-72.
- Hyre, D. E., I. Le Trong, et al. (2006). "Cooperative hydrogen bond interactions in the streptavidin-biotin system." Protein Sci 15(3): 459-67.
- Johnson, C. L. and C. G. Johnson (1992). "Characterization of receptors for substance P in human astrocytoma cells: radioligand binding and inositol phosphate formation." J Neurochem 58(2): 471-7.
- Kam, L., W. Shain, et al. (2001). "Axonal outgrowth of hippocampal neurons on micro-scale networks of polylysine-conjugated laminin." Biomaterials 22(10): 1049-54.
- Kandel, E. R., J. H. Schwartz, et al. Principles of Neuronal Science, McGraw-Hill.
- Katz, E. and I. Willner (2004). "Integrated nanoparticle-biomolecule hybrid systems: synthesis, properties, and applications." Angew Chem Int Ed Engl 43(45): 6042-108.
- Katzmann, D. J., G. Odorizzi, et al. (2002). "Receptor downregulation and multivesicular-body sorting." Nat Rev Mol Cell Biol 3(12): 893-905.
- Kegler, K., M. Salomo, et al. (2007). "Forces of interaction between DNA-grafted colloids: an optical tweezer measurement." Phys Rev Lett 98(5): 058304.
- Keller, H., P. Rentsch, et al. (2002). "Differences in cortical actin structure and dynamics document that different types of blebs are formed by distinct mechanisms." Exp Cell Res 277(2): 161-72.

- Kenakin, T. (2004). "Principles: receptor theory in pharmacology." Trends Pharmacol Sci 25(4): 186-92.
- Kim, M. J., K. Futai, et al. (2007). "Synaptic accumulation of PSD-95 and synaptic function regulated by phosphorylation of serine-295 of PSD-95." Neuron 56(3): 488-502.
- Knaus, G. A., H. G. Knaus, et al. (1991). "Complex allosteric interaction of heparin with neurokinin-1 receptors." Eur J Pharmacol 207(3): 267-70.
- Kohsaka, H., E. Takasu, et al. (2007). "In vivo induction of postsynaptic molecular assembly by the cell adhesion molecule Fasciclin2." J Cell Biol 179(6): 1289-300.
- Kojima, H., E. Muto, et al. (1997). "Mechanics of single kinesin molecules measured by optical trapping nanometry." Biophys J 73(4): 2012-22.
- Kole, T. P., Y. Tseng, et al. (2005). "Intracellular mechanics of migrating fibroblasts." Mol Biol Cell 16(1): 328-38.
- Kuo, S. C. and M. P. Sheetz (1992). "Optical tweezers in cell biology." Trends Cell Biol 2(4): 116-8.
- Kuricheti, K. K., V. Buschmann, et al. (2004). "Application of fluorescence correlation spectroscopy for velocity imaging in microfluidic devices." Appl Spectrosc 58(10): 1180-6.
- Kwik, J., S. Boyle, et al. (2003). "Membrane cholesterol, lateral mobility, and the phosphatidylinositol 4,5-bisphosphate-dependent organization of cell actin." Proc Natl Acad Sci U S A 100(24): 13964-9.
- Lau, C. G. and R. S. Zukin (2007). "NMDA receptor trafficking in synaptic plasticity and neuropsychiatric disorders." Nat Rev Neurosci 8(6): 413-26.
- Lauer, L., A. Vogt, et al. (2002). "Electrophysiological recordings of patterned rat brain stem slice neurons." Biomaterials 23(15): 3123-30.
- Lefkowitz, R. J. (1998). "G protein-coupled receptors. III. New roles for receptor kinases and beta-arrestins in receptor signaling and desensitization." J Biol Chem 273(30): 18677-80.
- Lefkowitz, R. J., K. Rajagopal, et al. (2006). "New roles for beta-arrestins in cell signaling: not just for seven-transmembrane receptors." Mol Cell 24(5): 643-52.
- Leitz, G., G. Weber, et al. (1994). "The laser microbeam trap as an optical tool for living cells." Physiol Chem Phys Med NMR 26(1): 69-88.
- Levinson, J. N. and A. El-Husseini (2007). "A crystal-clear interaction: relating neuroligin/neurexin complex structure to function at the synapse." Neuron 56(6): 937-9.
- Li, Z. and M. Sheng (2003). "Some assembly required: the development of neuronal synapses." Nat Rev Mol Cell Biol 4(11): 833-41.
- Liang, H., W. H. Wright, et al. (1993). "Micromanipulation of chromosomes in PTK2 cells using laser microsurgery (optical scalpel) in combination with laser-induced optical force (optical tweezers)." Exp Cell Res 204(1): 110-20.
- Lillemeier, B. F., J. R. Pfeiffer, et al. (2006). "Plasma membrane-associated proteins are clustered into islands attached to the cytoskeleton." Proc Natl Acad Sci U S A 103(50): 18992-7.
- Lin, Z., S. Cui, et al. (2003). "Studies on quantum dots synthesized in aqueous solution for biological labeling via electrostatic interaction." Anal Biochem 319(2): 239-43.
- Lipowsky, R. and R. Dimova (2003). "Domains in membranes and vesicles." J.Phys.: Condes. Matter 15: S31-S34.
- Lodish, Berk, et al. Molecular Cell Biology, W.H. FREEMAN AND COMPANY.
- Luo, C., H. Li, et al. (2007). "The combination of optical tweezers and microwell array for cells physical manipulation and localization in microfluidic device." Biomed Microdevices 9(4): 573-8.

- Luo, L. (2002). "Actin cytoskeleton regulation in neuronal morphogenesis and structural plasticity." Annu Rev Cell Dev Biol **18**: 601-35.
- Ma, H., J. Hyun, et al. (2004). ""Non-Fouling" Oligo(ethylene glycol)-Functionalized Polymer Brushes Synthesized by Surface-Initiated Atom Transfer Radical Polymerization." Adv.Mat. **16**(4): 338-341.
- Madara, J. L. (1998). "Regulation of the movement of solutes across tight junctions." Annu Rev Physiol **60**: 143-59.
- Maddugoda, M. P., M. S. Crampton, et al. (2007). "Myosin VI and vinculin cooperate during the morphogenesis of cadherin cell cell contacts in mammalian epithelial cells." J Cell Biol **178**(3): 529-40.
- Maggi, C. A. (1995). "The mammalian tachykinin receptors." Gen Pharmacol **26**(5): 911-44.
- Maggi, C. A. and T. W. Schwartz (1997). "The dual nature of the tachykinin NK1 receptor." Trends Pharmacol Sci **18**(10): 351-5.
- McConalogue, K., C. U. Corvera, et al. (1998). "Desensitization of the neurokinin-1 receptor (NK1-R) in neurons: effects of substance P on the distribution of NK1-R, Galphaq/11, G- protein receptor kinase-2/3, and beta-arrestin-1/2." Mol Biol Cell **9**(8): 2305-24.
- McConalogue, K., O. Dery, et al. (1999). "Substance P-induced trafficking of beta-arrestins. The role of beta- arrestins in endocytosis of the neurokinin-1 receptor." J Biol Chem **274**(23): 16257-68.
- McLaughlin, S., J. Wang, et al. (2002). "PIP(2) and proteins: interactions, organization, and information flow." Annu Rev Biophys Biomol Struct **31**: 151-75.
- McMahon, H. T. and J. L. Gallop (2005). "Membrane curvature and mechanisms of dynamic cell membrane remodelling." Nature **438**(7068): 590-6.
- Mehrishi, J. N. and J. Bauer (2002). "Electrophoresis of cells and the biological relevance of surface charge." Electrophoresis **23**(13): 1984-94.
- Meyer, B. H., K. L. Martinez, et al. (2006). "Covalent labeling of cell-surface proteins for in-vivo FRET studies." FEBS Lett **580**(6): 1654-8.
- Miller, K., E. Weisberg, et al. (1992). "Membrane-bound and solubilized brain 5HT3 receptors: improved radioligand binding assays using bovine area postrema or rat cortex and the radioligands 3H-GR65630, 3H-BRL43694, and 3H-LY278584." Synapse **11**(1): 58-66.
- Mills, J. W., S. Falsig Pedersen, et al. (2000). "Effect of cytochalasins on F-actin and morphology of Ehrlich ascites tumor cells." Exp Cell Res **261**(1): 209-19.
- Monastyrskaya, K., A. Hostettler, et al. (2005). "The NK1 Receptor Localizes to the Plasma Membrane Microdomains, and Its Activation Is Dependent on Lipid Raft Integrity." J Biol Chem **280**(8): 7135-7146.
- Montgomery, J. M., P. L. Zamorano, et al. (2004). "MAGUKs in synapse assembly and function: an emerging view." Cell Mol Life Sci **61**(7-8): 911-29.
- Muller, T., A. Pfennig, et al. (2003). "The potential of dielectrophoresis for single-cell experiments." IEEE Eng Med Biol Mag **22**(6): 51-61.
- Neher, E. and B. Sakmann (1976). "Single-channel currents recorded from membrane of denervated frog muscle fibres." Nature **260**(5554): 799-802.
- Neher, E. and B. Sakmann (1992). "The patch clamp technique." Sci Am **266**(3): 44-51.
- Niemeyer, C. M. (2004). "Semi-synthetic DNA-protein conjugates: novel tools in analytics and nanobiotechnology." Biochem Soc Trans **32**(Pt 1): 51-3.
- Panchin, Y. V. (2005). "Evolution of gap junction proteins-the pannexin alternative." J Exp Biol **208**(Pt 8): 1415-9.
- Pantaloni, D., C. Le Clainche, et al. (2001). "Mechanism of actin-based motility." Science **292**(5521): 1502-6.

- Park, K. S., E. K. Seo, et al. (2006). "Light stamping lithography: microcontact printing without inks." J Am Chem Soc **128**(3): 858-65.
- Parthasarathy, R., C. H. Yu, et al. (2006). "Curvature-modulated phase separation in lipid bilayer membranes." Langmuir **22**(11): 5095-9.
- Pedersen, S. F., E. K. Hoffmann, et al. (2001). "The cytoskeleton and cell volume regulation." Comp Biochem Physiol A Mol Integr Physiol **130**(3): 385-99.
- Pereda, A. E., J. E. Rash, et al. (2004). "Dynamics of electrical transmission at club endings on the Mauthner cells." Brain Res Brain Res Rev **47**(1-3): 227-44.
- Perrone, M. H., R. E. Diehl, et al. (1983). "Binding of [3H]substance P to putative substance P receptors in rat brain membranes." Eur J Pharmacol **95**(1-2): 131-3.
- Pick, H., E. L. Schmid, et al. (2005). "Investigating cellular signaling reactions in single attoliter vesicles." J Am Chem Soc **127**(9): 2908-12.
- Pilzer, D., O. Gasser, et al. (2005). "Emission of membrane vesicles: roles in complement resistance, immunity and cancer." Springer Semin Immunopathol **27**(3): 375-87.
- Piper, R. C. and J. P. Luzio (2001). "Late endosomes: sorting and partitioning in multivesicular bodies." Traffic **2**(9): 612-21.
- Pornillos, O., J. E. Garrus, et al. (2002). "Mechanisms of enveloped RNA virus budding." Trends Cell Biol **12**(12): 569-79.
- Pornillos, O., D. S. Higginson, et al. (2003). "HIV Gag mimics the Tsg101-recruiting activity of the human Hrs protein." J Cell Biol **162**(3): 425-34.
- Railborg, C., T. E. Rusten, et al. (2003). "Protein sorting into multivesicular endosomes." Curr Opin Cell Biol **15**(4): 446-55.
- Raucher, D., T. Stauffer, et al. (2000). "Phosphatidylinositol 4,5-bisphosphate functions as a second messenger that regulates cytoskeleton-plasma membrane adhesion." Cell **100**(2): 221-8.
- Reisler, E. and E. H. Egelman (2007). "Actin structure and function: what we still do not understand." J Biol Chem **282**(50): 36133-7.
- Reitsma, S., D. W. Slaaf, et al. (2007). "The endothelial glycocalyx: composition, functions, and visualization." Pflugers Arch **454**(3): 345-59.
- Revenu, C., R. Athman, et al. (2004). "The co-workers of actin filaments: from cell structures to signals." Nat Rev Mol Cell Biol **5**(8): 635-46.
- Richert, L., P. Lavallo, et al. (2004). "Layer by layer buildup of polysaccharide films: physical chemistry and cellular adhesion aspects." Langmuir **20**(2): 448-58.
- Ridley, A. J. (2001). "Rho family proteins: coordinating cell responses." Trends Cell Biol **11**(12): 471-7.
- Ridley, A. J. (2001). "Rho proteins: linking signaling with membrane trafficking." Traffic **2**(5): 303-10.
- Ridley, A. J. (2006). "Rho GTPases and actin dynamics in membrane protrusions and vesicle trafficking." Trends Cell Biol **16**(10): 522-9.
- Rossetti, F. F., I. Reviakine, et al. (2004). "Interaction of poly(L-lysine)-g-poly(ethylene glycol) with supported phospholipid bilayers." Biophys J **87**(3): 1711-21.
- Rozkiewicz, D. I., Y. Kraan, et al. (2006). "Covalent Microcontact Printing of Proteins for Cell Patterning." Chemistry **12**(24): 6290-6297.
- Satomi, T., Y. Nagasaki, et al. (2007). "Density control of poly(ethylene glycol) layer to regulate cellular attachment." Langmuir **23**(12): 6698-703.
- Schmidlin, F., O. Dery, et al. (2002). "Heterologous regulation of trafficking and signaling of G protein-coupled receptors: beta-arrestin-dependent interactions between neurokinin receptors." Proc Natl Acad Sci U S A **99**(5): 3324-9.

- Schnelle, T., T. Muller, et al. (1999). "Dielectric single particle spectroscopy for measurement of dispersion." Med Biol Eng Comput 37(2): 264-71.
- Schnelle, T., T. Muller, et al. (2000). "Dielectrophoretic manipulation of suspended submicron particles." Electrophoresis 21(1): 66-73.
- Sechi, A. S. and J. Wehland (2000). "The actin cytoskeleton and plasma membrane connection: PtdIns(4,5)P(2) influences cytoskeletal protein activity at the plasma membrane." J Cell Sci 113 Pt 21: 3685-95.
- Simmons, R. M., J. T. Finer, et al. (1993). "Force on single actin filaments in a motility assay measured with an optical trap." Adv Exp Med Biol 332: 331-6; discussion 336-7.
- Small, J. V., T. Stradal, et al. (2002). "The lamellipodium: where motility begins." Trends in Cell Biology 12(3): 112-120.
- Stamou, D., C. Duschl, et al. (2003). "Self-assembled microarrays of attoliter molecular vessels." Angew Chem Int Ed Engl 42(45): 5580-3.
- Staneva, G., M. I. Angelova, et al. (2004). "Phospholipase A2 promotes raft budding and fission from giant liposomes." Chem Phys Lipids 129(1): 53-62.
- Steubing, R. W., S. Cheng, et al. (1991). "Laser induced cell fusion in combination with optical tweezers: the laser cell fusion trap." Cytometry 12(6): 505-10.
- Stryer, L., J. M. Berg, et al. Biochemistry, W.H. FREEMAN AND COMPAGNY.
- Suh, K. Y., J. Seong, et al. (2004). "A simple soft lithographic route to fabrication of poly(ethylene glycol) microstructures for protein and cell patterning." Biomaterials 25(3): 557-63.
- Sun, Y., Z. Cheng, et al. (2002). "Beta-arrestin2 is critically involved in CXCR4-mediated chemotaxis, and this is mediated by its enhancement of p38 MAPK activation." J Biol Chem 277(51): 49212-9.
- Tadir, Y., W. H. Wright, et al. (1991). "Micromanipulation of gametes using laser microbeams." Hum Reprod 6(7): 1011-6.
- Tairi, A. P., R. Hovius, et al. (1998). "Ligand binding to the serotonin 5HT3 receptor studied with a novel fluorescent ligand." Biochemistry 37(45): 15850-64.
- Takeichi, M. and K. Abe (2005). "Synaptic contact dynamics controlled by cadherin and catenins." Trends Cell Biol 15(4): 216-21.
- Turcatti, G., S. Zoffmann, et al. (1997). "Characterization of non-peptide antagonist and peptide agonist binding sites of the NK1 receptor with fluorescent ligands." J Biol Chem 272(34): 21167-75.
- Urbanik, E. and B. R. Ware (1989). "Actin filament capping and cleaving activity of cytochalasins B, D, E, and H." Arch Biochem Biophys 269(1): 181-7.
- van der Flier, A. and A. Sonnenberg (2001). "Function and interactions of integrins." Cell Tissue Res 305(3): 285-98.
- Vogt, A. K., G. J. Brewer, et al. (2005). "Connectivity patterns in neuronal networks of experimentally defined geometry." Tissue Eng 11(11-12): 1757-67.
- Vogt, A. K., L. Lauer, et al. (2003). "Micropatterned substrates for the growth of functional neuronal networks of defined geometry." Biotechnol Prog 19(5): 1562-8.
- Vorobjev, I. A., H. Liang, et al. (1993). "Optical trapping for chromosome manipulation: a wavelength dependence of induced chromosome bridges." Biophys J 64(2): 533-8.
- Waggoner, P. S. and H. G. Craighead (2007). "Micro- and nanomechanical sensors for environmental, chemical, and biological detection." Lab Chip 7(10): 1238-55.
- Warrick, H. M., R. M. Simmons, et al. (1993). "In vitro methods for measuring force and velocity of the actin-myosin interaction using purified proteins." Methods Cell Biol 39: 1-21.

- Weber, G. and K. O. Greulich (1992). "Manipulation of cells, organelles, and genomes by laser microbeam and optical trap." Int Rev Cytol **133**: 1-41.
- Weinbaum, S., J. M. Tarbell, et al. (2007). "The structure and function of the endothelial glycocalyx layer." Annu Rev Biomed Eng **9**: 121-67.
- Weiss, J. M., P. H. Morgan, et al. (1996). "The cubic ternary complex receptor-occupancy model. I. Model description." J Theor Biol **178**(2): 151-67.
- Welch, H. C., W. J. Coadwell, et al. (2003). "Phosphoinositide 3-kinase-dependent activation of Rac." FEBS Lett **546**(1): 93-7.
- Wellershaus, K., J. Degen, et al. (2008). "A new conditional mouse mutant reveals specific expression and functions of connexin36 in neurons and pancreatic beta-cells." Exp Cell Res **314**(5): 997-1012.
- Whitesides, G. M., E. Ostuni, et al. (2001). "Soft lithography in biology and biochemistry." Annu Rev Biomed Eng **3**: 335-73.
- Xia, Y., E. Kim, et al. (1996). "Complex Optical Surfaces Formed by Replica Molding Against Elastomeric Masters." Science **273**(5273): 347-9.
- Yamagata, M., J. R. Sanes, et al. (2003). "Synaptic adhesion molecules." Curr Opin Cell Biol **15**(5): 621-32.
- Yamaji, S., A. Suzuki, et al. (2004). "Affixin interacts with alpha-actinin and mediates integrin signaling for reorganization of F-actin induced by initial cell-substrate interaction." J Cell Biol **165**(4): 539-51.
- Yang, Y. L., K. H. Yao, et al. (2003). "Three kinds of current in response to substance P in bullfrog DRG neurons." Brain Res **981**(1-2): 70-7.
- Yeung, C. K., L. Lauer, et al. (2001). "Modulation of the growth and guidance of rat brain stem neurons using patterned extracellular matrix proteins." Neurosci Lett **301**(2): 147-50.
- Zhang, C., J. Xu, et al. (2006). "PCR microfluidic devices for DNA amplification." Biotechnol Adv **24**(3): 243-84.
- Zhang, H., D. J. Webb, et al. (2003). "Synapse formation is regulated by the signaling adaptor GIT1." J Cell Biol **161**(1): 131-42.
- Zheng, J. H., E. T. Walters, et al. (2007). "Dissociation of dorsal root ganglion neurons induces hyperexcitability that is maintained by increased responsiveness to cAMP and cGMP." J Neurophysiol **97**(1): 15-25.
- Zheng, T., D. Peelen, et al. (2005). "Lectin arrays for profiling cell surface carbohydrate expression." J Am Chem Soc **127**(28): 9982-3.
- Ziaie, B., A. Baldi, et al. (2004). "Hard and soft micromachining for BioMEMS: review of techniques and examples of applications in microfluidics and drug delivery." Adv Drug Deliv Rev **56**(2): 145-72.
- Zicha, D., I. M. Dobbie, et al. (2003). "Rapid actin transport during cell protrusion." Science **300**(5616): 142-5.

Acknowledgments

First of all I would like to thank Prof. Horst Vogel for offering me the possibility to perform such PhD thesis in his laboratory, for the confidence he had on my ideas, but especially for his support during the discussions and his supervision. Thanks for the freedom and believing that collaborations are profitable experiences.

I would like to thank Prof. Karen Martinez for her supervision on my work during the time she was at the EPFL and for the encouragements her gave me. Only she knows how pessimistic I can be sometimes.

I would like to thank all LCPPM members, past or present, for their scientific support, for sharing knowledge and for the great ambiance at work and outside too. I would like to mention particularly my direct collaborators:

Dr. Erwin Ilegems for his introduction to siRNA world and the great friend you are.

Prof. Dimitrios Stamou for his introduction to Micro-Contact Printing and his detailed advises and tricks, which were essential for the final success.

Dr. Monika Bäumle for the interesting collaboration in the nanoparticles field, and the incredible atmosphere that you brought in our office.

Dr. Marinela Gjoni for introducing me to the field of laser tweezers. Working with you was motivating even in front of the difficulties but you kept your smile.

Joachim Piguet for his help with Igor and the time we share doing manipulations.

Davor Kosanic for his enthusiasm in collaborating, his ideas and the exchange we have. You are an extraordinary person and a good friend.

Dr. Ruud Hovius with who I have the most interesting discussion and for all the advices you share.

Special mention to Cédric Deluz, which help me in molecular biology and and Sylvain Etter for his advices and good mood. You are both very good friends.

Finally from the lab, I would like to thank Verena Tabet for her amability.

I would like to thank all the people from others laboratories:

Dr. Klaus Ehrmann for his spirit of innovation and the work we did together.

Dr. Urban Seger, who introduced me to dielectrophoresis.

The group of Prof. Claus Duschl at the Fraunhofer Institut in Berlin, for sharing their experience of the Evotech Technology.

Dr. Beate Sick for her knowledge in DNA microarrays.

All the members of the group of Prof. René Salathé with whom we developed the multi-tweezer setup. Especially I would like to thank Dr. Fabrice Merenda for the easy exchange of opinions, which finally led to this multidisciplinary collaboration.

The group of Prof. Daniel Bertrand at CMU of Geneva for sharing their knowledge about primary cell isolation. Especial thanks go to Dr. Marzia Lecchi for the attention she provided me.

I really would like to thank to the main correctors of my thesis, Dr. Samuel Terrettaz, Dr. Christophe Danelon, Dr. Horst Pick and Dr. Raissa Trend, not only for the work they did but also for their personalities. It was a pleasure to have you around me.

An especial citation for a particular group of friends that support me in the most difficult moment: Séverine Milon, Lydiane Saucède, Luigino Grasso, Angela Burki-Unholz, Megan Bowyer, Hoa Dang, Maude Niestlé, Joachim Piguet, Olivia Baud, Veronica Ponce de Leon and Cédric Deluz.

Finally I would like to thank my family... my best supporters.

Curriculum Vitae

Pedro PASCOAL

Born the 23 August 1977

Nationality: Portugal

Education

2003-2008	Ph. D. Thesis at Swiss Federal Institute of Technology	(EPFL-Lausanne)
2001-2002	M. Sc. in Biochemistry at Sciences II (Diplôme)	(University of Geneva)
1997-2001	B. Sc. in Biochemistry at Sciences II (Licence)	(University of Geneva)
1993-1997	High school at Collège Voltaire (Maturité Scientifique)	(Geneva)

Publications

“Covalent labeling of cell surface proteins for in vivo FRET studies.”

Meyer BH, Martinez KL, Segura JM, Pascoal P, Hovius R, George N, Johnsson K, Vogel H.

In FEBS Lett. 2006 Mar 6;580(6):1654-8.

“Sample patterning on NMR surface microcoils.”

Ehrmann K, Gersbach M, Pascoal P, Vincent F, Massin C, Stamou D, Besse PA, Vogel H, Popovic RS.

In J Magn Reson. 2006 Jan;178(1):96-105.